HEAT TRANSFER TO LIQUIDS IN SWIRLING MOTION

A THESIS

Presented to

the Faculty of the Graduate Division

by

Thomas Edward Stonecypher

In Partial Fulfillment

of the Requirements for the Degree

Doctor of Philosophy in the School

of Chemical Engineering

Georgia Institute of Technology

March 1961

"In presenting the dissertation as a partial fulfillment of the requirements for an advanced degree from the Georgia Institute of Technology, I agree that the Library of the Institution shall make it available for inspection and circulation in accordance with its regulations governing materials of this type. I agree that permission to copy from, or to publish from, this dissertation may be granted by the professor under whose direction it was written, or, in his absence, by the dean of the Graduate Division when such copying or publication is solely for scholarly purposes and does not involve potential financial gain. It is understood that any copying from, or publication of, this dissertation which involves potential financial gain will not be allowed without written permission.

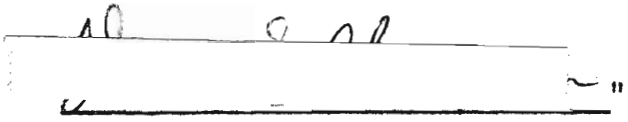

HEAT TRANSFER TO LIQUIDS IN SWIRLING MOTION

Approved:

Thesis Advisor

Date Approved by Chairman: 11/30/61

DEDICATION

This thesis is respectfully dedicated to the memory of the late Dr. Joseph M. DallaValle whose inspiration, encouragement, friendship and teaching were invaluable to the writer.

ACKNOWLEDGEMENTS

Many individuals have contributed to the completion of this work. The author is particularly indebted to the late Dr. J. M. DallaValle, who first suggested the research program and guided the initial phases of the investigation. The suggestions, guidance and friendship of Dr. H. V. Grubb throughout the study were invaluable. The association and stimulating discussions with Dr. J. D. Fleming, Jr., who was undertaking a similar investigation, were most helpful. The author is also indebted to Dr. W. B. Harrison, who first aroused his interest in heat transfer, and to Dr. Clyde Orr, Jr., from whom he gained invaluable practical research experience and training as an employee of the Engineering Experiment Station. The patience and encouragement throughout this undertaking of May Muse Stonecypher, wife of the author, are sincerely appreciated.

The author would also like to express his appreciation to the Dow Chemical Company for the graduate fellowship in the School of Chemical Engineering for the academic year 1957-1958.

NOMENCLATURE

Latin letter symbols

A	area	ft.^{2}
b	blade thickness	ft.
C	constant	
$\overline{c}_p$	mean specific heat	BTU/lbm-°F.
D	diameter	ft.
g_c	conversion factor	ft-lbm/lbf-sec^2.
h	steam enthalpy	BTU/lbm.
$\overline{h}$	local average film heat transfer coefficient	BTU/hr-ft^2-°F.
ΔH_f	fluid head loss	ft-lbf/lbm.
k	thermal conductivity	BTU/hr-ft-°F.
l	length	ft.
Nu	Nusselt number	
p	local pressure	lbf/ft^2
P	static pressure	lbf/ft^2
Pr	Prandtl number	
q	rate of heat transfer	BTU/hr
r	radius	ft.
Re	Reynolds number	
S	length	ft.
t	fluid temperature	°F.
T	wall temperature	°F.

u	local velocity	ft/sec.
U	velocity	ft/sec.
w	weight rate of flow	lbm/sec.
x	length	ft.
z	axial length	ft.

Greek letter symbols

α (alpha)	angle	
θ (theta)	angular coordinate	
μ (mu)	dynamic viscosity	lbm/ft-sec.
ρ (rho)	density	$lbm/ft.^3$
Δ (delta)	finite difference	
η (eta)	efficiency	

Subscripts

a	inside wall radius
b	thermocouple plane radius
c	condensate; channel
f	liquid phase
g	gas phase
i	inlet conditions
m	mean
n	normal direction
o	outlet conditions
t	tube
w	wall

z	axial direction
θ	angular direction
1	inside channel radius
2	outside channel radius
1, 2, 3, 4, 5, ...	designations for constants or positions

Superscripts

bar ($-$)	average conditions
prime (')	one channel

TABLE OF CONTENTS

LIST OF TABLES

LIST OF FIGURES

SUMMARY

A current and important problem in the field of heat transfer is the development of design concepts and techniques for handling high heat fluxes. Research in this area has been stimulated by recent advances in aeronautical science, nuclear technology and space technology. One concept which has been utilized to increase heat transfer rates in heat exchange equipment is that of imparting a swirling motion to the fluid removing heat from the system.

The purpose of this research program was the experimental investigation of a particular application of swirling motion to a common heat exchange system. The objectives of this study included the numerical evaluation of local average film heat transfer coefficients for fluids falling in a swirling film in a vertical tube heat exchanger, correlation of these results, and the evaluation of this model for purposes of handling high heat fluxes. General flow characteristics of the swirling falling film were sought also.

Investigations in this research program involved flow characterization studies and heat transfer studies. The principal effort in the early phases of this study was directed toward discovering and characterizing a suitable device for imposing swirling motion on a liquid film flowing vertically downward within a tube. Since fixed impeller devices in contrast to rotating mechanisms were simple to construct, operate and maintain, and had been demonstrated to be

suitable for producing swirling motion, design considerations were restricted to devices of this type.

The impeller which was developed and used throughout this study was fabricated by machining a cylindrical length of brass stock with square, triple threads at the rate of three threads per inch. This device was mounted in a jacketed enclosure which supplied fluid to each of the channels between the threads. Swirling motion was thus imposed on the fluid as it coursed down the spiral paths of the impeller channels and out into a flow visualization tube, a flow characterization tube or a heat transfer tube.

Flow characterization studies performed with the impeller assembly under conditions simulating those of the heat transfer system included measurements of the static pressure requirements of the device, visual observation of the flow pattern produced in a vertical glass tube attached to the assembly, and static pressure measurements at various distances from the impeller outlet in a copper tube attached to the assembly. The static pressure requirements of the impeller assembly were found to be quite high. The efficiency of conversion of static pressure to kinetic energy of fluid leaving the impeller was found to vary between approximately 12.5 per cent and 71.5 per cent. The static pressure requirements of the impeller were correlated with an impeller Reynolds number for the two fluids, water and ethylene glycol, which were investigated.

Flow characteristics of a descending swirling film of water in both a glass tube and in a plastic tube attached to the impeller outlet

were noted by visual observation and photographic recording for several flow rates. Short lengths of thread and dye injection were used to study the degree of turbulence. Wires and probes were inserted into the descending film to discover the effect on the overall flow pattern. The flow was found to be quite turbulent near the impeller outlet due to mixing of streams from the three channels; the apparent turbulence level decreased with increasing distance from the impeller. The ratio of apparent tangential to vertical velocity components in the swirling film decreased rapidly with increasing distance from the impeller also. Probes in the fluid stream apparently had little more than a local effect on the flow pattern.

This observation was confirmed impart by tube wall static pressure measurements; these studies indicated that the swirl velocity was quite low compared to its original value for distances greater than about fourteen inches from the impeller.

Heat transfer studies were performed using a 30-inch length of nominal 1-inch copper pipe for the heat exchange tube. Heat was transferred to the pipe by condensing steam. The pipe was mounted vertically in a steam chest and was surmounted by the impeller assembly. Thermocouples were imbedded in the pipe wall.

Local average film heat transfer coefficients for water and for ethylene glycol were determined at several flow rates for the first five inch length nearest the impeller, the following seven inch length, the next eight inch length and the last ten inch length of the heat exchange tube. Thermocouples mounted on a probe were used to determine the

fluid film temperature. In general the film heat transfer coefficients for the portion of the tube nearest the impeller were quite high, and film coefficients for the remaining lengths decreased with increasing distance from the impeller outlet. A correlation of the local average film heat transfer coefficients in terms of the Nusselt, Reynolds and Prandtl numbers for each of the fluids was obtained.

The results from this study indicated that induced swirling motion in fluids can have an appreciable effect on the local film heat transfer coefficients and thus the heat transfer characteristics of that fluid. Accordingly, the feasibility of applying this concept to the solution of novel heat transfer problems deserves further investigation.

The fixed impeller device used in this study to initiate the swirling motion in the fluid film produced satisfactory flow patterns, but the static pressure requirements were quite high. Methods for improving the impeller efficiency were suggested.

Based on experience gained from this investigation it is suggested that further research on this concept be designed to include theoretical studies of the fluid flow and heat transfer problem in conjunction with the experimental studies. Specifically, it is proposed that a fixed impeller design which produces a uniformly swirling flow be devised. It is recommended that the impeller extend throughout the heat exchange section to permit more accurate flow characterization and temperature measurement. Consideration should also be given to methods of producing a constant, uniform wall temperature. Attainment of this objective would simplify measurements, data reduction and

correlation of results as well as simplifying the theoretical analysis.

CHAPTER I

INTRODUCTION

A current and important problem in the field of heat transfer is the development of design concepts and techniques for handling high heat fluxes. Research in this area has been stimulated by recent advances in aeronautical science, nuclear technology and space technology. The advent of supersonic aircraft has produced a number of unique heat transfer problems requiring the fabrication of heat exchange equipment having small volume, low weight and high efficiency. The application of nuclear reactors to power generation has resulted in the development of novel methods of efficient heat exchange. In space technology a large effort has been devoted to the solution of the re-entry problem and the nozzle cooling problem, both of which are of paramount importance in determining the effectiveness, reliability and range of a missile system.

One concept which has been utilized to increase heat transfer rates in heat exchange equipment is that of imparting a swirling motion to the fluid removing heat from the system. Early investigations of this concept involved the use of turbulence promoters in the form of twisted metallic strips or wires which were placed within tubes in shell-and-tube heat exchangers. The results of these studies showed that heat transfer rates could be raised appreciably, but that there was an attendant increase in the pumping power requirements which limited the applicability of the concept. Other techniques for inducing swirling

motion in the heat exchange fluid have been investigated; these techniques have included tangential fluid entry into an axial flow system, rotation of the heat exchange tube about its axis, and fixed or rotating impellers. The improvement in heat transfer rates produced by the induced swirling motion has been ascribed to a number of mechanisms depending on the mode of heat transfer and the configuration of the equipment. Among these are included an increased turbulence intensity adjacent to the heat transfer surface, a pressure gradient favorable to convection from the heated surface, and a reduction in boundary layer thickness.

Purpose of This Research

The purpose of this research program was the experimental investigation of a particular application of swirling motion to a common heat exchange system. The objectives of this study included the numerical evaluation of local film heat transfer coefficients for fluids falling in a swirling film in a vertical tube heat exchanger, correlation of these results, and the evaluation of this model for purposes of handling high heat fluxes. General flow characteristics of the swirling falling film were sought also.

Related Literature

The literature particularly applicable to this investigation includes a number of studies of adiabatic swirling motion and studies of swirling motion with heat transfer. The studies of fluids in adiabatic swirling motion are useful in the development of a transport mechanism

to explain qualitatively the observed change in heat transfer rates. The heat transfer investigations give quantitative results for particular systems utilizing swirling motion.

Adiabatic swirling motion.—A comprehensive experimental investigation of the effect of curvature on the fully developed two-dimensional flow of air was undertaken by Wattendorf (1). The apparatus used in the investigation involved a bell-shaped entry having a honeycomb diffuser to reduce eddy currents. This was followed by a straight entry length of rectangular cross-section to insure fully developed flow. Tangent to the entry length and having the same cross-section was the curved section, which had constant radii of curvature and encompassed approximately 300 degrees of arc. At the outlet of the curved test section was the exhaust section, which contained a propeller to induce the flow through the apparatus. Provision was made for the measurement of the static pressure at the wall and for the measurement of the total pressure as a function of radial position at various stations in the straight entry section and in the curved test section.

Two experimental devices were built. The first device had an entry length of 305 cm. The radii of curvature of the test section were 45 cm and 50 cm. The channel cross-section was 5 cm in width and 90 cm in depth to minimize extraneous wall effects and to insure two-dimensional flow. The second experimental device differed slightly from the first. The entry section of this device was 285 cm in length, and the radii of curvature of the test section were 20 cm and 25 cm. The remaining dimensions of the system were the same as those in the

first device.

The measurements of the static pressure at the wall and of the mean total pressure as a function of radial position indicated that the velocity distributions in the curved channel differ considerably from those in the straight channel. The velocity profiles calculated from these measurements at various stations in the straight entry section had maxima at the center of the channel. The velocity profiles calculated at various stations in the curved test section had maxima which were displaced toward the center of curvature. The amount of displacement increased from zero upstream of the curved section to an essentially constant value at stations 90 degrees of arc from the entrance of the curved test section and beyond. In addition, the relative magnitude of the maximum velocity in the curved section was lower than the corresponding maxima in the straight entry section. This effect was compensated by an increase in the velocities near the outer wall of the curved section over corresponding values in the straight entry section.

The experimental results were compared with two potential flow velocity distributions. The first of these was formed by taking the product of the local velocity and the local radius to be constant, and the second was formed by taking the quotient of the local velocity and the local radius to be constant. It was found that the flow in the region away from the walls corresponded well to the first potential flow relation. Up to a distance of 1 cm from the walls the shape of the velocity distribution was similar to that of the usual fully developed turbulent flow profile. Also, it was found that there was only a slight increase in channel flow

resistance due to curvature for the test sections used.

In the discussion of the experimental results Wattendorf used the stability criterion proposed by Rayleigh (2) for flow in curved paths. In effect, this theory states that, for the case of a decreasing product of local velocity and radius with increasing radius, the centrifugal force on a fluid element displaced outward is greater than the centripetal pressure gradient. The motion of the element is unstable because the tendency is for the displaced particle to move further in the same direction. If the displacement is inward, the centrifugal force will be less than the centripetal pressure gradient and the element will be forced further inward. Similarly, for the case of an increasing product of local velocity and radius with increasing radius, the elements displaced from their equilibrium positions will be forced back to their original positions and the motion is stable. For a flow where the product of local velocity and radius is constant the stability is neutral. Accordingly, Wattendorf concluded that the flow in the curved channel is stable near the inner wall, neutral in the central portion of the channel, and unstable near the outer wall.

An extension of the investigations of Wattendorf to the experimental determination of the degree of turbulence, the shear stress, and velocity distributions in a similar apparatus was performed by Eskinazi and Yeh (3). The results of these studies, in general, confirmed and extended the results and conclusions obtained previously. In addition, however, it was noted that even a mild curvature of the mean flow influenced the turbulence quantities measured by these investigators to a

significant extent.

Many other investigations involving various geometrical configurations to produce swirling flow have been reported. Yeh (4) investigated the development of incompressible turbulent boundary layers along concave and convex stationary annular walls for air flowing spirally upward. Swirling vortex motion has been studied experimentally by Lay (5) and by Hartnett and Eckert (6). A theoretical analysis of the decay of a rotationally symmetric steady swirl superimposed on Poiseuille flow in a round pipe has been performed by Talbot (7).

Heat transfer to fluids in swirling motion.—A theoretical analysis and a limited amount of experimental data on convection to fluids in swirling motion were reported by Kreith (8). The model used in this study involved two-dimensional incompressible flow in a curved channel having a rectangular cross-section and constant radii of curvature. The theoretical analysis involved an extension of the analogy between heat transfer and momentum transfer. Expressions for the Nusselt number for concave surfaces and for convex surfaces were developed using the heat transfer equation in cylindrical polar coordinates for incompressible fully developed turbulent flow with constant fluid properties. The numerical evaluation of these expressions required the specification of the velocity distribution, the wall shearing stress, and the eddy diffusivity in a curved channel. This was accomplished using the experimental results of Wattendorf. For equivalent Reynolds numbers and Prandtl numbers greater than 0.7, the predicted values of the film heat transfer coefficient for typical concave surfaces encountered in practice

were from 25 to 60 per cent larger than those predicted for a convex surface.

Experimental results were obtained by Kreith for water and butyl alcohol flowing in a test section which had a mean radius of curvature of 1.5 inches. Heat was transferred to the fluid by a thin stainless steel resistance element located at the center of the channel. The heating element divided the test section into two flow regions. In the inner region heat was transferred from a wall concave to the flow, and in the outer region heat was transferred from a wall convex to the flow.

The results from the experiments generally confirmed the theory; the film heat transfer coefficient at the wall concave to the flow direction was larger than the film heat transfer coefficient in an equivalent straight channel. The film coefficient at the convex wall, conversely, was smaller than that for an equivalent straight channel.

An experimental investigation of heat transfer to liquids in swirling turbulent flow was conducted by Kreith and Margolis (9). The experimental apparatus involved a steam heated, horizontal, shell-and-tube heat exchanger. Swirling motion within the tube was induced by the use of a variety of twisted strips and twisted wires. It was observed that the inside film heat transfer coefficients were increased by as much as a factor of four compared to those for purely axial turbulent flow. The observed results were qualitatively explained by the mechanism of an increased turbulent mixing intensity near the concave surface and by the centrifugal force field acting on a favorable density gradient.

An analytical treatment of heat transfer in swirling pipe flow has

been given by Seigel and Perlmutter (10) in an extension of the theoretical analysis of Talbot. In this analysis a tangential swirl was superimposed on Poiseuille flow entering a straight round pipe under uniform wall heat flux. The tangential swirl decayed with axial distance. It was noted that in this case the increase in pressure drop caused by the swirling motion was larger than the net improvement in heat transfer.

A study of heat transfer from thin gold films to water in swirling motion was conducted by Fleming (11). The results of this study indicated that thin gold films may be feasible configurations for the generation of high heat flux at high surface temperatures; it was noted that the mode of heat transfer from these films was apparently forced convection.

Gambill and Green (12) have reported investigations of boiling heat transfer to water in swirling vortex motion. Boiling heat transfer coefficients considerably higher than those obtained in ordinary subcooled boiling studies were obtained.

CHAPTER II

INVESTIGATIONS AND RESULTS

Fluid Flow Studies

Design of the impeller assembly.—The principal effort in the early phases of this investigation was directed toward discovering a suitable device for imposing swirling motion on a liquid film flowing vertically downward within a tube. A number of concepts capable of producing the desired flow were considered. Among these were fixed impeller devices, rotating impeller mechanisms, systems employing tangential entry of the fluid, and arrangements utilizing rotation of the tube containing the fluid film. Since it was felt that suitable swirling motion could be induced in a fluid by a tangential inlet device or by a fixed impeller arrangement, all design considerations were limited to devices of these types.

Preliminary investigations to determine the feasibility of using a design based on tangential fluid inlets were conducted using a Plexiglas model. In this device, four equally spaced tangential holes 1/16-inch in diameter were drilled in an axial plane in a nominal 1-inch plastic pipe. Surrounding these inlet holes was a concentric jacket which provided a uniform source of fluid. The jacket was made from nominal 4-inch plastic pipe and 1/8-inch sheet stock. Fluid entered the jacket through four equally spaced holes on its perimeter; these holes were aligned with the tangential inlets in the 1-inch pipe. The supplementary equipment

used with this model included a vertical mounting frame for the plastic impeller-tube assembly, a manifold to supply fluid to the impeller jacket, and the necessary piping, fittings, and valves to permit attachment to an existing water supply.

A number of preliminary experiments to determine the feasibility of this apparatus were undertaken using various water flow rates. The results from these studies generally indicated that the tangential inlet type of impeller configuration was not desirable. As the fluid passed through a tangential inlet, it experienced a centrifugal force as it began to follow the curvature of the vertical tube. This produced a deformation from the original circular cross-section into a flattened elliptical shape. The meeting of two of these streams of fluid from adjacent circular inlets produced a highly turbulent zone at the juncture. This effect was most pronounced near the impeller. The result was a fluctuating flow pattern which extended for some distance down the tube. For this reason this configuration was abandoned and a more suitable device was sought.

The impeller assembly used by Sineath (13) in his investigations of particulate separation and classification was then considered. The impeller used in this device consisted of a circular cylinder having a conical streamlining shape on the upstream end and an ogival shape on the downstream end. Equally spaced around the cylindrical surface were a number of curved blades. These blades were fabricated to follow the contour of an arc of a circle projected on the cylinder. At any cross-section of the impeller the blade thickness centerline of any blade cross-

section passed through the axis of the cylinder. Thus, the lines shown in the blade cross-section which corresponded to blade flow surfaces were parallel to radial lines. The blade surfaces on the upstream end of the assembly were parallel to the approaching flow. A pipe which had an internal diameter corresponding to the external diameter of the impeller was used to encase this device, thus forming the impeller assembly.

A number of tests using the impeller assembly of Sineath were conducted. It was found that the swirling motion produced by this device was quite stable and relatively free of turbulent fluctuations, although regions of flow which corresponded to fluid leaving individual blades separated by the turbulent interference zone described previously still existed.

Accordingly, it was decided to utilize an impeller of similar design. Attempts to construct a curved blade fixed impeller suitable for these investigations were entirely unsuccessful. The principal difficulty in producing a scaled version of the Sineath impeller was in the fabrication and attachment of the small, compound curved blades required for exact duplication.

To alleviate the fabrication problem, it was decided to replace the curved impeller blades having a continuously varying slope with blades of fixed slope. This impeller blade configuration, of course, was much easier to fabricate, since it required only the cutting of square threads on a circular cylinder to produce impeller blades having any desired slope and pitch.

The impeller which was used throughout these investigations is shown in Fig. 1. This device was fabricated from brass rod stock. The cylindrical section was first machined to a diameter of 1.068 inches, and then the stock was triple threaded at three threads per inch with square threads. The root diameter of the threads was 0.750 inch, and the total length of the threaded section was three inches. The open space between two adjacent thread surfaces measured in the axial direction was 0.078 inch. A uniform distribution of flow from the three channels was insured by machining the downstream end of the blades plane in the radial direction. The burr produced by this operation was removed by careful filing. An ogival shape 1.5 inches in length was then machined on the root diameter at this end of the impeller.

The remainder of the impeller assembly consisted of a jacket to furnish a uniform source of fluid to the impeller and an enclosure for the impeller. These components with the impeller and flanges for tube attachment are shown in Fig. 2. The jacket was fabricated from two end plates of 1/8-inch brass plate and a 1-1/2-inch length of nominal 4-inch copper pipe. First, a groove to accommodate end plates having diameters slightly greater than the inside diameter of the pipe was machined to a depth of 1/8-inch in both ends of the pipe. The brass end plates were machined from flat stock and shrunk into place. A groove at each exposed copper-brass interface was then machined so that the juncture could be soldered conveniently. Three equally spaced holes were then drilled and tapped on the periphery of the pipe to accommodate pipe fittings, and the centers of the end plates were bored to a shrink

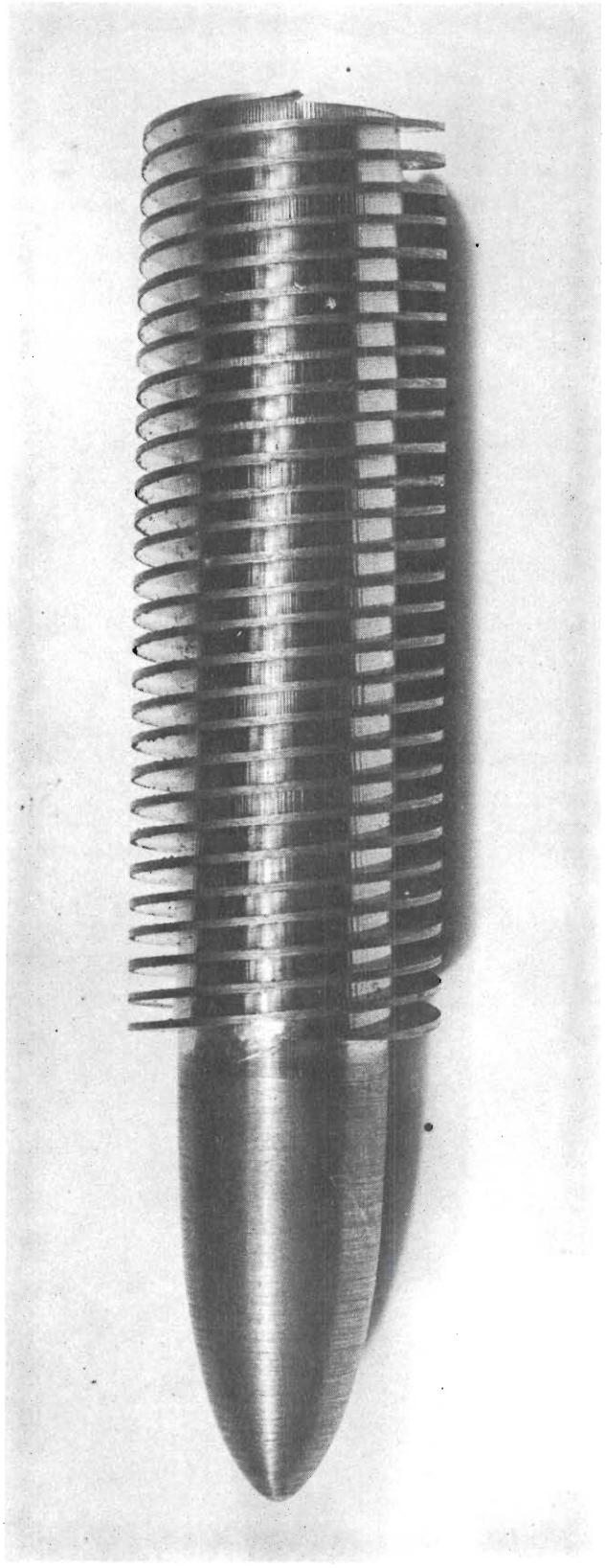

Figure 1. Impeller.

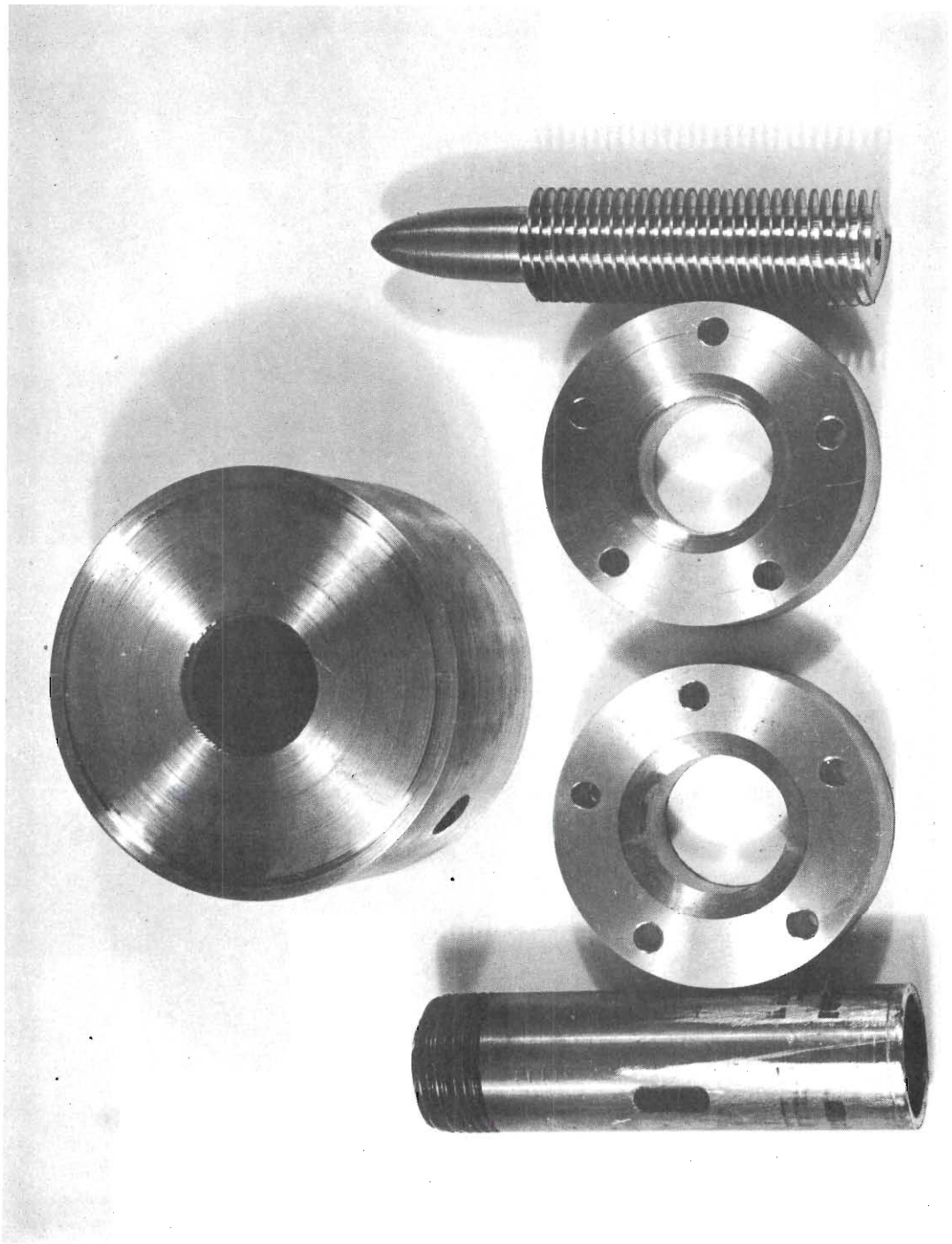

Figure 2. Components of Impeller Assembly.

fit on the external diameter of the pipe used to enclose the impeller.

The impeller enclosure was fabricated from nominal 1-inch copper pipe. One end of a 4-1/2-inch length of pipe was machined plane in the radial direction, and the other was threaded with 1-inch pipe threads. Three fluid inlet slots equally spaced around the periphery of the pipe were milled in an axial direction. These slots were 1/8-inch wide and 3/4-inch long and were located 1-3/4-inches from the plane surface. The outer surface of each slot was tangent to the inner surface of the pipe.

The fabrication of the complete impeller assembly from the various components was conducted as follows. First, the impeller was firmly fixed in the impeller enclosure by means of a shrink fit. The slightly oversized impeller was mounted in a vertical position with the outlet plane of the blades resting on a smooth, plane surface. The enclosure was heated and placed around the impeller and its plane surface was aligned with the outlet plane of the blades. This assembly was then allowed to cool. The impeller enclosure was shrunk into the jacket and soldered in place. The exposed copper-brass junctures in the jacket were then soldered. A nominal 1-inch iron pipe cap was used to seal the upper end of the impeller enclosure.

To facilitate the alignment and attachment of flow visualization tubes and heat transfer tubes to the impeller outlet, the flanges shown in Fig. 2 were machined from 3-inch brass rod stock. As shown in the schematic drawing of the complete impeller assembly in Fig. 3, one flange was soldered to the impeller enclosure, and the other was used

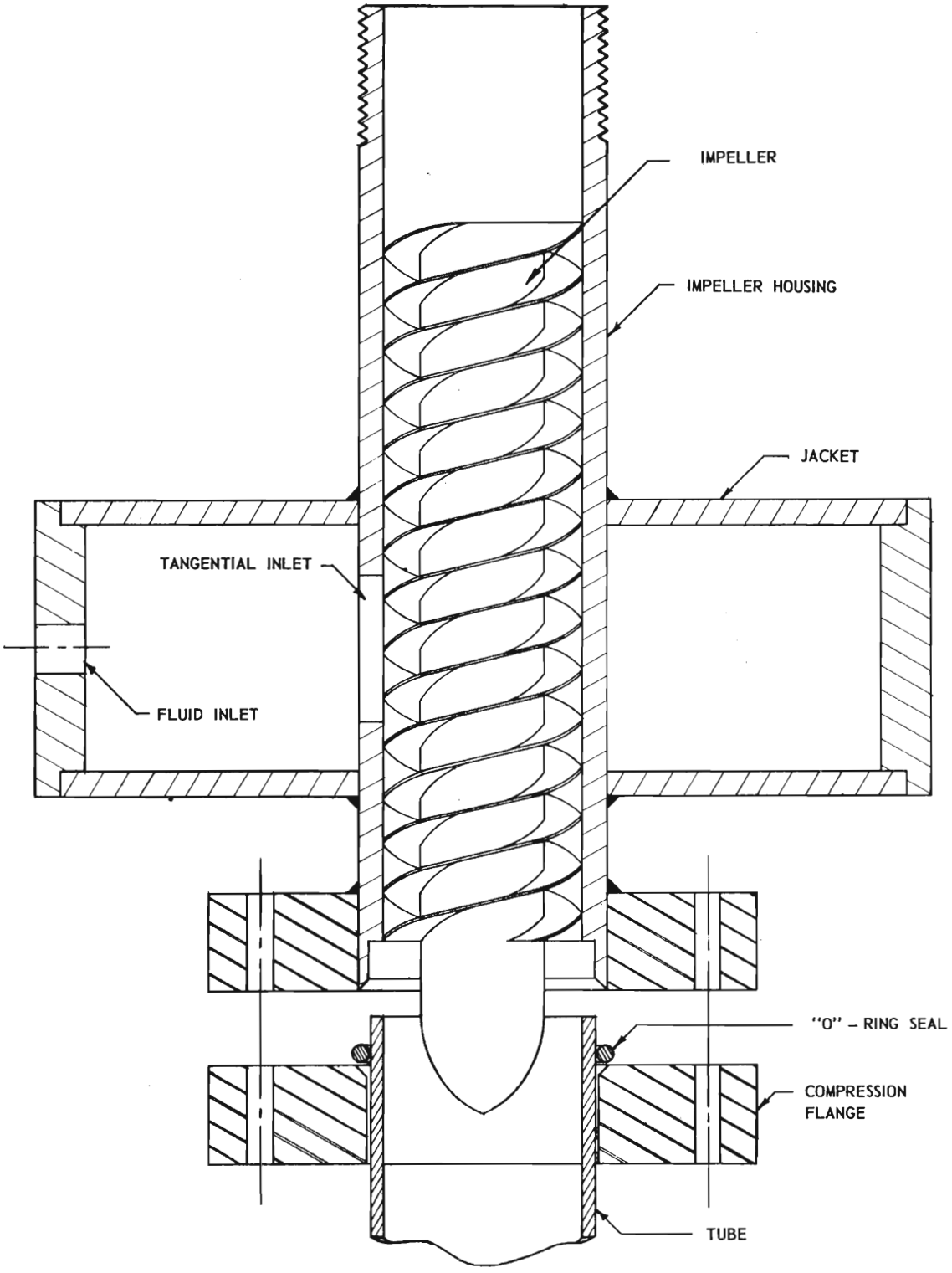

Figure 3. Schematic Drawing of Impeller Assembly.

to compress an O-ring encircling the tube to be attached to the impeller. The exposed inner surface of the attached flange was machined concentric with the inner surface of the enclosure, with a diameter slightly greater than that of the enclosure. Since the outside diameter of the tubes to be attached to the impeller assembly was the same as the inside diameter of the attached flange, this arrangement served to align the inner surfaces of the impeller enclosure and the flow visualization tube or heat transfer tube.

Flow characterization.—To determine the characteristics of the swirling flow produced by the impeller assembly, two series of investigations were undertaken. The first of these involved flow visualization studies, and the second series was concerned with static pressure determinations at various locations along the tube containing the fluid.

For the flow visualization studies the apparatus shown in Fig. 4 was constructed. Water was supplied to the impeller assembly from existing water mains or from a 20 gpm centrifugal pump connected to a storage tank. The fluid then passed through a metering section, which was composed of two rotameters mounted in parallel. The rotameters were manufactured by the Fischer-Porter Company of Hatboro, Pennsylvania, and had full scale ratings of 4.35 and 9.40 gpm for liquids having a specific gravity of 1.0. These instruments were calibrated with water before installation in the apparatus using the customary weighing technique. The results of the calibration tests are shown in Fig. 22 in the Appendix.

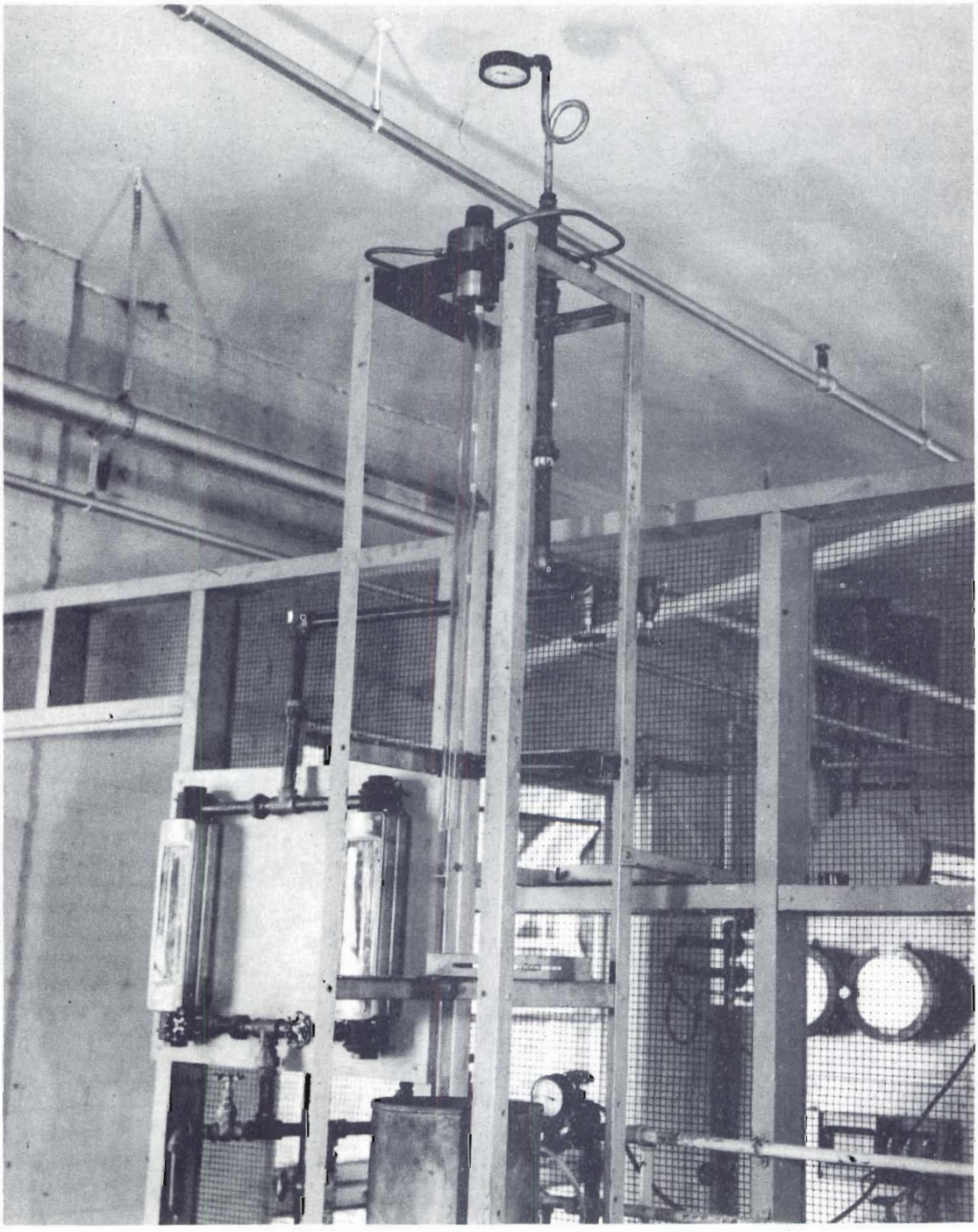

Figure 4. Flow Visualization Apparatus.

Following the metering section was a pressure manifold, which was made from a length of 1-1/2-inch pipe. Three equally spaced holes around the circumference of the pipe were drilled and 1/4-inch tubing fittings were attached. Copper tubing was connected to these fittings and to the corresponding fittings in the jacket of the impeller assembly.

The impeller assembly was mounted in an angle-iron frame approximately six feet higher than the water supply to the metering section. Attached to the outlet of the impeller assembly was a 36-inch length of Pyrex tubing having an internal diameter corresponding to that of nominal 1-inch pipe, 1.063 inches. This tubing was attached to the impeller using the O-ring clamping flanges described previously. Numerical designations indicating the distance from the plane of the impeller outlet in inches were attached to the surface of the tube with cellophane tape. A tank to receive the fluid leaving the Pyrex tube was provided. Fluid from this tank could be directed to the drain or returned to the storage tank.

Tests at a number of flow rates were conducted to determine flow patterns prevailing at various stations in the tube. Photographs of typical flow patterns are shown in Figs. 5 through 8.

Other flow visualization tests to ascertain the effect of introducing various disturbances into the swirling flow were undertaken. These studies were conducted so that a satisfactory method for measuring the fluid film temperature at various axial locations in the heat transfer tube could be developed. In the first series of tests fine copper wires were placed chordally at several axial locations in a plastic tube which

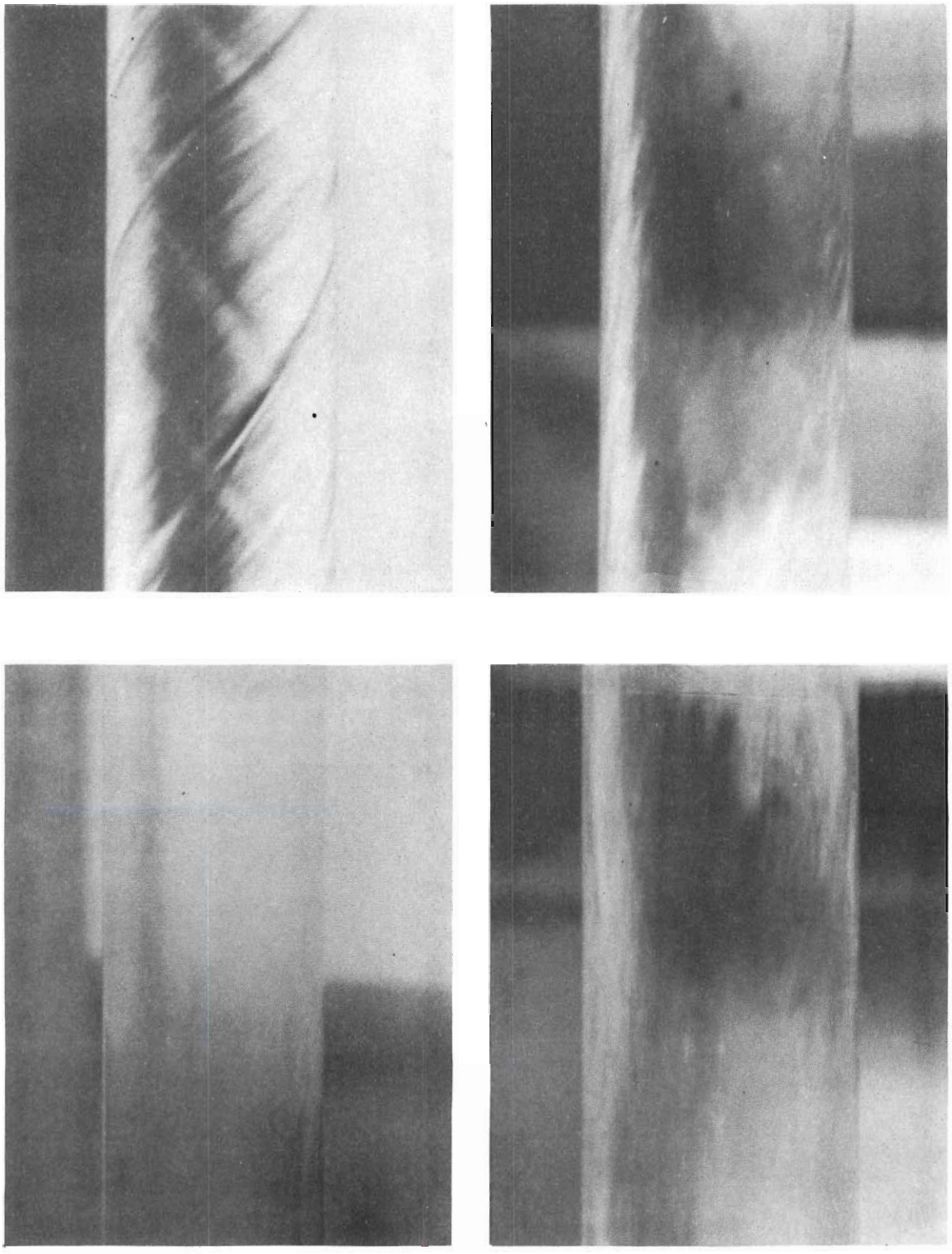

Figure 5. Flow Visualization Study. Flow Rate of 0.21 lb_m/sec.

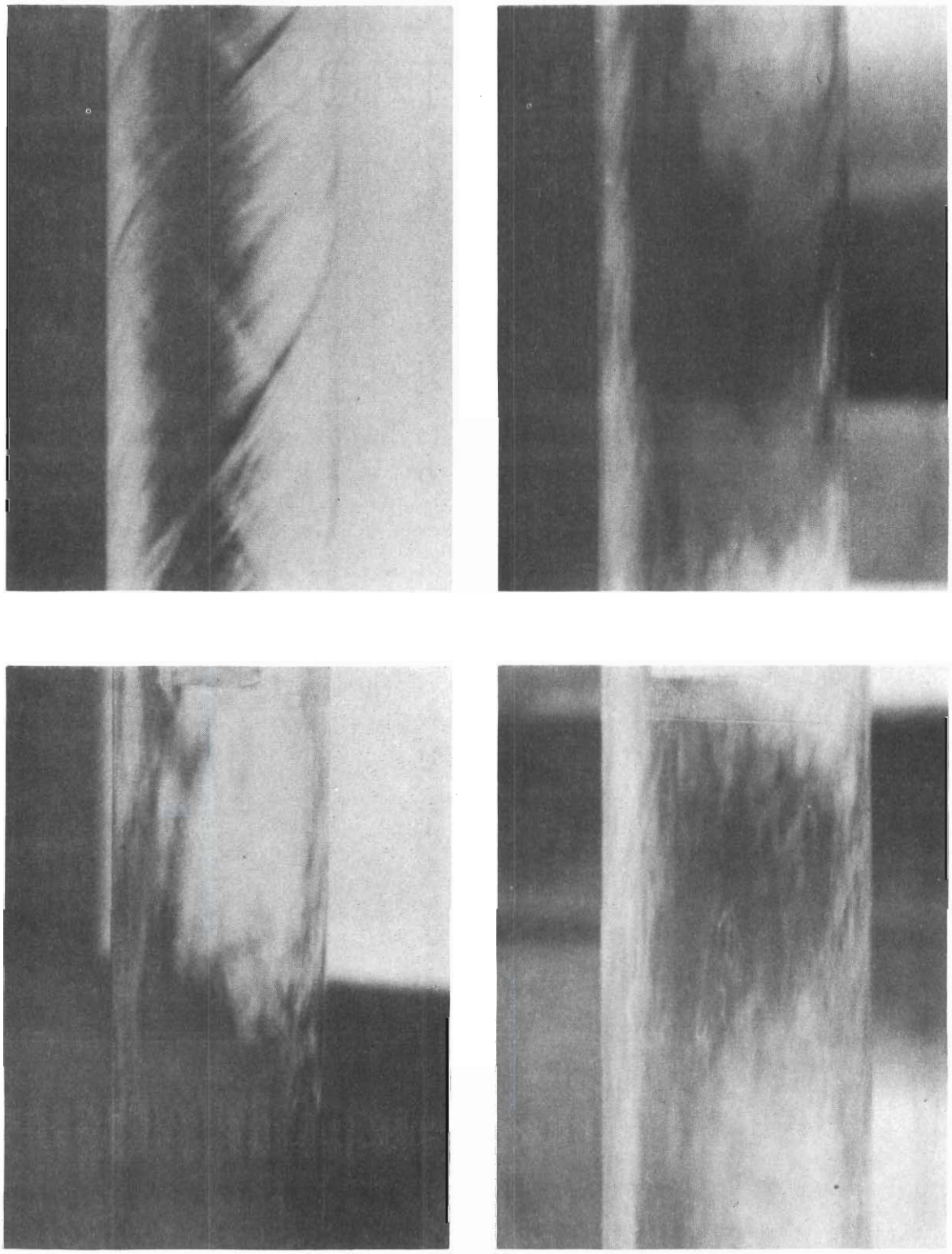

Figure 6. Flow Visualization Study. Flow Rate of 0.30 lb_m/sec.

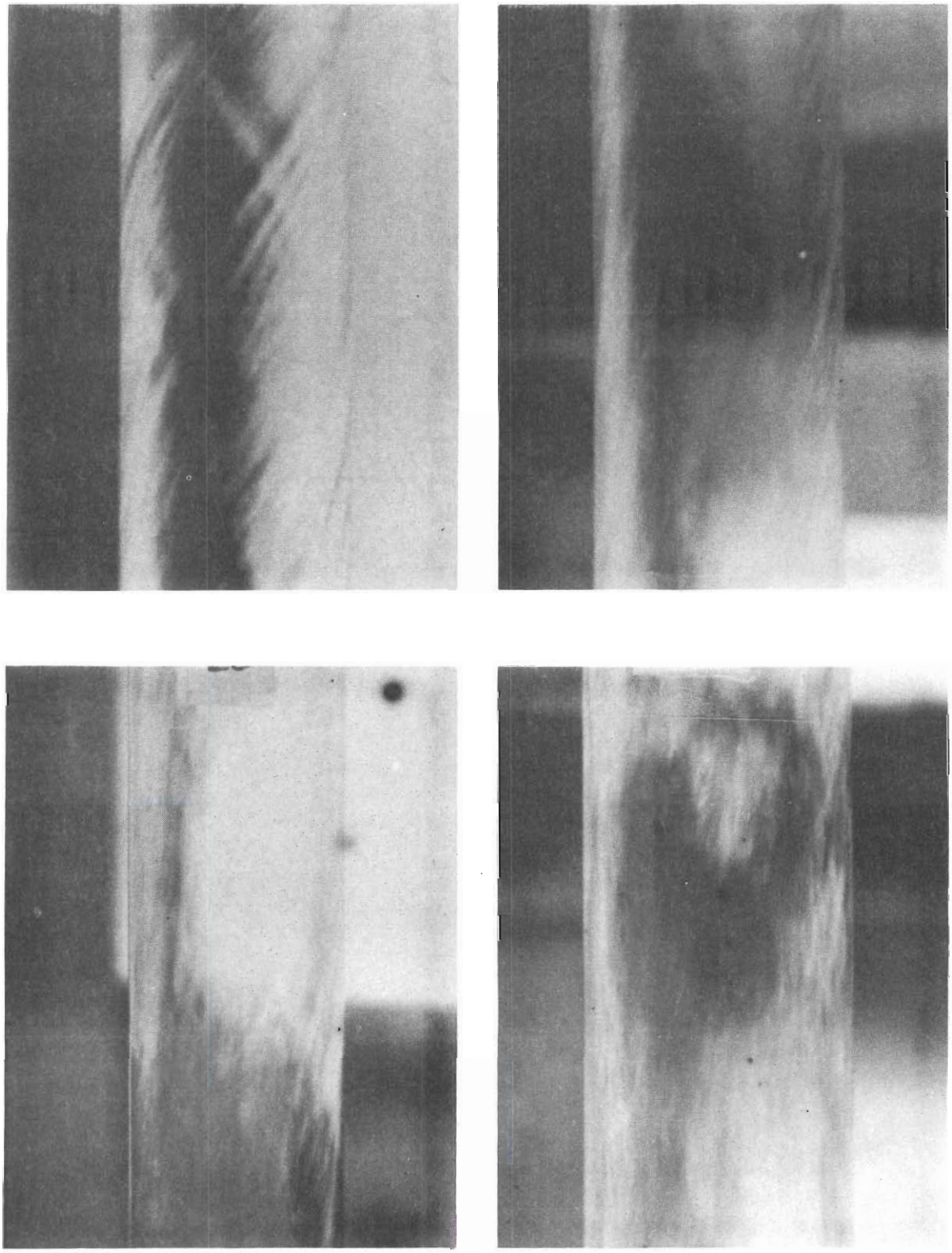

Figure 7. Flow Visualization Study. Flow Rate of 0.33 lb_m/sec.

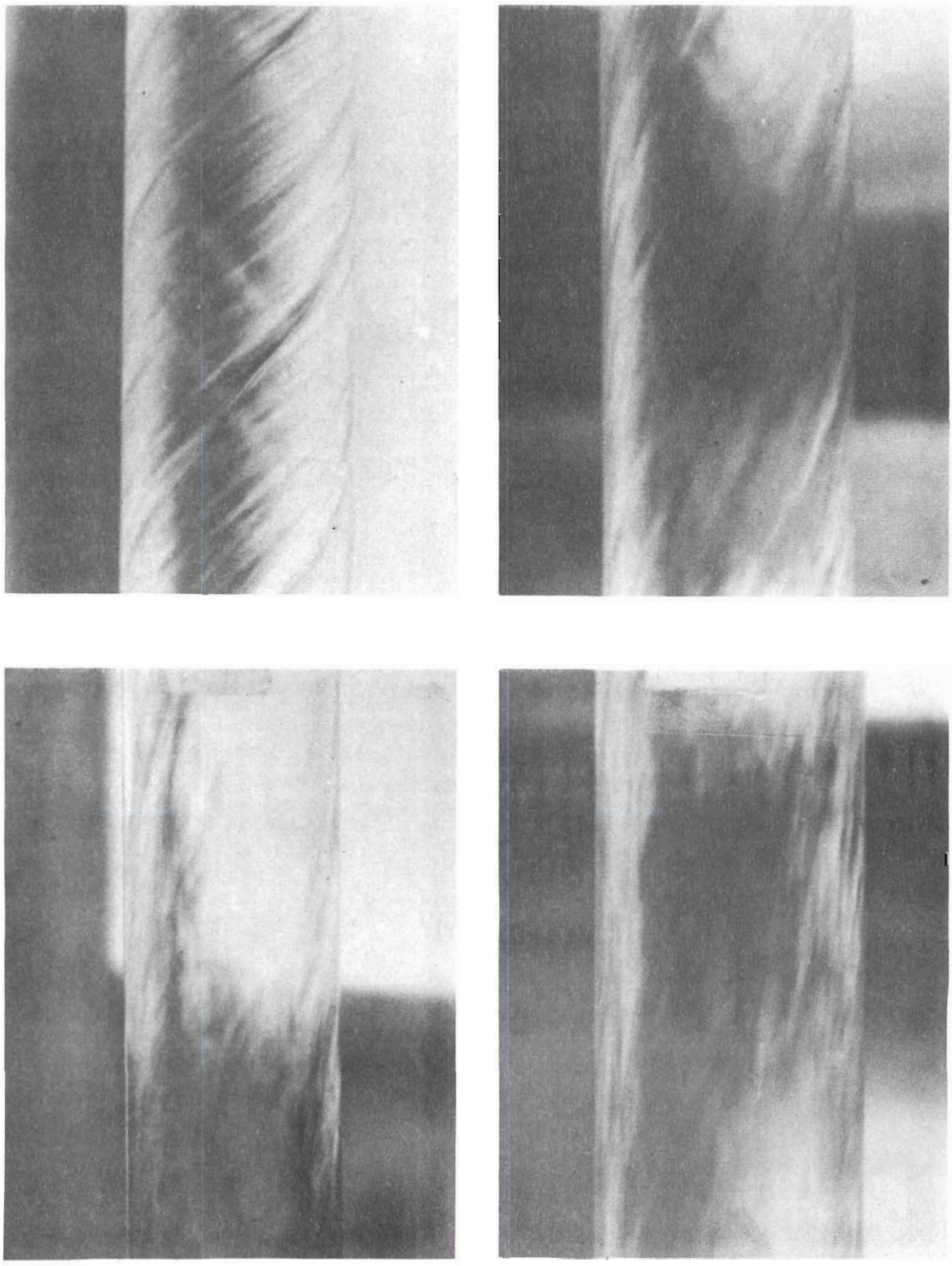

Figure 8. Flow Visualization Study. Flow Rate of 0.44 $lb_m/sec.$

had been machined on one end to fit the outlet of the impeller assembly. The tube was attached to the flow visualization apparatus and the flow pattern in the neighborhood of the wires was observed. It was noted that the wires did not seem to affect either the upstream or the downstream swirling flow pattern to a great extent.

The second series of tests was performed using a larger flow disturbance. In these studies the tip of a length of 1/8-inch rod was allowed to come into contact with the inner surface of the tube at various distances from the outlet of the impeller assembly. It was noted that a small wake upstream of the disturbance and a larger wake downstream of the disturbance were produced. The downstream wake apparently resumed the more uniform swirling pattern one or two inches beyond the disturbance, however.

The rapid recovery of the disturbed flow into the swirling flow, which was noted in both series of investigations, was attributed to a high level of turbulence in the swirling flow. To permit the testing of this hypothesis, small holes at a number of axial locations were drilled through the wall of the plastic tube and 1-inch lengths of black thread were passed through to the interior of the tube and cemented in place. A hole to accommodate a length of hypodermic tubing for dye injection was drilled at a location approximately three inches from the outlet of the impeller assembly. A number of tests at various fluid flow rates were conducted using these devices to qualitatively determine the degree of turbulence. It was found in the dye injection experiments that practically complete dissipation occurred approximately one inch down-

stream from the point of injection for all but the lowest flow rates. A violent agitation of the loose thread ends was also apparent at the higher flow rates and near the outlet of the impeller. A reduction in the degree of agitation was noted for lower flow rates and for locations more distant from the impeller outlet. These observations appeared to confirm the hypothesis of a highly turbulent swirling motion.

The second type of flow characterization investigations involved the determination of the static pressure in the fluid film as a function of the distance from the impeller. The tube used in these studies was fabricated from a 36-inch length of nominal 1-inch copper pipe. One end of this tube was machined so that it could be attached to the impeller outlet by means of the O-ring clamping device described previously. To provide a plane surface for the pressure tap locations, two diametrically opposed slots 0.100 inch deep were milled with a 1/4-inch end mill for the entire length of the tube. Locations for the pressure taps were selected, and two diametrically opposed holes 1/32-inch in diameter were drilled through the tube wall in a radially inward direction. The holes were centrally located in the slots. Following the drilling operation, short lengths of 1/8-inch copper tubing were fitted into the slots around each hole, and these were soldered in place. Since the drilling operation had slightly deformed the inner surface of the tube in the vicinity of the holes, the interior of the tube was polished with fine emery paper until the surface irregularities could no longer be observed. The static pressure holes were cleared with the drill and the smoothness of the inner surface of the tube was again verified.

This device was mounted in the impeller assembly, which had been mounted in the flow visualization apparatus described previously. The complete apparatus used in the static pressure determinations is shown in Fig. 9. Tygon tubing was used to connect diametrically opposed pressure taps to a 1/8-inch glass "Y" connector. The third side of each of these "Y" connectors was attached to a corresponding vertical glass tube mounted on a manometer board, using Tygon tubing as before. The outside diameter of this glass tubing was approximately 1/4-inch.

The experimental procedure involved filling the glass tubes and Tygon tubing with water, removing all entrapped air bubbles, and measuring the height of the liquid meniscus in each tube at static conditions. Flow through the impeller was started and readings of the equilibrium height of each meniscus, the liquid flow rate and the barometric pressure were taken. The static pressure tube was rotated approximately 75 degrees and the test was repeated under the same flow conditions. Following this determination, the tube was again rotated approximately 75 degrees and the third and final set of data for a particular experiment was recorded. An arithmetic average of the pressure reading at each station was calculated, the tube was returned to its original location, and the next experiment was begun.

The experimental data recorded in these determinations are given in Table 3 in the Appendix. The static pressure distribution as a function of the distance from the outlet of the impeller for a number of water flow rates is shown in Fig. 10.

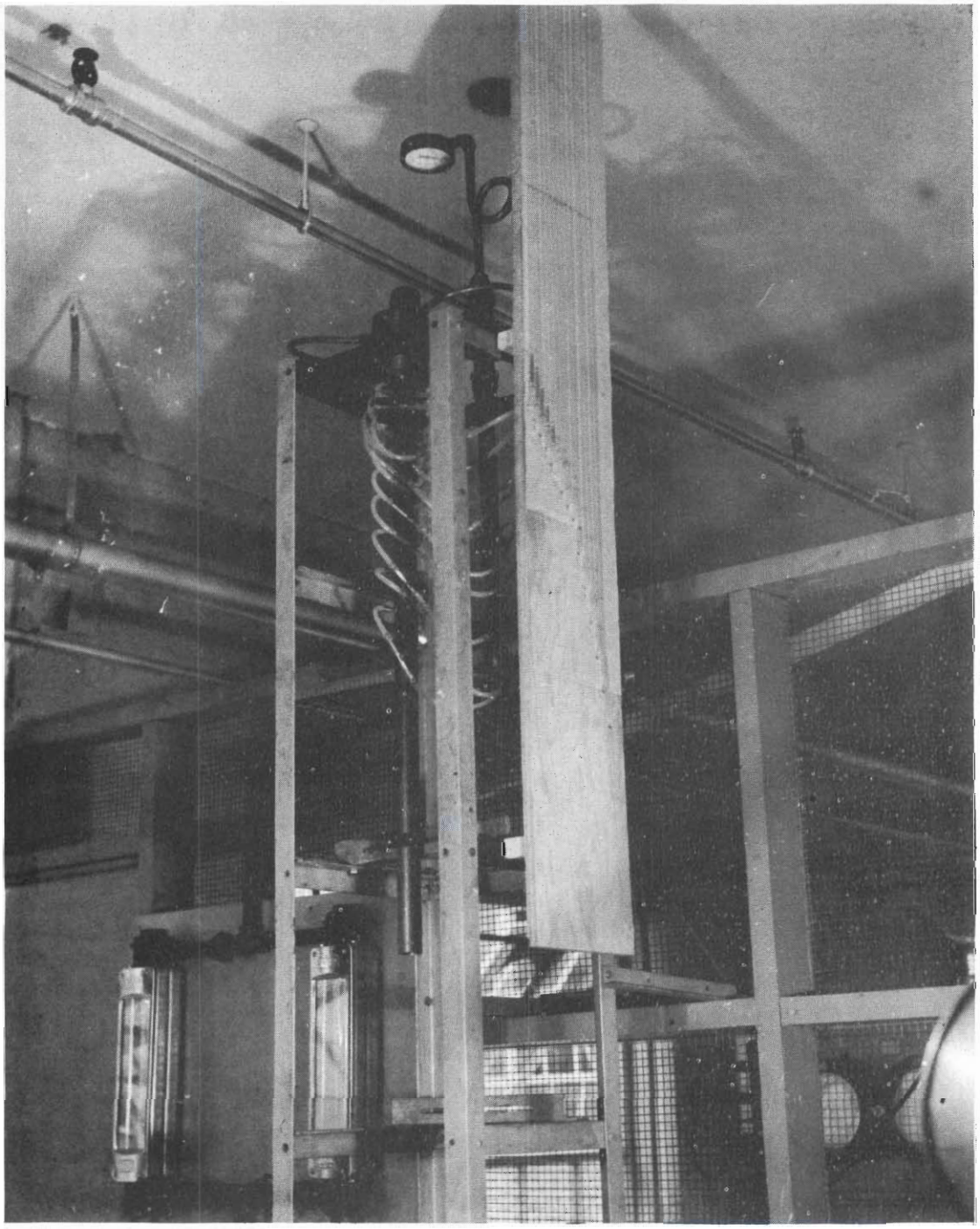

Figure 9. Static Pressure Apparatus.

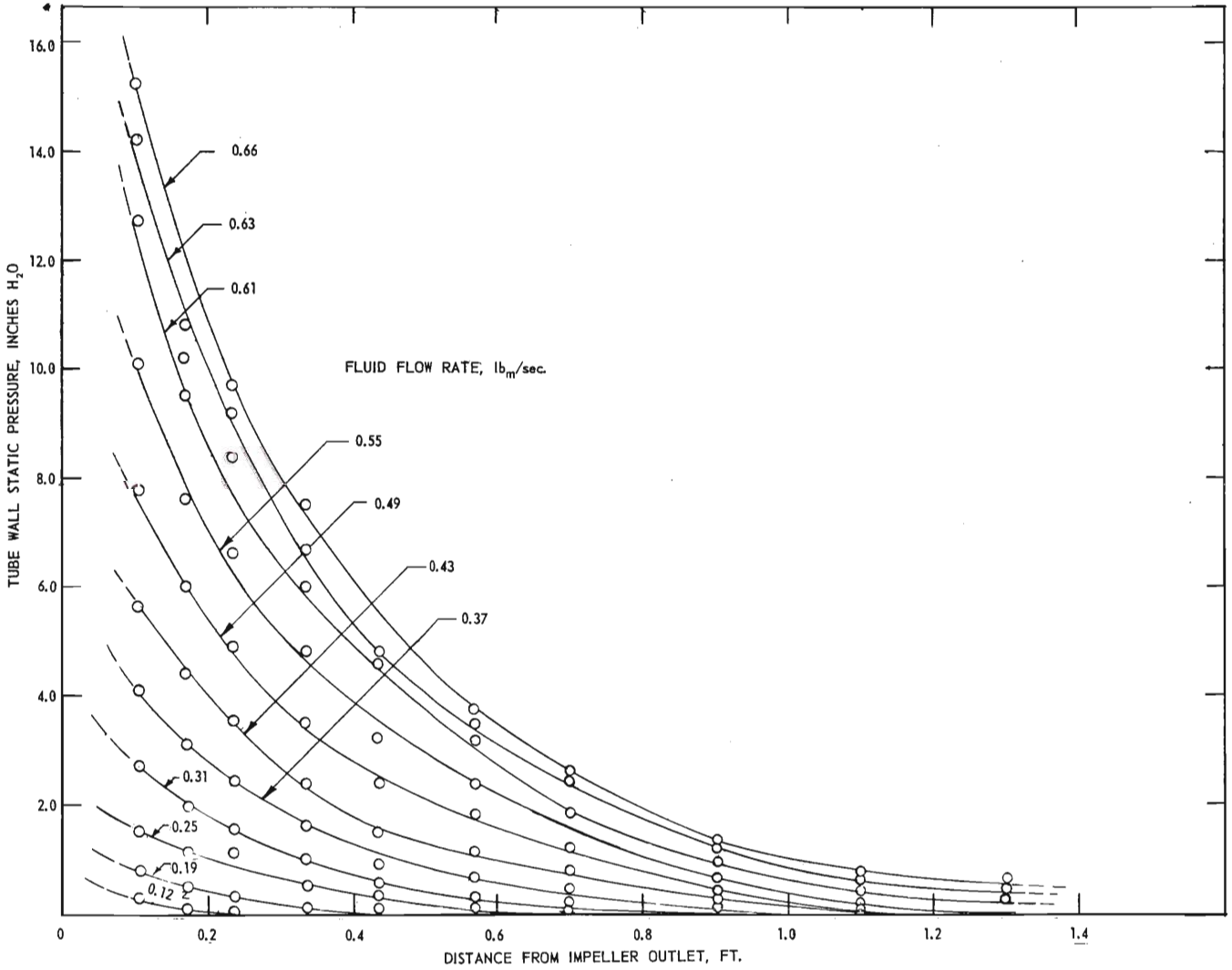

Figure 10. Tube Wall Static Pressure Distributions.

Heat Transfer Studies

Apparatus.—The apparatus used in the heat transfer investigations is shown schematically in Fig. 11, and a photograph of the assembled equipment is shown in Fig. 12. The apparatus was composed of a heat transfer section, a fluid supply section, a fluid preheat and temperature control section, and accessory piping, fittings, and instrumentation.

The heat transfer section is shown schematically in greater detail in Fig. 13. The design of this section was influenced to a considerable extent by that of Orr (14). Principal components in this section included the steam jacket, the steam jacket closure plates, the adiabatic wall separator, and the heat exchange tube. The steam jacket was fabricated from nominal 6-inch iron pipe. A flange two inches in width was welded to each end of the pipe to permit the attachment of the closure plates. The exterior surface of each flange was machined to give an overall jacket length of 29.75 inches. A tangential inlet for admitting steam to the jacket was milled at a distance of six inches from the upper end of the jacket, and a short length of nominal 1-inch iron pipe which had been ground to the proper shape was welded in place over the opening. An outlet for the thermocouples imbedded in the heat exchange tube was provided as follows. First a short length of nominal 2-inch iron pipe was ground to the surface contour of the 6-inch pipe. This was welded in place 15 inches from the upper end of the jacket. The wall of the 6-inch pipe enclosed by the 2-inch pipe was then drilled through. A flange to fit the 2-inch pipe was machined from 3-inch brass rod stock and was threaded to fit. The flange was attached and the threads were

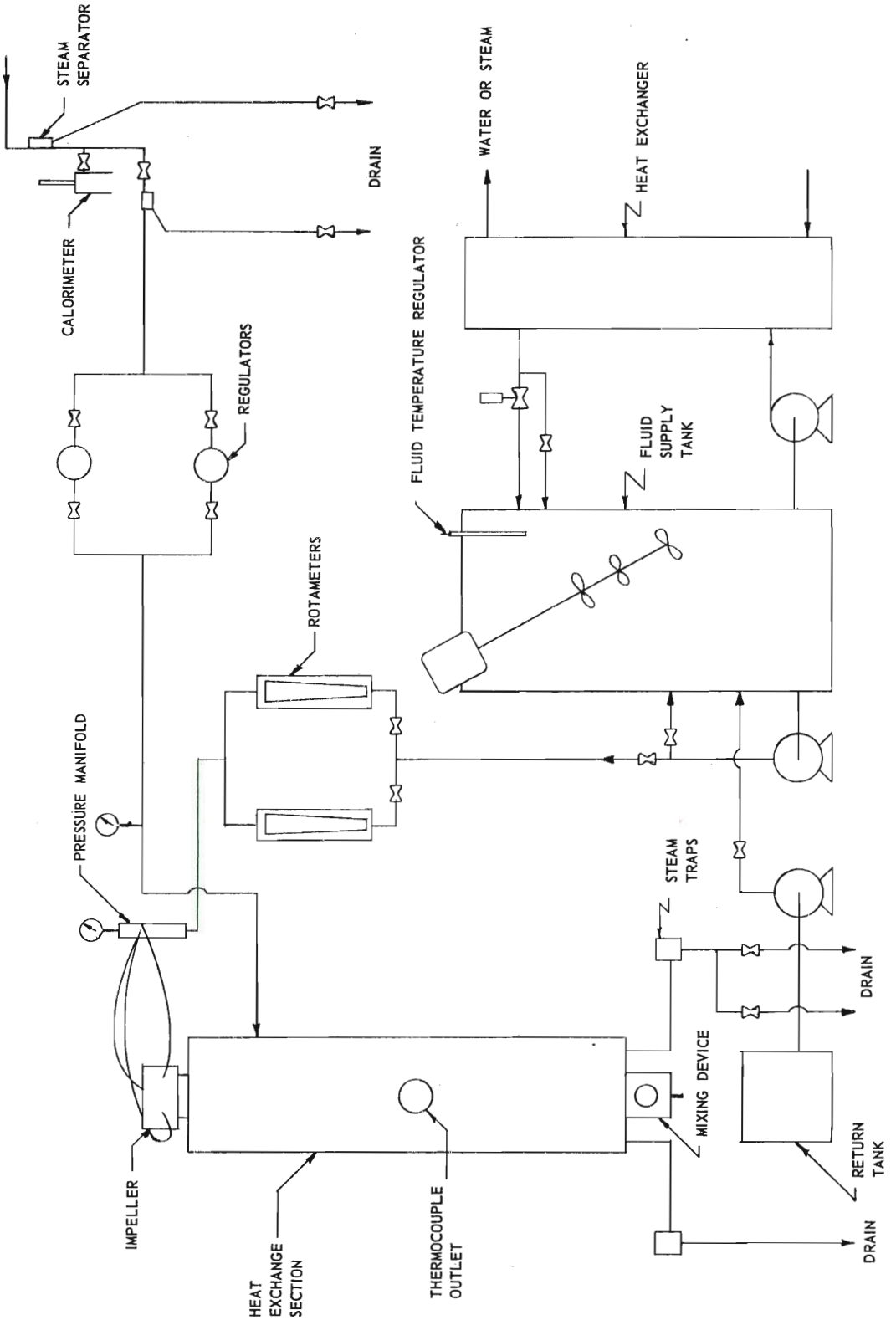

Figure 11. Schematic Drawing of Heat Transfer Apparatus.

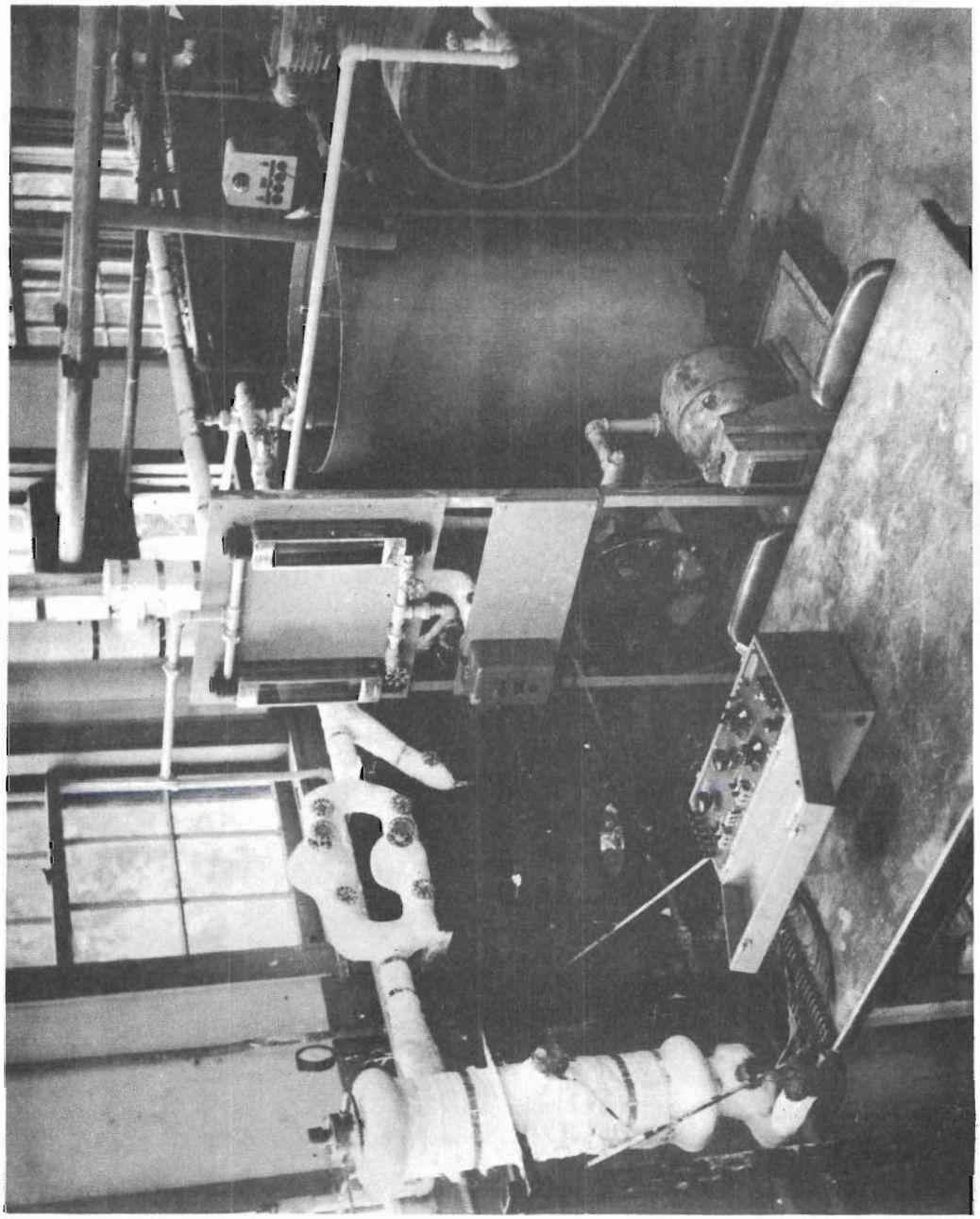

Figure 12. Heat Transfer Apparatus.

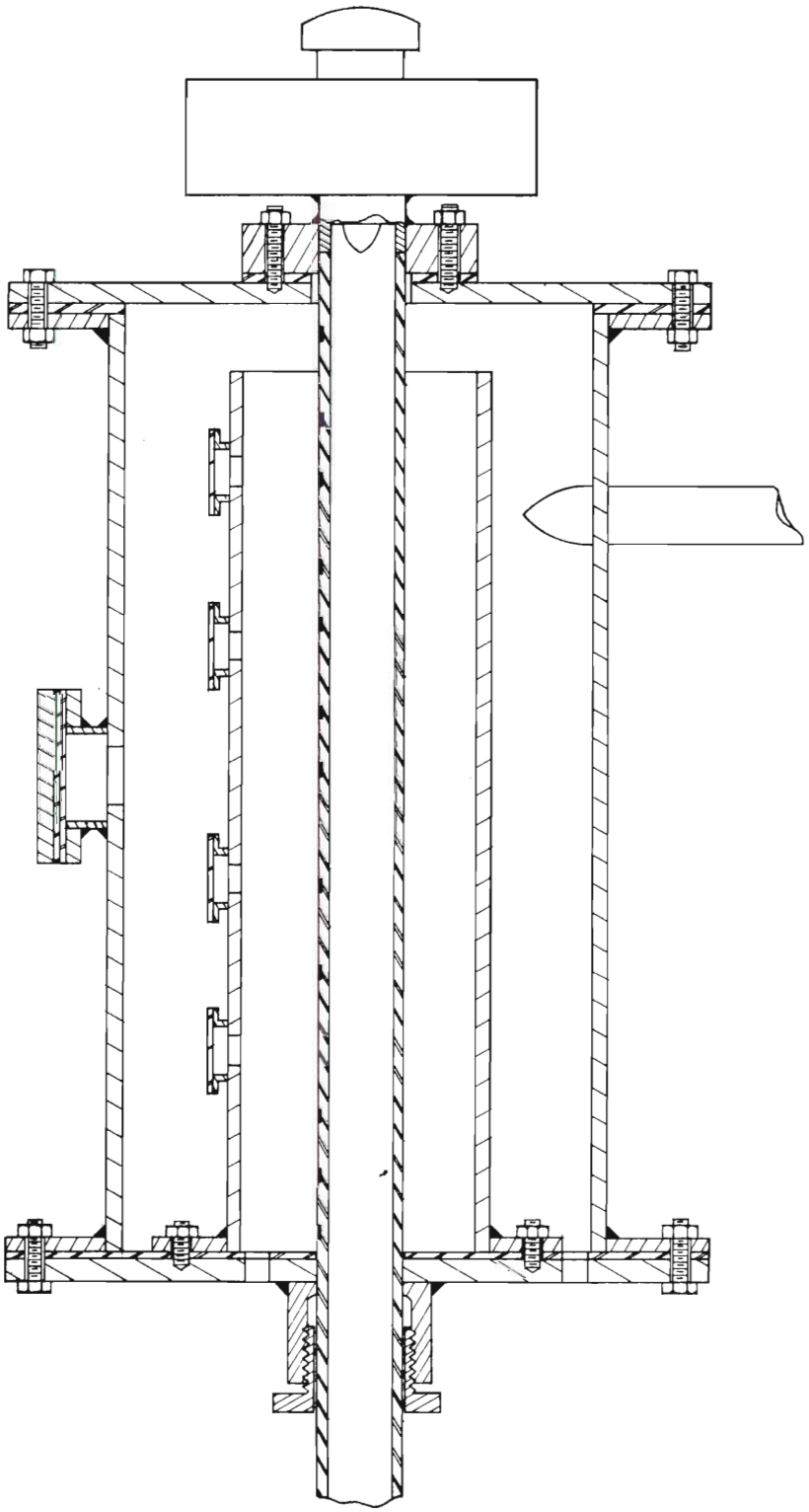

Figure 13. Schematic Drawing of Heat Exchange Section.

sealed by brazing. A flange closure plate for this outlet was prepared using the same rod stock. Matching bolt holes were drilled in the flange and its closure plate to permit sealing with a gasket.

The jacket closure plates were machined from 1/4-inch steel plate to match the flanges on either end of the jacket. An outlet for the heat exchange tube to pass through was bored in each closure plate, and 12 equally spaced bolt holes for attaching the closure plates to the flanges were drilled through the plates and flanges. The upper closure plate had five studs equally spaced on a 2-1/2-inch bolt circle on its outer surface to facilitate the attachment and sealing of the impeller. The lower closure plate had six equally spaced studs on a 4-1/2-inch bolt circle on its inner surface to permit the attachment of the adiabatic wall separator. Two diametrically opposed condensate outlets were drilled and tapped in the lower closure plate for nominal 1/2-inch pipe fittings; this permitted the separation of condensate produced inside and outside the adiabatic wall. A packing gland and packing nut were attached to the outer surface of the lower closure plate to permit sealing of the lower end of the heat exchange section.

The adiabatic wall separator was fabricated from nominal 4-inch iron pipe. The exterior surface of this pipe was machined to give a wall thickness of approximately 1/10-inch. A flange was welded on one end of this pipe and was drilled to match the studs in the lower closure plate. The overall length of the separator was 29 inches. This gave a 3/4-inch space between the upper end of the separator and the upper closure plate for the passage of steam to the heat exchange tube. Three openings

approximately 3/4-inch in diameter were spaced along the separator wall for the thermocouple wires. The openings were provided with covers made from 1/8-inch rubber gasket material to prevent free passage of steam and also to keep the various wires separated.

The heat exchange tube was fabricated from nominal 1-inch copper pipe. To permit the measurement of wall temperatures, thermocouple slots were approximately equally spaced at seven intervals along the tube axis. At a particular axial location, two diametrically opposed slots approximately 1-inch in length, 1/8-inch wide, and 0.100 inch deep were milled in the axial direction. Thermocouples made from No. 20 B.&S. gauge copper-constantan wire were installed in the slots. This was accomplished by carefully peening the bead into the bottom surface of the slot, insulating the wires with glass cloth shields, and covering the slot with a strip of copper. The copper strip was then soldered to the tube with tin, and the excess solder and copper were filed away to the contour of the original tube surface. To facilitate the attachment of the impeller to this heat exchange tube, one end of the tube was machined to the internal diameter of the impeller outlet so that the tube could be inserted to the depth of the plane of the impeller blades.

The assembly of the heat transfer section was accomplished as follows. First, the heat exchange tube was inserted into the impeller outlet and was then soldered in place using tin solder. The heat exchange tube was then passed through the upper closure plate, which had been fitted with a gasket cut from 1/8-inch rubber gasket material. The studs in the upper closure plate were passed through holes in the gasket and

through the holes in the flange on the impeller, nuts and washers were affixed, gasket cement was applied, and the whole was aligned and tightened. Thus, the plane of the blades in the impeller outlet was located 1.0 inch from the upper end of the heated portion of the heat exchange tube.

The upper closure plate was bolted to the corresponding flange on the steam jacket, using gasket cement and 1/8-inch gasket material. The adiabatic wall separator was attached to the lower closure plate. A gasket seal for this device was provided to insure separation of the condensate streams.

Thermocouple wires from the upper end of the heat exchange tube were drawn through the upper passage in the adiabatic wall separator and were passed through the thermocouple outlet in the flange. The adiabatic wall separator was inserted into the jacket for a short distance and the procedure was repeated for thermocouple wires near the middle of the heat exchange tube, and again for thermocouple wires near the lower end of the heat exchange tube. The lower closure plate was bolted to the lower end of the jacket, using a rubber gasket as before. To complete the closure of the heat transfer section, two rubber gaskets were attached to the thermocouple outlet, with liberal quantities of cement on each face, and the thermocouple wires were passed between them. The cover plate for the thermocouple plate was then bolted on, compressing the wires between the gaskets and removing the excess cement, thus making an effective seal. A graphite-coated stem packing was inserted into the packing gland around the projecting end of the heat

exchange tube, and the packing nut was tightened to seal the system. The complete assembly is shown in Fig. 14.

Steam for the heat exchange section was taken from an existing overhead high pressure steam line. Steam to the system first passed through the separator constructed by Orr. Located a few feet beneath the separator on the steam line was a calorimeter (also constructed by Orr) which permitted the determination of the enthalpy of the steam entering the system. This was done by permitting a small flow of steam to enter the calorimeter where it expanded to atmospheric pressure. The temperature of the superheated steam was measured accurately, and the steam enthalpy at the measured temperature and pressure was determined from the tables of Keenan and Keyes (15).

To maintain constant pressure in the heat transfer section, two regulators manufactured by the Crane Company of Chicago, Illinois, were used in parallel. The low pressure regulator had a range of 0 to 30 psig, and the high pressure regulator had a range of 0 to 100 psig. The regulator assembly was connected to the tangential inlet on the heat exchange section. A Bourdon pressure gauge which had been calibrated prior to installation by using a dead weight tester was included in the connecting line to measure the pressure in the steam chest.

The removal of the condensate from the heat exchange section was accomplished using the two condensate openings in the lower closure plate. To each opening a conventional 1/2-inch bucket type steam trap was attached. Flow from the trap attached to the opening for the condensate produced outside the adiabatic wall separator was conducted

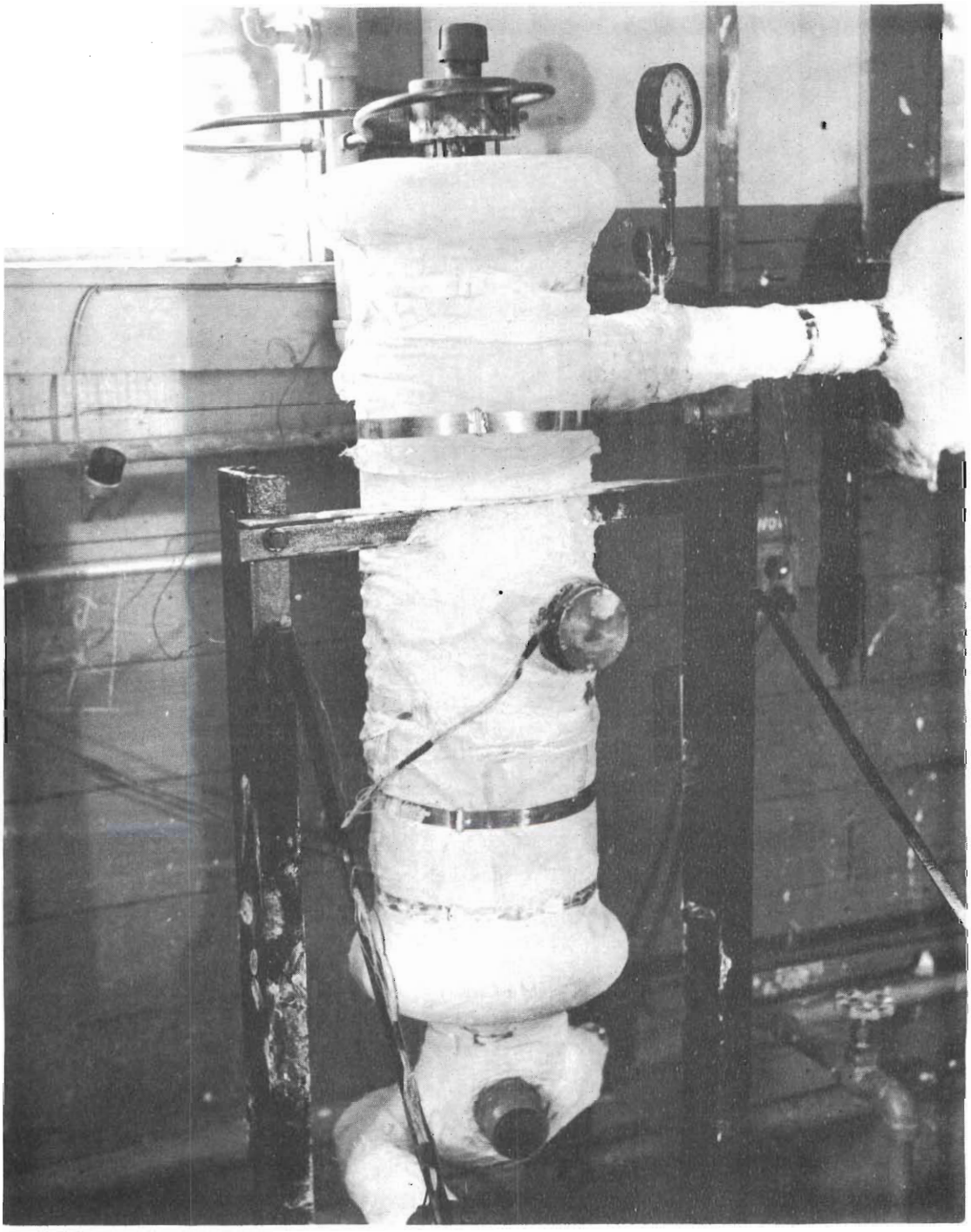

Figure 14. Heat Exchange Section.

directly to the drain, while the outlet from the remaining trap was arranged so that the condensate flow could be diverted to the drain or measured in a cooled, tared receiving flask.

A mixing device to insure uniform outlet temperature measurements was attached to the lower closure plate. This device was fabricated from a nominal 2-inch iron tee, a 1/2-inch to 2-inch pipe bushing, and a short length of 2-inch pipe. A schematic drawing of this device is shown in Fig. 15. Fluid entered the mixing device through one side of the run of the tee, impinging and mixing with the fluid retained by the bushing and thermocouple mounted in the other side of the run. The well-mixed fluid then passed out of the device through the branch of the tee.

After the heat exchange section and its supplementary equipment were assembled, the exposed surfaces of the heated portions of the equipment were insulated with appropriate thicknesses of 85 per cent magnesia pipe insulation.

The accessory equipment used with the copper-constantan thermocouples in the heat transfer section included a Model 8662 potentiometer and a sixteen point thermocouple switch, both manufactured by Leeds & Northrup Company, Philadelphia, Pennsylvania. The reference junction was maintained at 0°C in an ice bath in a Dewar flask.

A probe to measure the fluid film temperature was made from short lengths of 1/8-inch steel rod having threaded ends so that they could be connected, a spacing device to hold the thermocouples in the fluid film, and two copper-constantan thermocouples. The 1/8-inch rod

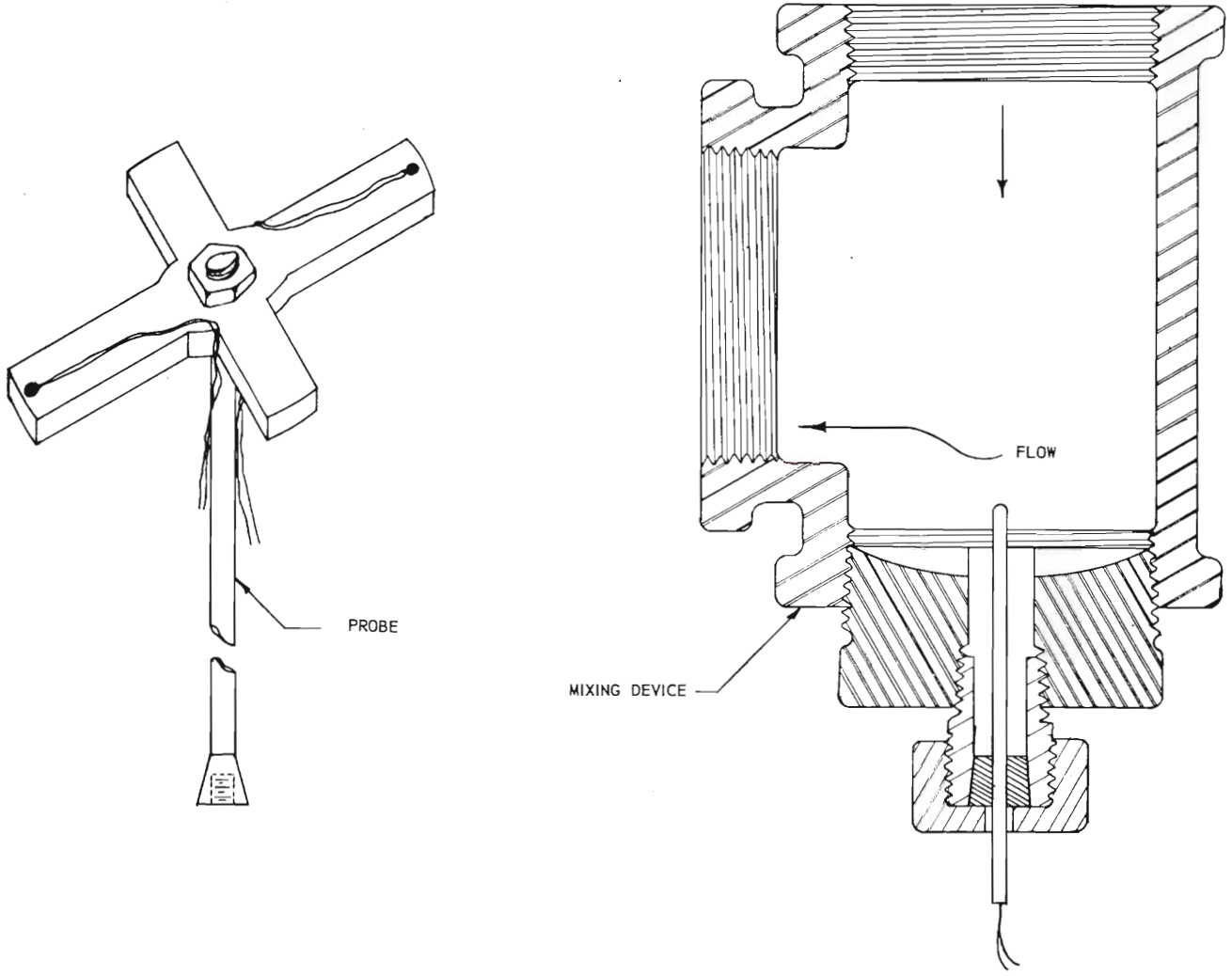

Figure 15. Schematic Drawing of Mixing Section and Thermocouple Probe Assembly.

sections were used to locate the spacing device which surmounted the first section in the heat exchange tube. The spacing device was made from a disk of 1/8-inch stiff sheet rubber. This material was first cut into a disk having a diameter slightly greater than the inside diameter of the heat exchange tube. Four sectors of material were removed, which produced a cruciform shape having four segments approximately 1/8-inch wide. A hole in the center of the cruciform spacer was cut to admit the threaded end of one of the 1/8-inch rods. A washer and nut to retain the spacer were used to complete the assembly of the first segment of the probe.

The thermocouples were attached to two opposite segments on the spacer with cotton thread. The thermocouple beads on the segments were located so that, when the probe was inserted into the tube, they were held in the flowing stream but away from the tube wall. The leads from these two thermocouple junctions extended down the heat exchange tube and passed out the water outlet port in the mixing device. The probe assembly is shown in Fig. 15 also.

To permit location and adjustment of the temperature probe in the heat exchange tube, the mounted thermocouple in the mixing device was removed. The first segment of the thermocouple assembly was placed in the mixing device with the thermocouples and spacer within the heat exchange tube. The threaded end of the first segment projected through the fitting for the mounted thermocouple and was sealed with a packing assembly. Probe location was accomplished by adding the necessary number of segments to the first segment. The mounted

thermocouple which had been removed was carefully relocated in the mixing device.

The thermocouples used for the probe, for measuring the inlet and outlet temperatures, and several other unmounted thermocouples were calibrated using a well-stirred oil bath. Temperature control and heat input in these calibrations were accomplished using a temperature relay manufactured by the Precision Scientific Company of Chicago, Illinois, a 500 watt and a 700 watt resistance heater, and a Precision Scientific Company Microset Thermoregulator. Temperatures were measured using a National Bureau of Standards certified thermometer having a range of -5°C to 105°C in 0.1°C intervals. The standard cell in the Leeds & Northrup Model 8662 potentiometer was calibrated using a low temperature coefficient form standard cell manufactured by the Eppley Laboratories of Newport, Rhode Island.

The fluid supplied to the heat exchange section for the heat transfer investigations was held in a large storage tank having a capacity of approximately 150 gallons. Fluid from the tank was passed through a screened inlet to a rotary pump manufactured by the Viking Pump Company of Cedar Rapids, Iowa. The fluid leaving the pump was separated into two streams; one stream was returned to the storage tank and the other was directed to the flow measuring equipment.

The equipment used to measure the rate of flow of fluid to the impeller assembly was the same set of Fischer-Porter rotameters described in the preceding section. These rotameters were connected in parallel as before and were calibrated in place for ethylene glycol

using the weighing technique used for the calibrations with water. The results from the calibration studies are shown in Fig. 22 in the Appendix.

After leaving the rotameter section, the fluid entered a manifold where the temperature and static pressure of the fluid were measured. For these determinations a calibrated, mounted copper-constantan thermocouple and a Bourdon pressure gauge which had been calibrated on a dead weight tester were used. The manifold was connected to the impeller assembly by three lengths of 1/4-inch copper tubing.

On leaving the impeller, the fluid passed down the vertical heat exchange tube at atmospheric pressure. On leaving the vertical tube, the fluid entered the mixing device and overflowed into a small receiving tank. Fluid from this tank was then returned to the large storage tank by a small centrifugal pump.

The temperature of the fluid in the storage tank was established initially and was continuously regulated by the fluid and temperature control section. Both of these functions were accomplished using a shell-and-tube heat exchanger as shown in Fig. 11. Fluid from the storage tank was pumped to the tube side of the exchanger using a centrifugal pump manufactured by Ingersoll-Rand Company, New York, New York. Fluid leaving the tube side of the heat exchanger was separated into two streams. The first stream was controlled by a manually operated globe valve in the line, and the second stream was controlled by a normally-closed solenoid valve in the line. Both streams returned to the storage tank. The solenoid valve was actuated by a modification of two relays manufactured by the Precision Scientific Company of Chicago,

Illinois. The temperature sensing element for the relays was adapted from a thermoregulator manufactured by the Bronwill Scientific Company in Western Germany.

The temperature of the fluid in the large storage tank was controlled during a series of experimental determinations as follows. First, cooling water was admitted to the shell side of the heat exchanger. The centrifugal pump circulating fluid to the temperature control section was started, and the manually operated valve was adjusted so that the heat input from the heat exchange section was slightly greater than that removed by the shell-and-tube exchanger in the temperature control section. The thermoregulator was then set for the desired temperature and the solenoid relay system was energized. When the tank temperature exceeded the prescribed value, the relay system opened the solenoid valve and the cooling rate was increased. When the tank temperature returned to the desired value, the relay system de-energized the solenoid valve, which closed and reduced the rate of cooling.

To provide a well-mixed fluid in the storage tank, a 1/4 h.p. Lightnin mixer manufactured by the Mixing Equipment Company of Rochester, New York, was used. This mixer utilized a shaft having three propellers for fluid agitation. The rate of rotation was 1750 rpm.

The shell-and-tube heat exchanger was also used in preheating the fluid in the storage tank to a desired temperature range or for deaeration purposes. For this function, the centrifugal pump circulating fluid from the storage tank to the temperature control section was started, with both the manually operated globe valve and the solenoid

valve open. The shell side of the heat exchanger was then exposed to low pressure steam, and the fluid was rapidly heated to the desired level.

Experimental procedure.—The procedure for each complete experiment involved four tests. Each test in a particular experiment differed from the others, as far as possible, only in the location of the temperature probe which was used to measure the fluid film temperature. The first test of an experiment was conducted with the temperature probe entirely removed from the heat exchange tube. The second, third, and fourth tests were conducted so that the temperature of the fluid film at distances of 10-, 18-, and 25-inches from the lower end of the heated length of the tube, respectively, were measured. The total heated length of the tube was 30 inches.

For a particular series of experiments, the procedure was first to fill the fluid supply tank with the fluid to be investigated. The fluid in the tank was then heated to the desired temperature using the shell-and-tube heat exchanger in the temperature control section. Circulation of fluid to this section was stopped and adjustments were made to provide cooling water instead of steam to the shell side of the heat exchanger. The valve to the steam calorimeter was opened, permitting steam to expand in the body of the device.

Flow was then started in the heat exchange section, and the valves controlling the fluid flow rates in the various parts of the system were adjusted. Steam was admitted to the heat exchange section and the

pressure in the steam chest was adjusted to the desired value. The *entire system was then allowed to come to thermal equilibrium. During* this time the rate of flow of the fluid to the shell-and-tube heat exchanger was adjusted with the manually operated globe valve, the tank mixer was started, and the solenoid relay system was energized. Thus, by the time the heat exchange section had come to thermal equilibrium the fluid supply tank had reached an essentially constant temperature.

At this time, recordings of the thermocouple millivolt readings were made. The temperature reading given by the thermometer in the steam calorimeter was determined, the pressures in the steam chest and in the impeller manifold were recorded, and the rotameter scale reading was taken. Then, the rate of steam condensation on the heat exchange tube was determined by weighing the amount of condensate leaving this section in a measured time interval. The condensate for this determination was diverted from its usual direct path to the drain to a tared flask retained in a bucket containing ice and water. Following this measurement, which took several minutes, the thermocouple millivolt readings were again taken and compared with those recorded previously; this was done to insure that the process was operating at equilibrium.

After the completion of the first test in an experiment, the thermocouple probe was inserted into the heat exchange tube to the predetermined distance and the system was again allowed to equilibrate. Since the thermocouple probe did not disturb the flow pattern excessively in any but the last test of an experiment, thermal equilibrium was

achieved much sooner than in the first test of an experiment. The complete series of data readings were again recorded as before, the condensate rate was measured, and the thermocouple millivolt readings were again determined for purposes of comparison. The third and fourth tests in an experiment were conducted in a similar manner. The subsequent experiments in a series were performed following the same general procedure.

Data.—A number of experiments were undertaken using both water and ethylene glycol as the heat transfer fluid. A summary of the recorded data for these experiments is given in Table 1. Numerical values given in this table for the tube wall temperature were obtained by constructing the best straight line through the data points.

Calculation procedure.— The calculation procedures involved in reducing the heat transfer data to a more useful form were concerned with three types of calculated results. These were (1) the calculation of the rate of heat input to the heat exchange tube, (2) the rate of removal of heat by the fluid in the heat exchange tube, and (3) the average local film heat transfer coefficients.

The calculation of the rate of heat input to the heat exchange tube was based on the rate of steam condensation within the adiabatic wall separator. The equation used for this calculation was

$$q_i = 3600\ w_c[h_g - h_f] \qquad (1)$$

where q is the rate of heat transfer, BTU/hr.; w is the weight rate of

Table 1. Experimental Heat Transfer Data.

Experiment Number	Steam Line Pressure (psia)	Exchange Section Pressure (psia)	Barometric Pressure (mm Hg)	Manifold Pressure (psia)	Fluid Flow Rate (lb_m-sec^{-1})	Condensate Flow Rate (lb_m-sec^{-1} x 10^3)	Calorimeter Temperature (°C)	Pipe Wall Temperature Inlet (°F)	Pipe Wall Temperature Outlet (°F)	Fluid Temperature at Stated Distance from Exchange Section Inlet 0.0 in. (°F)	5.0 in. (°F)	12.0 in. (°F)	20.0 in. (°F)	30.0 in. (°F)
1	60.8	18.8	738	17.3	0.12	13.5	115.0	202.5	221.2	104.0	137.5	166.0	188.1	207.5
2	60.6	18.8	737	18.9	0.20	19.6	115.4	197.5	211.1	104.3	129.0	150.2	172.6	198.8
3	61.1	18.8	738	26.5	0.30	25.0	115.3	191.0	220.3	98.9	120.0	137.5	157.5	182.7
4	61.1	18.8	738	37.8	0.40	29.0	114.5	182.2	219.5	101.4	118.0	133.0	149.0	169.5
5	60.1	18.8	735	50.9	0.50	31.0	115.5	174.0	220.9	99.9	115.5	129.3	143.9	161.7
6	59.6	18.8	737	66.0	0.60	32.1	115.0	161.5	219.2	102.6	116.0	128.2	140.7	153.4
7	60.1	18.8	735	75.3	0.70	33.2	116.9	151.8	213.5	103.1	115.1	124.2	135.0	149.7
8	61.9	18.8	738	104.3	0.80	33.9	116.7	142.0	211.5	102.9	114.0	123.8	134.0	147.5
9	61.9	18.8	737	27.0	0.30	17.6	116.6	191.1	217.2	132.4	148.0	160.0	172.5	188.6
10	62.0	18.8	738	36.7	0.40	19.2	115.0	185.2	210.5	133.1	145.0	154.5	165.0	175.0
11	61.1	18.8	737	47.9	0.50	19.4	115.5	177.5	205.0	129.5	141.8	150.7	159.1	169.0
12	61.0	18.8	738	62.0	0.60	21.3	116.8	173.4	205.6	130.6	141.5	149.3	156.0	165.5
13	61.1	18.8	739	78.3	0.70	26.7	115.5	165.3	212.5	134.3	145.2	151.2	159.0	169.5
14	61.1	18.8	738	98.3	0.80	30.0	114.9	159.0	208.8	130.2	138.5	145.5	154.0	164.0
15	61.1	18.8	738	25.5	0.30	15.2	115.0	190.0	215.5	148.8	161.0	169.5	179.5	190.6
16	60.2	18.8	737	36.2	0.40	15.7	114.8	188.8	215.2	149.1	159.5	166.5	174.8	184.8
17	61.1	18.8	738	47.4	0.50	16.9	115.2	185.0	216.5	149.8	158.0	165.1	172.2	181.0
18	61.1	18.8	737	60.9	0.60	16.7	115.0	180.0	218.2	152.1	159.5	166.5	172.5	179.5
19	61.0	18.8	738	76.3	0.70	18.8	115.5	176.0	214.1	151.7	158.5	164.2	171.0	178.2
20	61.1	18.8	737	97.3	0.80	22.1	114.7	172.2	214.0	155.2	159.7	165.6	172.3	181.0
21	61.1	29.3	739	66.0	0.60	33.2	114.8	186.5	243.0	106.2	124.0	134.8	146.9	161.5
22	61.1	29.3	739	81.0	0.70	37.1	115.2	181.0	243.0	110.4	124.5	136.2	147.0	160.3
23	58.6	29.3	737	103.0	0.80	35.4	115.3	170.5	241.0	110.7	126.0	133.6	142.1	153.0
24	58.6	24.3	738	65.5	0.60	31.9	115.0	174.0	220.2	109.6	123.2	133.3	145.0	159.8
25	59.1	24.3	739	81.0	0.70	31.9	116.1	164.8	218.0	111.7	125.8	134.4	144.0	156.1
26	59.6	24.3	738	103.0	0.80	34.1	117.0	156.5	215.0	113.0	124.5	133.2	142.1	153.5
27	60.1	21.5	737	50.9	0.50	30.2	116.5	180.0	217.2	105.1	120.8	131.9	144.7	160.5
28	59.6	21.5	739	65.5	0.60	30.8	115.2	178.9	212.0	107.6	124.0	133.8	144.0	156.1
29	60.6	21.5	739	81.0	0.70	29.3	114.9	171.0	213.0	109.4	122.5	130.0	138.5	149.2
30	59.6	21.5	738	103.3	0.80	35.1	113.8	150.0	220.1	110.1	121.5	130.5	140.7	153.2
31	58.1	18.8	740	98.3	0.80	23.0	110.5	165.5	215.5	147.7	154.2	160.0	166.7	174.5
32	61.1	18.8	740	47.4	0.50	19.9	114.9	181.5	216.0	144.0	154.8	161.7	169.7	179.8
33	61.1	18.8	737	60.9	0.60	17.9	115.9	175.2	217.5	147.6	155.0	160.5	168.5	176.0
34	61.1	18.8	738	76.3	0.70	20.5	115.5	171.4	217.0	145.6	152.6	157.9	163.9	171.4
35	59.6	18.8	737	78.7	0.70	24.1	115.0	157.0	214.5	127.1	137.5	144.0	151.2	160.3
36	61.1	18.8	738	102.3	0.80	25.5	116.2	151.5	212.0	125.5	135.5	141.5	148.5	156.5

(Continued)

Table 1 (Continued). Experimental Heat Transfer Data.

Experiment Number	Steam Line Pressure (psia)	Exchange Section Pressure (psia)	Barometric Pressure (mm Hg)	• Manifold Pressure (psia)	Fluid Flow Rate (lb_m-sec^{-1})	Condensate Flow Rate (lb_m-sec^{-1} x 10^3)	Calorimeter Temperature (°C)	Pipe Wall Temperature Inlet (°F)	Pipe Wall Temperature Outlet (°F)	Fluid Temperature at Stated Distance from Exchange Section Inlet 0.0 in. (°F)	5.0 in. (°F)	12.0 in. (°F)	20.0 in. (°F)	30.0 in. (°F)
37	62.8	18.8	737	36.3	0.21	3.9	113.0	212.4	221.2	93.4	116.2	119.1	121.1	123.6
38	62.6	18.8	738	66.5	0.38	6.3	114.5	204.8	220.4	93.4	112.5	115.5	118.0	121.0
39	62.6	18.8	738	84.6	0.45	7.2	113.8	203.1	222.2	94.9	112.0	115.3	118.1	121.7
40	62.6	18.8	738	105.5	0.58	9.3	114.9	198.4	221.7	100.3	115.4	119.0	122.2	126.2
41	62.6	24.3	737	36.3	0.21	4.3	115.3	222.6	232.6	101.3	125.0	128.2	130.9	133.5
42	61.6	24.3	737	66.6	0.38	7.1	115.1	217.7	233.2	103.3	123.7	127.3	130.4	134.4
43	61.6	24.3	738	84.3	0.45	8.0	115.7	215.7	235.5	103.8	122.5	125.9	128.8	132.2
44	62.1	24.3	739	105.0	0.58	10.6	115.6	210.7	234.1	102.8	120.0	124.1	128.3	133.3
45	60.6	47.3	740	37.5	0.21	5.1	115.6	244.7	257.6	85.5	115.0	118.8	121.5	124.8
46	60.1	47.3	741	67.0	0.38	8.4	115.8	232.0	256.3	94.4	119.8	122.8	126.6	130.8
47	62.1	47.3	740	84.5	0.45	10.2	115.6	231.8	256.3	99.4	123.0	128.3	132.0	136.5
48	60.6	47.3	740	105.0	0.58	12.5	115.6	225.6	259.5	103.7	124.3	129.2	132.5	139.2
49	63.1	18.8	739	28.3	0.21	2.9	115.5	215.5	219.5	143.6	158.1	160.2	162.2	164.2
50	63.1	18.8	740	52.3	0.38	5.6	115.5	210.0	221.6	132.7	146.8	149.4	155.8	155.8
51	62.6	18.8	740	66.0	0.45	7.1	115.7	209.5	219.4	142.5	158.9	161.3	164.1	167.7
52	62.8	18.8	738	82.5	0.58	9.9	115.8	207.2	218.1	145.4	153.6	156.5	158.9	161.9
53	63.1	24.3	738	28.5	0.21	3.2	115.3	223.5	232.0	139.5	156.0	158.3	160.4	162.9
54	62.6	24.3	739	51.5	0.38	5.2	116.4	219.7	232.6	143.4	157.4	160.2	162.2	164.7
55	62.6	24.3	738	66.5	0.45	6.9	115.7	217.1	233.5	135.9	149.8	152.7	156.0	159.9
56	62.6	24.3	738	82.5	0.58	8.1	116.4	215.7	232.2	139.2	151.2	154.6	158.3	161.8
57	61.6	39.3	738	28.3	0.21	4.2	115.7	249.6	261.0	141.4	163.3	166.7	169.3	172.6
58	61.6	39.3	737	47.3	0.38	8.1	116.0	242.7	261.0	147.7	168.7	173.3	176.7	181.1
59	62.1	39.3	738	66.3	0.45	9.1	115.8	239.4	260.2	135.4	153.7	157.6	162.0	167.3
60	62.1	39.3	738	78.5	0.58	10.0	116.4	238.1	260.0	145.4	159.6	163.3	167.5	172.8
61	62.1	24.3	739	26.5	0.21	1.6	116.4	224.7	229.8	190.6	198.2	199.6	200.9	202.2
62	61.6	24.3	739	41.8	0.38	3.5	116.3	227.3	234.4	187.4	195.3	197.1	199.1	201.1
63	61.6	24.3	739	54.5	0.45	3.5	116.7	222.0	231.0	189.2	195.3	196.7	198.4	200.5
64	61.6	24.3	740	69.5	0.58	5.7	116.3	224.0	233.0	186.6	193.5	195.7	198.4	201.5
65	61.6	39.3	740	26.2	0.21	3.1	116.7	250.4	261.5	183.5	198.9	201.4	203.4	205.8
66	62.6	39.3	738	41.8	0.38	5.3	116.7	241.8	261.3	188.3	199.2	202.0	205.3	209.6
67	62.6	39.3	739	54.5	0.45	6.9	115.9	241.8	261.3	184.4	195.2	198.8	202.7	207.7
68	61.6	39.3	739	69.0	0.58	8.2	116.9	242.0	261.0	188.7	197.6	201.0	204.8	209.6
69	62.6	49.3	738	26.1	0.21	4.4	116.7	267.7	275.4	178.5	198.5	201.6	204.1	209.6
70	62.6	49.3	738	42.3	0.38	7.5	116.4	262.1	276.2	185.6	201.2	205.1	209.6	215.2
71	62.6	49.3	738	54.5	0.45	7.9	116.8	255.6	272.2	186.1	199.8	203.5	207.7	213.0
72	62.6	49.3	738	69.5	0.58	10.3	116.9	254.6	276.5	184.1	195.0	199.5	204.8	211.3

flow of fluid, lb_m/sec; h is the enthalpy of the steam, BTU/lb_m; and subscripts i, g, f and c refer to inlet conditions, the gas phase, the liquid phase, and condensate, respectively. The enthalpy of the steam entering the exchange section was determined from the steam calorimeter temperature and the prevailing barometric pressure, using the steam tables of Keenan and Keyes. The enthalpy of the condensate leaving the exchange section was taken to be the enthalpy of saturated water at the pressure prevailing in the exchange section; this value was also taken from the steam tables.

The rate at which heat was removed from the exchange section by the heat transfer fluid was calculated according to the relation

$$q_o = 3600\ w_f\ \bar{c}_p\ [t_o - t_i] \qquad (2)$$

where $\bar{c}_p$ is the specific heat of the fluid evaluated at its arithmetic mean temperature, $BTU/lb_m\text{-}°F$; t is fluid temperature, °F; and subscript o refers to outlet conditions.

Average local film heat transfer coefficients were calculated using the relation

$$3600\ w_f\ \bar{c}_p(\Delta t) = 2\pi r_a(\Delta x)\bar{h}(\Delta T)_m, \qquad (3)$$

where $\bar{h}$ is an average local film heat transfer coefficient, $BTU/hr.\text{-}ft^2\text{-}°F$; (Δt) is the change in the fluid temperature, °F; r is radius, ft.; (Δx) is the length of the heat transfer tube over which the fluid temperature change (Δt) occurred, ft.; $(\Delta T)_m$ is the logarithmic mean temperature difference, °F; and subscript a refers to the inside wall.

The logarithmic mean temperature difference is defined

$$(\Delta T)_m = \frac{(T_i - t_i) - (T_o - t_o)}{ln\left(\frac{T_i - t_i}{T_o - t_o}\right)}, \qquad (4)$$

where T is the inner surface temperature of the heat transfer tube, °F; and subscripts i and o refer to conditions at the inlet and outlet ends of the particular portion of the tube under consideration, respectively. For a number of calculations the logarithmic mean temperature difference was replaced by the arithmetic mean temperature difference since the temperature differences at the inlet and outlet section were of similar magnitude.

Four average local film heat transfer coefficients were determined from each experiment. The first of these, $\bar{h}_1$, was computed for the first five inches of the heated tube as measured from the upstream end. The second was computed for the next seven inches, the third was computed for the following eight inches, and the fourth was computed for the remaining ten inches; these were designated $\bar{h}_2$, $\bar{h}_3$, and $\bar{h}_4$, respectively.

The measured pipe wall temperatures were corrected to the pipe inner surface temperature using the one-dimensional heat conduction equation

$$q = -2\pi r(\Delta x)\, k\left(\frac{dT}{dr}\right), \qquad (5)$$

where k is thermal conductivity, BTU/hr-ft-°F. Integration of the above equation gave

$$q = \frac{2\pi k(\Delta x)(T_a - T_b)}{\ln\left(\frac{r_b}{r_a}\right)}, \qquad (6)$$

where subscripts a and b refer to the inside radius and to the radius of the thermocouple plane, respectively.

For 1-inch nominal copper pipe the inside radius is 0.5315 inches. The radius to the plane of the thermocouples was 0.5575 inches. The thermal conductivity of the copper pipe was taken to be 217.6 BTU/hr-ft-°F. Substitution of these constants into Eq. 6 and simplifying gave

$$(T_b - T_a) = 3.493 \times 10^{-5} \frac{q}{\Delta x}, \qquad (7)$$

where $(T_b - T_a)$ is the temperature correction, °F, to be subtracted from the measured pipe wall temperatures.

Sample calculation.—To illustrate the calculation procedure followed in reducing the heat transfer data a typical investigation, Experiment 14, was chosen. The data used in this calculation are given in Table 1.

The heat input to the system was computed using Eq. 1. The enthalpy of the steam supplied to the heat exchange section was obtained from steam tables using the calorimeter data; for an atmospheric pressure of 14.25 psia and a calorimeter temperature of 238.8°F this value is 1163.6 BTU/lb_m. The enthalpy of the condensate leaving the exchange section was determined for saturated liquid at a pressure of 18.8 psia; this value was 192.6 BTU/lb_m. Thus, the heat entering the exchange section was

$$q_i = (3600)(0.030)(1163.6 - 192.6), \text{ or}$$

$$q_i = 1.949 \times 10^5 \text{ BTU/hr.}$$

The heat removed from the heat exchange section by the heat transfer fluid was computed using Eq. 2.

$$q_o = (0.80)(3600)(1.00)(164.0 - 130.2), \text{ or}$$

$$q_o = 9.73 \times 10^4 \text{ BTU/hr.}$$

To facilitate the calculation of the local heat transfer coefficients, figures giving temperature distributions in the fluid and in the pipe wall as a function of distance down the heated tube length were prepared for each experiment. Fig. 16 gives the distributions used in Experiment 14. Four local film heat transfer coefficients were calculated using Eq. 3 in conjunction with Eq. 4. The first film heat transfer coefficient, $\bar{h}_1$, was computed for the first five inches of the heated tube. The temperature correction to be applied to the pipe wall temperatures was computed from Eq. 7, as follows:

$$(T_b - T_a) = \frac{(3.493 \times 10^{-5})(0.80)(3600)(1.00)(138.5 - 130.2)}{\left(\frac{5}{12}\right)} \text{ or}$$

$$(T_b - T_a) = 2.01°\text{F.}$$

The measured pipe wall inlet and outlet temperatures were 159.0°F and 167.3°F, respectively. The fluid film temperatures at the inlet and outlet were 130.2°F and 138.5°F, respectively. The mean temperature

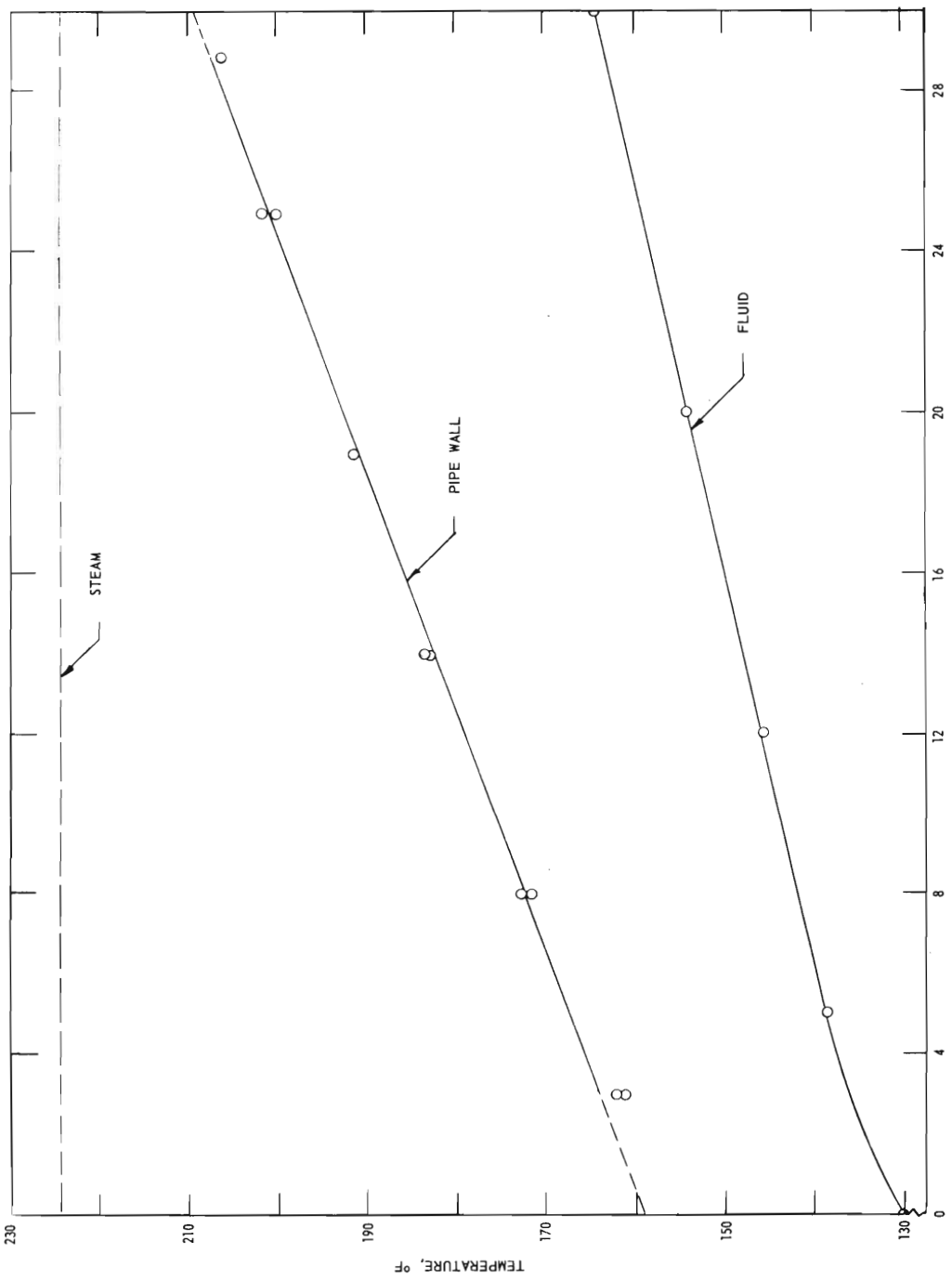

Figure 16. Temperature Distributions for Experiment 14.

difference was

$$(\Delta T)_m = \frac{(159.0 - 2.01 - 130.2) + (167.3 - 2.01 - 138.5)}{2}, \text{ or}$$

$$(\Delta T)_m = 26.79°F.$$

The average local film heat transfer coefficient for this section was computed from Eq. 3.

$$\bar{h}_1 = \frac{(3600)(0.80)(1.00)(138.5 - 130.2)}{2\pi\left(\frac{0.5315}{12}\right)\left(\frac{5}{12}\right)(26.79)}, \text{ or}$$

$$\bar{h}_1 = 7700 \text{ BTU/hr-ft}^2\text{-°F}.$$

The second average film heat transfer coefficient was calculated in a similar manner for the following seven inches of heated tube length. The measured pipe wall inlet and outlet temperatures were 167.3°F and 178.9°F, respectively; and the fluid film temperatures at the inlet and outlet were 138.5°F and 145.5°F. The pipe wall temperature correction was, from Eq. 7,

$$(T_b - T_a)_1 = \frac{(3.493 \times 10^{-5})(0.80)(3600)(1.00)(145.5 - 138.5)}{\left(\frac{7}{12}\right)}, \text{ or}$$

$$(T_b - T_a)_1 = 1.21°F.$$

The mean temperature difference was

$$(\Delta T)_m = \frac{(178.9 - 1.21 - 145.5) + (167.3 - 1.21 - 138.5)}{2}, \text{ or}$$

$$(\Delta T)_m = 29.89°F.$$

The local film heat transfer coefficient for the second section was

$$\bar{h}_2 = \frac{(3600)(0.80)(1.00)(145.5 - 138.5)}{2\pi\left(\frac{0.5315}{12}\right)\left(\frac{7}{12}\right)(29.89)}$$

$$\bar{h}_2 = 4150 \text{ BTU/hr-ft}^2\text{-°F.}$$

The third average film heat transfer coefficient was computed for the following eight inches of heated tube. The pipe wall temperature correction was

$$(T_b - T_a) = \frac{(3.493 \times 10^{-5})(0.80)(1.00)(154.0 - 145.5)}{\left(\frac{8}{12}\right)}, \text{ or}$$

$$(T_b - T_a) = 1.29°F.$$

The mean temperature difference was

$$(\Delta T)_m = \frac{(192.2 - 1.29 - 154.0) + (178.9 - 1.29 - 145.5)}{2}, \text{ or}$$

$$(\Delta T)_m = 34.50°F.$$

The average local film heat transfer coefficient for the third length was

$$\bar{h}_3 = \frac{(3600)(0.80)(1.00)(154.0 - 145.5)}{2\pi\left(\frac{0.5315}{12}\right)\left(\frac{8}{12}\right)(34.50)}, \text{ or}$$

$$\bar{h}_3 = 3820/\text{hr-ft}^2\text{-°F.}$$

The fourth average local film heat transfer coefficient was computed for the remaining ten inches of heated tube. The pipe wall correction was

$$(T_b - T_a) = \frac{3.493 \times 10^{-5})(3600)(0.80)(1.00)(164.0 - 154.0)}{\left(\frac{10}{12}\right)}, \text{ or}$$

$$(T_b - T_a) = 1.21°F.$$

The mean temperature difference was

$$(\Delta T)_m = \frac{(208.8 - 1.21 - 164.0) + (192.2 - 1.21 - 154.0)}{2}, \text{ or}$$

$$(\Delta T)_m = 40.3°F.$$

The average local film heat transfer coefficient for the fourth section was

$$\bar{h}_4 = \frac{(3600)(0.80)(1.00)(164.0 - 154.0)}{2\pi\left(\frac{0.5315}{12}\right)\left(\frac{10}{12}\right)(40.3)}, \text{ or}$$

$$\bar{h}_4 = 3070 \text{ BTU/hr-ft}^2\text{-°F}.$$

Calculated results.—The calculated results for all of the heat transfer experiments are given in Table 2. The data for the specific heat of water were taken from Perry (16), and the data for the specific heat of ethylene glycol were taken from publications (17, 18) by the manufacturer.

Table 2. Calculated Heat Transfer Data.

Experiment	Heat into Exchange Section	Heat Out of Exchange Section	Local Film Heat Transfer Coefficients and Mean Temperature Differences							
			First Section		Second Section		Third Section		Fourth Section	
			$\overline{h_1}$	$(\Delta T_m)_1$	$\overline{h_2}$	$(\Delta T_m)_2$	$\overline{h_3}$	$(\Delta T_m)_3$	$\overline{h_4}$	$(\Delta T_m)_4$
	(BTU-sec^{-1})	(BTU-sec^{-1})	(BTU-hr^{-1}-ft^{-2}-°F^{-1})		(BTU-hr^{-1}-ft^{-2}-°F^{-1})		(BTU-hr^{-1}-ft^{-2}-°F^{-1})		(BTU-hr^{-1}-ft^{-2}-°F^{-1})	
1	13.1	12.4	1525	81.5	1395	54.5	1505	34.1	1880	19.2
2	19.0	18.9	1925	79.8	1560	60.4	2080	41.8	3970	20.5
3	24.3	25.1	2410	81.5	1690	68.9	2030	57.4	2670	44.0
4	28.2	27.2	2810	73.5	2015	66.1	2075	59.9	2420	52.8
5	30.1	30.9	3575	67.8	2420	63.4	2320	61.1	2350	59.0
6	31.2	30.4	4580	54.6	2995	54.2	2575	56.5	1930	61.4
7	32.2	32.6	5750	45.4	2930	48.3	2720	53.8	2705	59.3
8	32.9	35.7	7510	36.7	4240	41.1	3245	48.7	2900	58.0
9	17.1	16.9	2825	51.5	1825	43.7	1910	38.1	2375	31.6
10	18.6	16.8	3165	46.8	2030	41.5	2165	37.6	1760	35.4
11	18.8	19.7	4520	42.3	2590	38.1	2230	36.5	2165	35.6
12	20.7	21.0	5330	38.1	2865	36.2	2095	37.2	2300	38.6
13	25.9	24.5	8750	27.1	3180	29.3	3125	33.9	2930	39.0
14	29.1	27.0	7710	26.8	4160	29.9	3830	34.5	3090	40.3
15	14.8	12.6	3140	36.2	1805	31.4	2040	28.5	2015	25.7
16	15.3	14.3	3560	35.4	1900	32.7	2000	32.2	2015	30.9
17	16.4	15.6	3905	32.6	2500	31.6	2120	32.5	2015	34.0
18	16.2	16.4	5280	26.1	3460	27.0	2310	30.2	1855	35.2
19	18.3	18.6	6510	22.7	3600	24.6	3320	27.8	2415	32.4
20	21.4	20.6	6500	17.2	5140	20.4	4250	24.5	3700	29.3
21	31.4	33.2	4540	73.0	2005	71.8	1890	74.5	1740	78.2
22	35.2	34.9	4660	65.7	2740	66.4	2060	71.1	1860	77.7
23	33.5	33.8	7000	54.3	2275	59.4	1915	69.0	1690	80.3
24	30.6	30.1	4300	59.0	2095	57.8	2340	58.2	2345	58.8

(Continued)

Table 2 (Continued). Calculated Heat Transfer Data.

Experiment	Heat into Exchange Section	Heat Out of Exchange Section	Local Film Heat Transfer Coefficients and Mean Temperature Differences							
			First Section		Second Section		Third Section		Fourth Section	
	$\overline{q}$	$\overline{q}$	$\overline{h_1}$	$(\Delta T_m)_1$	$\overline{h_2}$	$(\Delta T_m)_2$	$\overline{h_3}$	$(\Delta T_m)_3$	$\overline{h_4}$	$(\Delta T_m)_4$
	(BTU-sec^{-1})	(BTU-sec^{-1})	(BTU-hr^{-1}-ft^{-2}-°F^{-1})		(BTU-hr^{-1}-ft^{-2}-°F^{-1})		(BTU-hr^{-1}-ft^{-2}-°F^{-1})		(BTU-hr^{-1}-ft^{-2}-°F^{-1})	
25	30.6	31.0	6450	47.5	2755	48.5	2470	52.7	2280	57.8
26	32.6	32.4	7160	39.9	3870	42.8	2835	48.8	2525	56.1
27	29.1	27.6	3600	67.8	1955	63.0	2060	60.4	2145	57.2
28	29.7	29.1	4870	62.7	2245	58.1	2100	56.4	2050	55.0
29	28.2	27.8	5110	55.8	2100	55.6	1985	58.1	1905	61.1
30	33.8	34.4	7600	37.3	3780	42.3	3140	50.3	2600	59.8
31	22.4	21.4	9450	17.1	4760	21.6	3740	27.8	5190	34.8
32	19.3	17.9	5020	33.4	2370	32.3	2325	33.4	1670	34.9
33	17.4	17.6	5280	26.1	2555	28.7	2875	32.4	1865	37.5
34	19.9	18.0	6210	24.5	2930	28.1	2420	33.7	2000	40.7
35	23.4	23.2	8280	27.3	3195	31.6	2505	39.1	2055	48.3
36	24.8	24.8	10500	23.6	3660	29.1	2880	37.7	2080	47.8
37	3.79	3.74	806	107.0	81	97.1	49	97.0	49	97.5
38	6.12	6.18	1345	96.0	161	90.1	110	96.3	104	98.1
39	7.00	7.11	1490	99.5	206	94.6	151	96.5	151	99.0
40	9.04	8.94	1770	91.5	314	87.5	238	90.0	230	93.4
41	4.12	4.03	828	108.4	88	98.8	65	98.3	50	98.7
42	6.80	7.04	1325	103.0	179	96.5	134	97.0	137	98.1
43	7.65	7.60	1510	103.1	208	96.9	153	98.8	139	101.6
44	10.15	10.51	1865	98.9	330	93.0	291	96.7	269	99.1
45	4.68	4.91	780	143.4	73	131.4	49	131.3	47	132.2
46	7.21	8.23	1375	123.8	122	117.4	132	120.1	111	123.5
47	9.35	9.91	1615	120.5	279	112.9	168	114.5	160	117.7
48	11.45	12.25	1970	112.3	346	108.3	196	112.7	306	117.6

(Continued)

Table 2 (Continued). Calculated Heat Transfer Data.

Experiment	Heat into Exchange Section	Heat Out of Exchange Section	Local Film Heat Transfer Coefficients and Mean Temperature Differences							
			First Section		Second Section		Third Section		Fourth Section	
			$\overline{h_1}$	$(\Delta T_m)_1$	$\overline{h_2}$	$(\Delta T_m)_2$	$\overline{h_3}$	$(\Delta T_m)_3$	$\overline{h_4}$	$(\Delta T_m)_4$
	(BTU-sec^{-1})	(BTU-sec^{-1})	(BTU-hr^{-1}-ft^{-2}-°F^{-1})		(BTU-hr^{-1}-ft^{-2}-°F^{-1})		(BTU-hr^{-1}-ft^{-2}-°F^{-1})		(BTU-hr^{-1}-ft^{-2}-°F^{-1})	
49	2.82	2.68	882	64.5	102	57.4	87	56.5	70	55.7
50	5.44	5.35	1460	70.2	207	65.1	195	65.2	200	65.5
51	6.89	6.97	2420	57.8	281	52.1	287	52.0	298	51.7
52	5.73	5.89	1565	57.9	415	55.1	302	55.1	299	55.7
53	3.07	3.02	859	75.3	94	68.7	75	68.7	71	68.9
54	4.98	5.01	1465	69.5	218	64.5	139	65.3	136	66.9
55	6.61	6.65	1600	74.2	252	70.3	247	71.3	229	72.6
56	7.75	8.05	1890	70.2	400	67.2	378	67.7	281	69.2
57	3.90	4.06	887	96.6	98	87.7	73	87.6	73	88.0
58	7.53	7.93	1820	83.9	313	76.7	200	77.2	203	78.8
59	8.45	8.83	1655	94.3	266	89.5	259	90.5	247	91.9
60	9.30	9.85	1825	86.1	354	82.6	356	84.1	342	85.9
61	1.53	1.57	1020	30.3	150	27.2	122	27.1	96	27.4
62	3.35	3.33	1665	35.8	290	33.5	282	33.4	229	33.0
63	3.35	3.26	1840	29.7	315	28.4	327	29.1	314	29.9
64	5.45	5.58	2455	32.4	591	30.6	606	32.0	562	31.8
65	2.88	3.02	1110	56.9	137	53.3	95	53.9	90	54.5
66	4.93	5.18	1700	48.4	324	46.7	322	48.4	324	50.4
67	6.40	6.75	1820	53.1	461	50.1	425	51.2	425	52.6
68	7.62	7.95	1965	50.4	585	47.8	558	49.0	550	50.3
69	4.03	4.21	1032	78.8	114	69.7	92	68.9	167	67.2
70	6.86	7.25	1700	69.4	335	62.7	341	62.0	345	61.2
71	7.24	7.81	1950	62.7	406	58.5	401	58.6	404	58.9
72	9.42	10.18	1900	66.3	586	63.2	596	63.7	582	64.4

CHAPTER III

ANALYSIS OF RESULTS

Fluid Flow Studies

Impeller performance.—A striking feature of the operation of the fluid flow system was the energy required to produce the swirling motion. The principal resistance to flow in the system was the impeller assembly. The static pressure decrease which was obtained experimentally was not anticipated when the assembly was being designed, and thus no attempt was made to minimize the losses.

The considerable decrease in static pressure from the fluid manifold to the impeller outlet can be attributed to entrance losses, exit losses, friction losses and an increase in the kinetic energy of the fluid. To permit an estimate of the magnitude of the static pressure decrease due to friction and abrupt area changes, the mechanical energy equation was written in the form

$$\frac{\overline{P}_i}{\rho} + \frac{\overline{U}_i^2}{2g_c} = \frac{\overline{P}_o}{\rho} + \frac{\overline{U}_o^2}{2g_c} + \Delta H_f, \qquad (8)$$

where P is static pressure, lbf/ft^2; ρ is density, lbm/ft^3; U is velocity, ft/sec; ΔH_f is the fluid heat decrease due to all apparent friction losses, ft-lbf/lbm; and the bar denotes suitable averaged conditions. The effect of compressibility and changes in elevation were neglected.

The system over which Eq. 8 was applied included the fluid

manifold, the copper tubing connections between the manifold and the impeller assembly, and the impeller assembly. Inlet conditions for the system were taken at the plane of the static pressure taps in the fluid manifold. Outlet conditions for the system were taken at the plane of the outlet of the impeller channels.

Numerical evaluation of the velocity terms appearing in Eq. 8 was accomplished using the continuity equation for incompressible flow:

$$w = \rho \int_{o}^{A_n} u \, dA_n \tag{9}$$

where u is local velocity, ft/sec; A is area, ft^2; and subscript n denotes direction normal to A. For simplicity the integral appearing in Eq. 9 for the inlet plane of the system was defined

$$\int_{o}^{A_n} u \, dA_n = \overline{U}_i A_i, \tag{10}$$

where A_i is the cross-sectional area of the fluid manifold. From the dimensions of the system,

$$A_i = \frac{\pi}{4} \left(\frac{1.61}{12} \right)^2 = 1.414 \times 10^{-2} \text{ ft}^2.$$

Combining the above numerical value with Eqs. 9 and 10 gave

$$\overline{U}_i = 70.7 \frac{w}{\rho} \ . \tag{11}$$

Thus, by using Eq. 11 in conjunction with the measured values of static

pressure and mass flow rate the energy input to the system as defined by the left member of Eq. 8 was completely described.

The static pressure term and the kinetic energy term appearing in the right member of Eq. 8 were not so easily obtained. In any one of the three channels of the impeller the direction of the flow was along streamlines bounded by the channel walls. Accordingly, the area normal to the direction of flow was also the area normal to the channel walls. The differential area dA'_n normal to one channel, as shown in Fig. 17, was given by

$$dA'_n = \cos \alpha \, dA' = \Delta z \cos \alpha \, dr, \qquad (12)$$

where α is the angle between the direction of the approaching fluid and the outward drawn normal of the differential element dA' of the r-z plane in the channel, and Δz is the distance between channel walls measured parallel to the axis of the impeller, ft. The numerical value of the angle α was obtained from the machining dimensions as follows. From the geometrical configuration shown in Fig. 17,

$$\cos \alpha = \frac{r d\theta}{[(r d\theta)^2 + (dz)^2]^{1/2}} . \qquad (13)$$

Since the impeller was triple threaded with square threads at the rate of three threads per inch, the relationship between angular position and axial position was specified.

$$\frac{d\theta}{dz} = \left(3 \frac{\text{rev.}}{\text{in.}}\right)\left(2\pi \frac{\text{rad.}}{\text{rev.}}\right)\left(12 \frac{\text{in.}}{\text{ft}}\right) = 72\pi \frac{\text{rad.}}{\text{ft}} . \qquad (14)$$

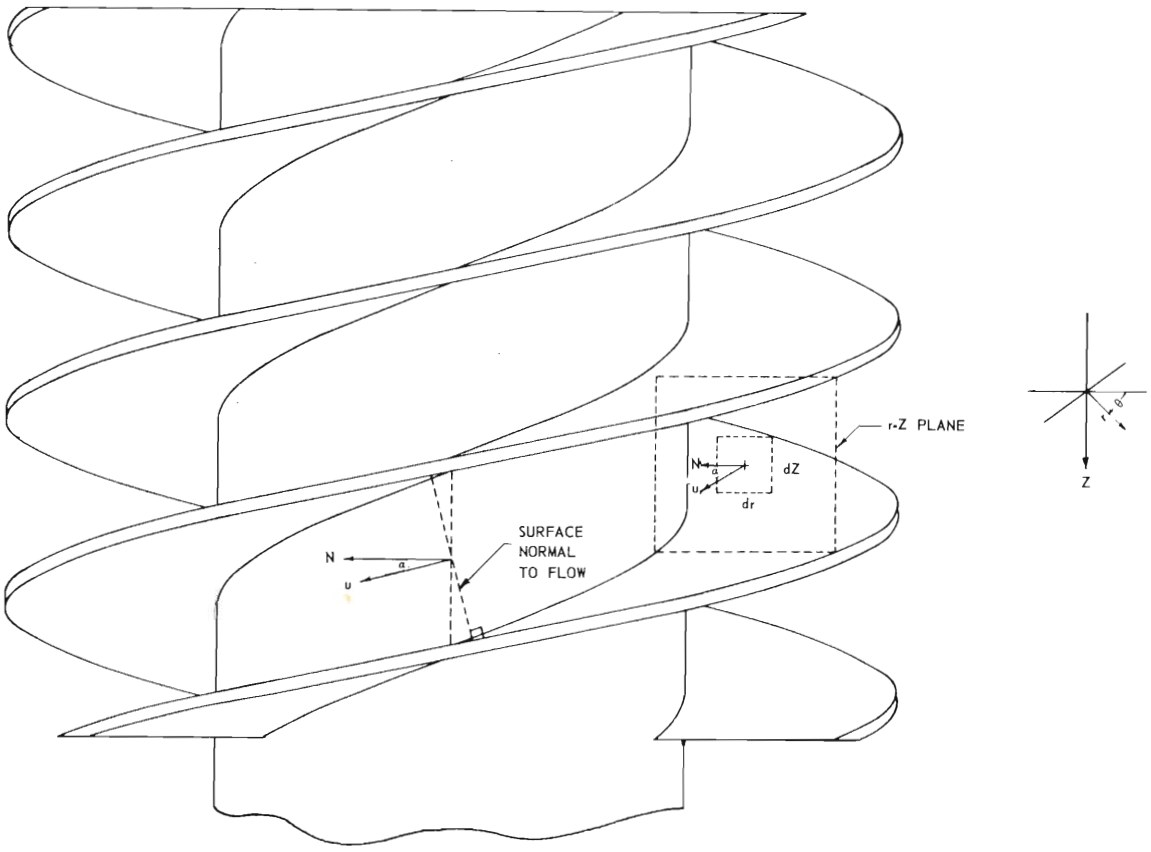

Figure 17. Schematic Drawing of Impeller.

Substitution of Eq. 14 into Eq. 13 and simplifying gave

$$\cos \alpha = \frac{72\pi r}{[(72\pi r)^2 + 1]^{1/2}} . \tag{15}$$

Substitution of Eq. 15 into Eq. 12 gave

$$dA'_n = \frac{72\pi \Delta z \, r dr}{[(72\pi r)^2 + 1]^{1/2}} . \tag{16}$$

Integration of Eq. 16 for constant Δz gave

$$A'_n = \frac{\Delta z}{72\pi}\left\{[(72\pi r_2)^2 + 1]^{1/2} - [(72\pi r_1)^2 + 1]^{1/2}\right\}, \tag{17}$$

where subscripts 1 and 2 refer to the inside and the outside radius of the impeller channel, ft, respectively. Substitution of the numerical values $r_1 = 3.125 \times 10^{-2}$ ft, $r_2 = 4.429 \times 10^{-2}$ ft, and $\Delta z = 6.5 \times 10^{-3}$ ft into Eq. 17 and simplifying gave

$$A'_n = 8.418 \times 10^{-5} \text{ ft}^2. \tag{18}$$

The total area normal to the direction of flow at the impeller outlet was given by

$$A_n = 3A'_n = 25.254 \times 10^{-5} \text{ ft}^2. \tag{19}$$

The kinetic energy term appearing in the right member of Eq. 8 may be evaluated from the definition

$$\frac{\overline{U}_o^2}{2g_c} = \frac{3(U_o')^2}{2g_c} = \frac{3}{\left(\frac{2g_c w}{3\rho}\right)} \int_o^{A'_n} u^3 dA'_n , \qquad (20)$$

provided the velocity distribution in the channel is known.

Three types of velocity profiles analogous to those studied by Wattendorf were considered in the calculation of the fluid energy leaving the outlet plane of the impeller. These were

Case 1. $u_z = C_1$, (21)

$u_\theta = C_2$, (22)

and thus $u = [(C_1)^2 + (C_2)^2]^{1/2}$. (23)

Case 2. $u_z = C_1$, (24)

$u_\theta = C_3 r$, (25)

and thus $u = [(C_1)^2 + (C_3 r)^2]^{1/2}$. (26)

Case 3. $u_z = C_1$, (27)

$u_\theta = C_4\left(\frac{1}{r}\right)$, (28)

and thus $u = \left[(C_1)^2 + \left(\frac{C_4}{r}\right)^2\right]^{1/2}$. (29)

In the above equations the quantities C_n are constants, and subscripts θ and z refer to angular position and axial position, respectively.

Constant C_1 may be determined readily from Eq. 9 by considering the flow through the r-θ plane of one channel. For this calculation Eq. 9 becomes

$$\frac{w}{3} = \rho \int_0^{A'_z} u_z dA'_z$$

or

$$C_1 = \frac{1}{3A'_z}\left(\frac{w}{\rho}\right), \tag{30}$$

where A'_z is the area of the r-θ plane exposed in one channel. This area was calculated from

$$A'_z = \frac{1}{3}\left[\frac{2\pi - (3)(72\pi b)}{2\pi}\right]\left[\pi(r_2^2 - r_1^2)\right], \tag{31}$$

where b is the blade thickness measured in the direction of the axis of the impeller, ft. Numerical evaluation of Eq. 31 for $b = 2.759 \times 10^{-3}$ ft gave

$$A'_z = 7.242 \times 10^{-4}\ \text{ft}^2. \tag{32}$$

Substitution of Eq. 32 into Eq. 30 and simplifying gave

$$C_1 = 460.3\left(\frac{w}{\rho}\right). \tag{33}$$

A relation for the constant C_2 appearing in Case 1 was developed in a similar manner. From Eq. 9

$$\frac{w}{3} = \rho \int_{o}^{A'_\theta} u_\theta \, dA'_\theta , \tag{34}$$

where A'_θ is the area of the r-z plane bounded by one channel, as before. Substitution of Eq. 22 into Eq. 34, integrating and simplifying gave

$$C_2 = \frac{1}{3\Delta z(r_2 - r_1)} \left(\frac{w}{\rho} \right)$$

or

$$C_2 = 3.93 \times 10^3 \left(\frac{w}{\rho} \right). \tag{35}$$

Substitution of Eqs. 33 and 35 into Eq. 23 and simplifying gave

$$u = 3.96 \times 10^3 \left(\frac{w}{\rho} \right). \tag{36}$$

Substitution of Eq. 36 into Eq. 20 gave

$$\frac{\overline{U}_o^2}{2g_c} = 3 \left[\frac{1}{\left(\frac{2g_c w}{3\rho} \right)} \int_{o}^{A'_n} \left(3.96 \times 10^3 \, \frac{w}{\rho} \right)^3 dA'_n \right].$$

Integration and numerical evaluation of the above equation gave

$$\frac{\overline{U}_o^2}{2g_c} = 7.32 \times 10^5 \left(\frac{w}{\rho} \right)^2. \tag{37}$$

Eq. 37 is the derived expression for the kinetic energy term in the right member of Eq. 8 for Case 1 defined by Eqs. 21 and 22.

An expression for the constant C_3 appearing in Case 2 was developed as follows. From Eq. 9

$$\frac{w}{\rho} = 3\int_{o}^{A'_\theta} u_\theta dA'_\theta ,$$

or

$$\frac{w}{\rho} = 3\int_{r_1}^{r_2} C_3 r(\Delta z dr) . \tag{38}$$

Integration of Eq. 38 and simplifying gave

$$C_3 = \frac{2}{3\Delta z(r_2^2 - r_1^2)}\left(\frac{w}{\rho}\right) .$$

Numerical evaluation of the above equation gave

$$C_3 = 1.041 \times 10^5 \left(\frac{w}{\rho}\right) . \tag{39}$$

Substitution of Eqs. 33 and 39 into Eq. 26 gave

$$u = [(460.3)^2 + (1.041 \times 10^5 r)^2]^{1/2}\left(\frac{w}{\rho}\right) . \tag{40}$$

Substitution of the above relation and Eq. 16 into Eq. 20 and simplifying gave, as before,

$$\frac{\overline{U}_o^2}{2g_c} = \frac{324\pi\Delta z}{g_c}\left(\frac{w}{\rho}\right)^2 \int_{r_1}^{r_2} \frac{[(460.3)^2 + (1.041 \times 10^5 r)^2]^{3/2} rdr}{[(72\pi r)^2 + 1]^{1/2}} . \tag{41}$$

The integral appearing in Eq. 41 was evaluated using graphical methods. The right member of Eq. 41 was then evaluated giving

$$\frac{\overline{U}_o^2}{2g_c} = 7.36 \times 10^5 \left(\frac{w}{\rho} \right)^2. \qquad (42)$$

Eq. 42 is the derived expression for the kinetic energy term in the right member of Eq. 8 for Case 2.

An expression for the constant C_4 appearing in Case 3 was developed as follows. From Eq. 9

$$\frac{w}{\rho} = 3 \int_{r_1}^{r_2} \frac{C_4}{r} \Delta z dr.$$

Integration of the above expression gave

$$C_4 = \frac{1}{3\Delta z \ln\left(\frac{r_2}{r_1} \right)} \left(\frac{w}{\rho} \right),$$

and numerical evaluation gave

$$C_4 = 1.475 \times 10^2 \left(\frac{w}{\rho} \right). \qquad (43)$$

Substitution of Eqs. 33 and 43 into Eq. 29 gave

$$u = \left[(460.3)^2 + \left(\frac{147.5}{r} \right)^2 \right]^{1/2} \left(\frac{w}{\rho} \right). \qquad (44)$$

Substitution of Eq. 44 and Eq. 16 into Eq. 20 and simplifying gave

$$\frac{\overline{U}_o^2}{2g_c} = \frac{324\pi\Delta z}{g_c}\left(\frac{w}{\rho}\right)^2 \int_{r_1}^{r_2} \frac{\left[(460.3)^2 + \left(\frac{147.5}{r}\right)^2\right]^{3/2} r\,dr}{[(72\pi r)^2 + 1]^{1/2}} . \quad (45)$$

The integral appearing in Eq. 45 was evaluated using graphical methods and the right member of Eq. 45 became, on simplification,

$$\frac{\overline{U}_o^2}{2g_c} = 7.53 \times 10^5 \left(\frac{w}{\rho}\right)^2 . \quad (46)$$

Eq. 46 is the derived expression for the kinetic energy term in the right member of Eq. 8 for Case 3.

The pressure term appearing in the right member of Eq. 8 was then determined for the three cases described above. The equation defining the radial pressure distribution for a frictionless, incompressible fluid flowing in a curved channel was obtained using the configuration shown in Fig. 18. The force balance on the differential element of fluid gave

$$p[(r\,d\theta)\,dz] + \frac{\rho u_\theta^2}{g_c r}\left[\left(r + \frac{dr}{2}\right) d\theta\,dr\,dz\right] = (p+dp)[(r+dr)\,d\theta\,dz] .$$

The above relation was simplified, neglecting second order infinitesimals, to give

$$\frac{d(pr)}{dr} = \frac{\rho}{g_c} u_\theta^2 , \quad (47)$$

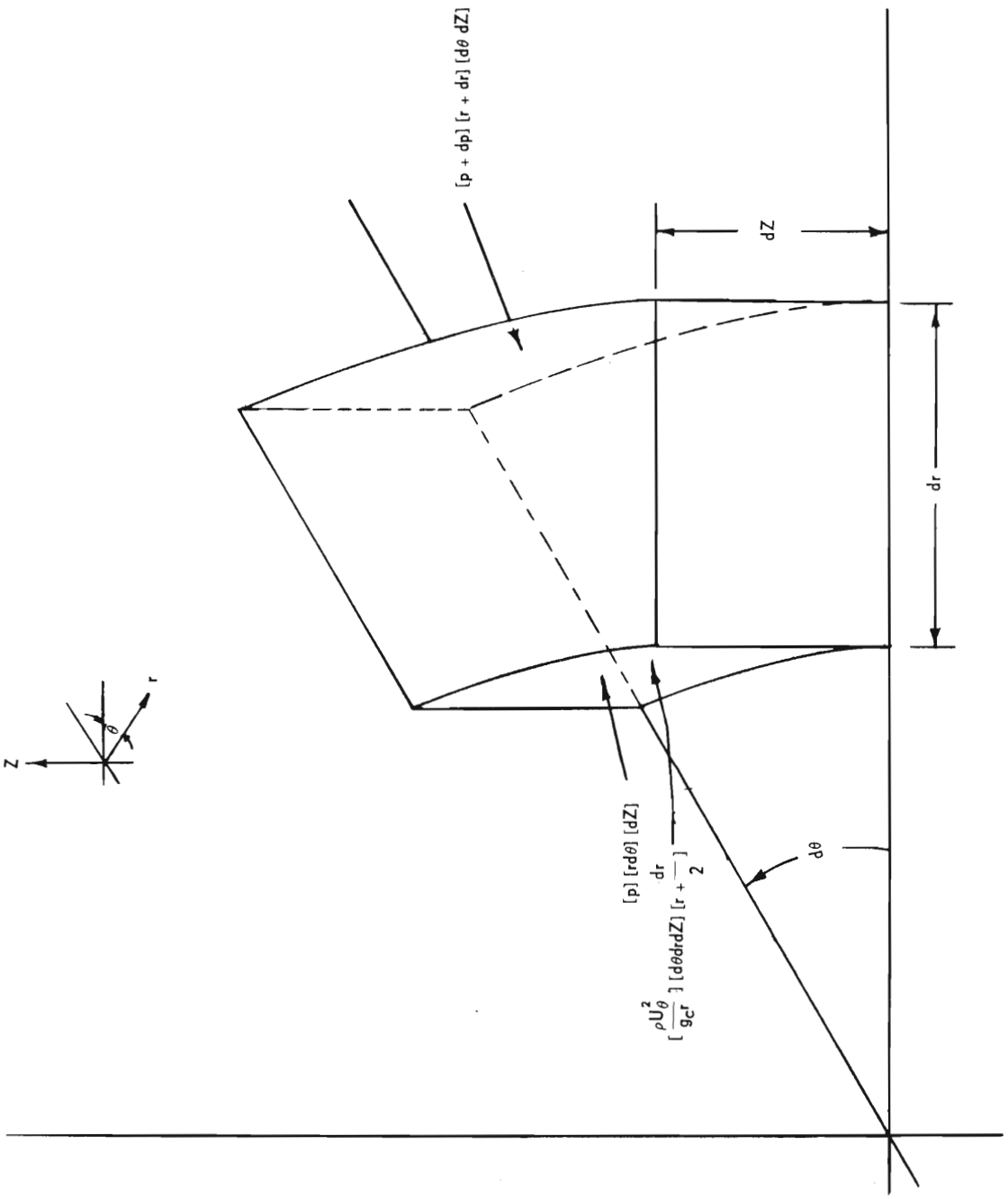

Figure 18. Force Balance.

where p is local pressure, lbf/ft^2.

The radial pressure distribution for the first case was obtained by substituting Eq. 22 into Eq. 47 and integrating. This gave

$$p = \frac{\rho C_2^2}{g_c}\left[1 - \frac{r_1}{r}\right] + \left(\frac{r_1}{r}\right)p_1. \tag{48}$$

For the second case the radial pressure distribution was obtained by substituting Eq. 25 into Eq. 47 and integrating. This gave

$$p = \frac{\rho C_3^2}{3g_c}\left[r^2 - \frac{r_1^3}{r}\right] + \left(\frac{r_1}{r}\right)p_1. \tag{49}$$

For the third case the radial pressure distribution was obtained by substituting Eq. 28 into Eq. 47 and integrating. This gave

$$p = \frac{\rho C_4^2}{g_c}\left[\frac{1}{r_1 r} - \frac{1}{r^2}\right] + \left(\frac{r_1}{r}\right)p_1. \tag{50}$$

The average pressure at the outlet of an impeller channel was defined

$$\overline{P}_o = \frac{1}{A'}\int_o^{A'} p\,dA',$$

or

$$\overline{P}_o = \frac{2}{r_2^2 - r_1^2}\int_{r_1}^{r_2} pr\,dr. \tag{51}$$

The average pressure for Case 1 was obtained by substituting Eq. 48 into Eq. 51 and integrating. This gave

$$\overline{P}_o = \frac{\rho C_2^2}{g_c}\left[\frac{r_2 - r_1}{r_2 + r_1}\right] + \left(\frac{2r_1}{r_2 + r_1}\right) p_1. \qquad (52)$$

Numerical evaluation of Eq. 52 was accomplished using the dimensions of the impeller assembly and Eq. 35. This gave

$$\overline{P}_o = 8.30 \times 10^4 \frac{w^2}{\rho} + 0.828\, p_1. \qquad (53)$$

The average pressure for Case 2 was obtained by substituting Eq. 49 into Eq. 51 and integrating. This gave

$$\overline{P}_o = \frac{2\rho C_3^2}{3g_c}\left[\frac{(r_2^2 + r_1^2)}{4} - \frac{r_1^3}{(r_1 + r_2)}\right] + \left(\frac{2r_1}{r_1 + r_2}\right) p_1. \qquad (54)$$

Numerical evaluation of Eq. 54 was accomplished using the impeller dimensions and Eq. 39. This gave

$$\overline{P}_o = 7.43 \times 10^4 \frac{w^2}{\rho} + 0.828\, p_1. \qquad (55)$$

The average pressure for Case 3 was obtained by substituting Eq. 50 into Eq. 51 and integrating. This gave

$$\overline{P}_o = \frac{2\rho C_4^2}{g_c}\left[\frac{1}{r_1(r_2 + r_1)} - \frac{1}{(r_2^2 - r_1^2)} \ln \frac{r_2}{r_1}\right] + \left(\frac{2r_1}{r_2 + r_1}\right) p_1. \qquad (56)$$

Numerical evaluation of Eq. 56 was accomplished using the impeller dimensions and Eq. 43. This gave

$$\overline{P}_o = 9.58 \times 10^4 \frac{w^2}{\rho} + 0.828\, p_1. \qquad (57)$$

The final expression for apparent friction losses in the impeller assembly for the velocity distribution of Case 1 was obtained by substituting Eqs. 11, 37, and 53 into Eq. 8. This gave

$$\Delta H_f = \frac{\overline{P}_i - 0.828\, p_1}{\rho} - 8.15 \times 10^5 \left(\frac{w}{\rho} \right)^2. \qquad (58)$$

A similar expression for the velocity distribution of Case 2 was obtained by substituting Eqs. 11, 42 and 55 into Eq. 8. This gave

$$\Delta H_f = \frac{\overline{P}_i - 0.828\, p_1}{\rho} - 8.10 \times 10^5 \left(\frac{w}{\rho} \right)^2. \qquad (59)$$

The final expression for the velocity distribution of Case 3 was obtained by sutstituting Eqs. 11, 46 and 57 into Eq. 8. This gave

$$\Delta H_f = \frac{\overline{P}_i - 0.828\, p_1}{\rho} - 8.49 \times 10^5 \left(\frac{w}{\rho} \right)^2. \qquad (60)$$

The expressions for the apparent friction loss in the impeller assembly, Eqs. 58, 59 and 60, were strikingly similar. The difference in the equations occurred in the coefficient of the bulk velocity term in the right members; the maximum difference in the coefficients was approximately 5 per cent. Since the cases studied were based on idealized velocity distributions, none of the resulting equations was an exact representation of actual flow conditions.

For the correlation of data Eq. 60 was chosen. This relation was developed using the velocity distribution determined experimentally by Wattendorf for flow removed from the vicinity of the wall. The correlating parameter was the impeller Reynolds number, which was defined

$$Re = \frac{D_h \overline{U} \rho}{\mu}, \tag{61}$$

where D_h is the hydraulic diameter of one channel, ft, and μ is viscosity, lbm/ft-sec. The hydraulic diameter is defined

$$D_h = \frac{4A'_n}{S'_n}, \tag{62}$$

where S'_n is the wetted perimeter of the area A'_n, ft.

Two sides of the wetted perimeter of the flow channel were obtained from the difference in the inner and outer radii. The remaining two sides were obtained from the relation

$$dS = \cos \alpha \, dz \tag{63}$$

which was developed using the configuration shown in Fig. 17. Substitution of Eq. 15 into Eq. 63 gave, on integration at constant radius,

$$S = \left[\frac{(72\pi r)^2}{(72\pi r)^2 + 1} \right]^{1/2} \Delta z. \tag{64}$$

Substitution of the numerical values $\Delta z = 6.5 \times 10^{-3}$ ft and $r_1 = 3.125 \times 10^{-2}$ ft into Eq. 64 gave $S_1 = 6.45 \times 10^{-3}$ ft. Substitution of

$\Delta z = 6.5 \times 10^{-3}$ ft and $r_2 = 4.429 \times 10^{-2}$ ft gave $S_2 = 6.47 \times 10^{-3}$ ft. Thus, the wetted perimeter was

$$S_n = 2(4.429 - 3.125) \times 10^{-2} + 6.45 \times 10^{-3} + 6.47 \times 10^{-3} \text{ ft},$$

or

$$S_n = 3.9 \times 10^{-2} \text{ ft}. \tag{65}$$

The expression for the average velocity in a flow channel was developed from Eqs. 9 and 44. Thus,

$$\overline{U} = \frac{1}{A'_n} \int_o^{A'_n} \left[(460.3)^2 + \left(\frac{147.5}{r} \right)^2 \right]^{1/2} \left(\frac{w}{\rho} \right) dA'_n.$$

Substitution of Eq. 16 into the above expression and simplifying gave

$$\overline{U} = \frac{72\pi\Delta z}{A'_n} \frac{w}{\rho} \int_{r_1}^{r_2} \left[\frac{(460.3r)^2 + (147.5)^2}{(72\pi r)^2 + 1} \right]^{1/2} dr. \tag{66}$$

Numerical evaluation of Eq. 66 was accomplished using graphical techniques. The resulting expression for the average velocity in the impeller channel was

$$\overline{U} = \frac{0.3346}{A'_n} \frac{w}{\rho}. \tag{67}$$

Substitution of Eqs. 62, 65, and 67 into Eq. 61 and simplifying gave

$$Re = 34.2\left(\frac{w}{\rho}\right). \tag{68}$$

A correlation of the static pressure data shown in Table 1 was attempted by assuming the functional relationship

$$\frac{\Delta H_f}{\left(\frac{\overline{U}_o^2}{2g_c}\right)} = f(Re). \tag{69}$$

The apparent friction loss ΔH_f was calculated for each experiment using Eq. 60. The kinetic energy of the fluid leaving the impeller $\frac{\overline{U}_o^2}{2g_c}$ was calculated using Eq. 46, and the Reynolds number was calculated from Eq. 68. All fluid properties were evaluated at the inlet temperature. The results of the calculations are shown in Fig. 19.

Flow characterization.—The results from the flow characterization studies included photographic records of flow patterns and data from tube wall pressure measurements. Illustrations of typical flow patterns at various stations in a nominal 1-inch glass tube for several flow rates were presented in Figs. 5 through 8. Averaged tube wall static pressure data were presented in Fig. 10. The photographic records indicate the change in the general fluid flow pattern with axial distance from the impeller and thus give a measure of the relative magnitude of the axial and tangential velocity components. No systematic attempt was made to determine slopes of the flow patterns from the photographic records, since this method of analysis is subject to numerous inaccuracies.

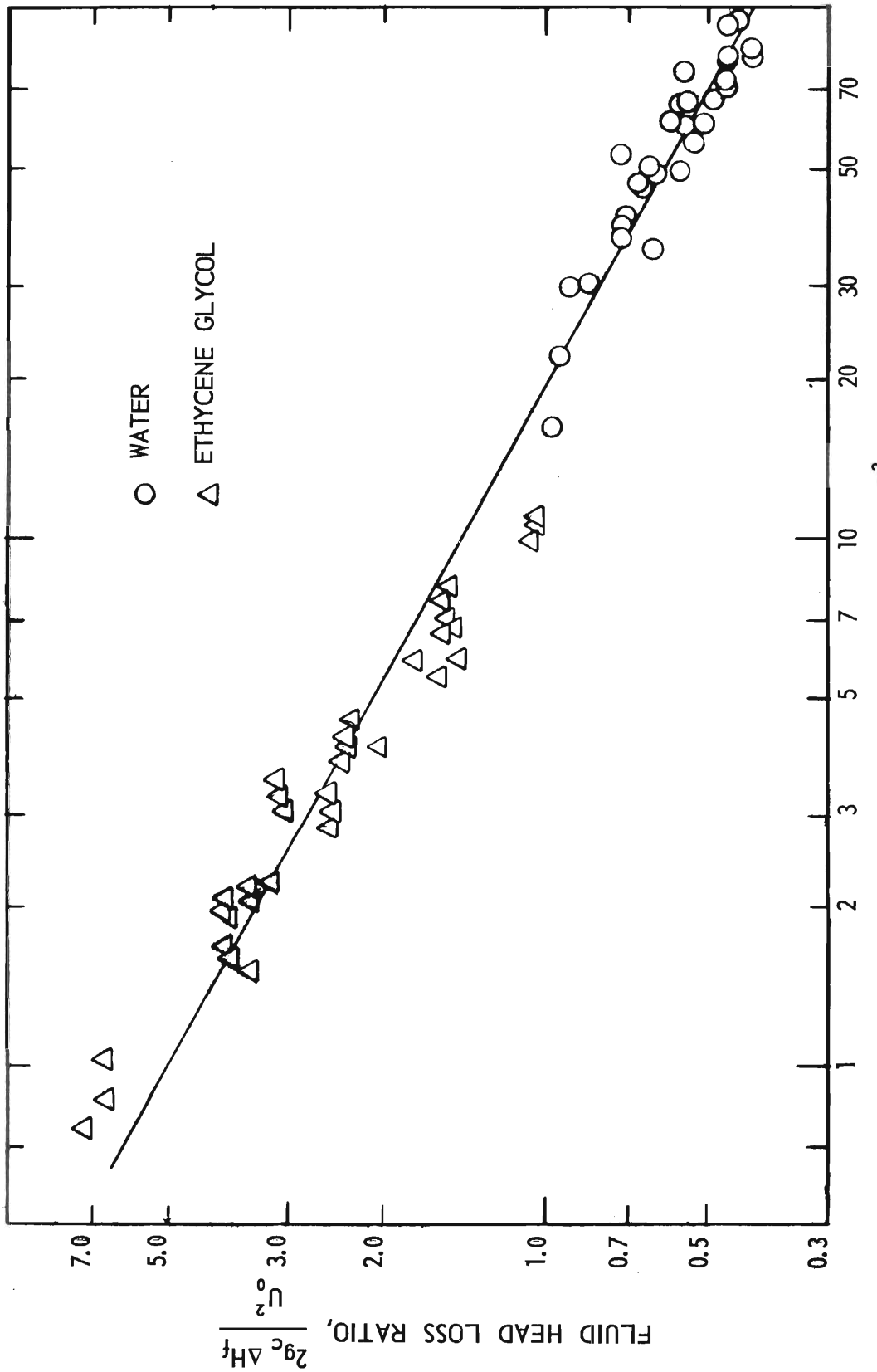

Figure 19. Correlation of Impeller Pressure Loss Data.

The tube wall static pressure measurements, in principle, may be used to determine the tangential velocity component of the flow pattern, provided the radial distribution of tangential velocity and the inner radius of the fluid film are known. The method of analysis is based on Eq. 47 from the preceding section:

$$\frac{d(pr)}{dr} = \frac{\rho}{g_c} u_\theta^2. \tag{47}$$

If, for example, the tangential velocity distribution described by Wattendorf is assumed,

$$u_\theta = \frac{C_4}{r}. \tag{28}$$

Substitution of the velocity distribution into the differential equation describing the radial pressure distribution and integrating gave

$$p_2 r_2 - p_1 r_1 = \frac{\rho}{g_c} C_4^2 \left(\frac{1}{r_1} - \frac{1}{r_2} \right). \tag{70}$$

Experimental data for the inner and outer radii of the fluid film and the corresponding pressures may be used to determine the numerical value of the constant C_4 appearing in Eq. 70, thus determining the tangential velocity. Unfortunately it was not feasible to determine the inner radius r_1 of the fluid film. The reason for this difficulty is readily apparent in the static pressure data in Table 3 in the Appendix. At tube stations where the tube wall static pressure was appreciable, there was a considerable variation in static pressure with angular position. This effect was produced by inhomogenities in the fluid film, which prevented

accurate estimates of film thickness. Accordingly, no attempts were made to estimate tangential velocity components from the tube wall static pressure data.

Heat transfer studies.—Experimental data from the heat transfer experiments with water and with ethylene glycol were presented in Table 1, and calculated local average film heat transfer coefficients for each experiment were presented in Table 2. A correlation of the experimental data and the calculated film coefficient at a particular tube section for each fluid at the various flow conditions was sought. In this analysis the empirical relation

$$Nu = \phi\left[Re^{0.8}\, Pr^{0.4}\left(\frac{\mu_m}{\mu_w}\right)^{0.14}\right], \tag{71}$$

where Nu is the Nusselt number, ϕ is a functional notation, Pr is the Prandtl number, and subscripts m and w refer to properties evaluated at the mean bulk temperature and the wall temperature, respectively, was utilized. The local Nusselt number was defined

$$Nu = \frac{hD_h}{k_m}. \tag{72}$$

The characteristic length appearing in the Nusselt number was assumed to be the hydraulic diameter of the impeller channel defined by Eq. 62.

The Reynolds number of the fluid was defined by Eq. 68. The viscosity of the fluid was evaluated at the arithmetic average of the bulk fluid temperatures at the inlet and outlet of the particular test section.

The characteristic length implicit in this definition was consistent with the one used in Eq. 72 for the Nusselt number.

The Prandtl number of the fluid was defined

$$Pr = \left(\frac{\bar{c}_p \mu}{k} \right)_m . \qquad (73)$$

Thermodynamic and transport properties appearing in Eq. 73 were evaluated at the arithmetic mean of the inlet and outlet temperature of the fluid for the particular test section as before.

At a particular tube section in each experiment the independent variable appearing in the right member of Eq. 71 was evaluated from the data of Table 1. The corresponding local Nusselt number, the dependent variable in Eq. 71, was evaluated from Eq. 72 with the data from Table 2. The process was repeated for the four tube sections for all experiments. The results of this analysis are shown in Fig. 20 for the experiments utilizing water and in Fig. 21 for the experiments using ethylene glycol.

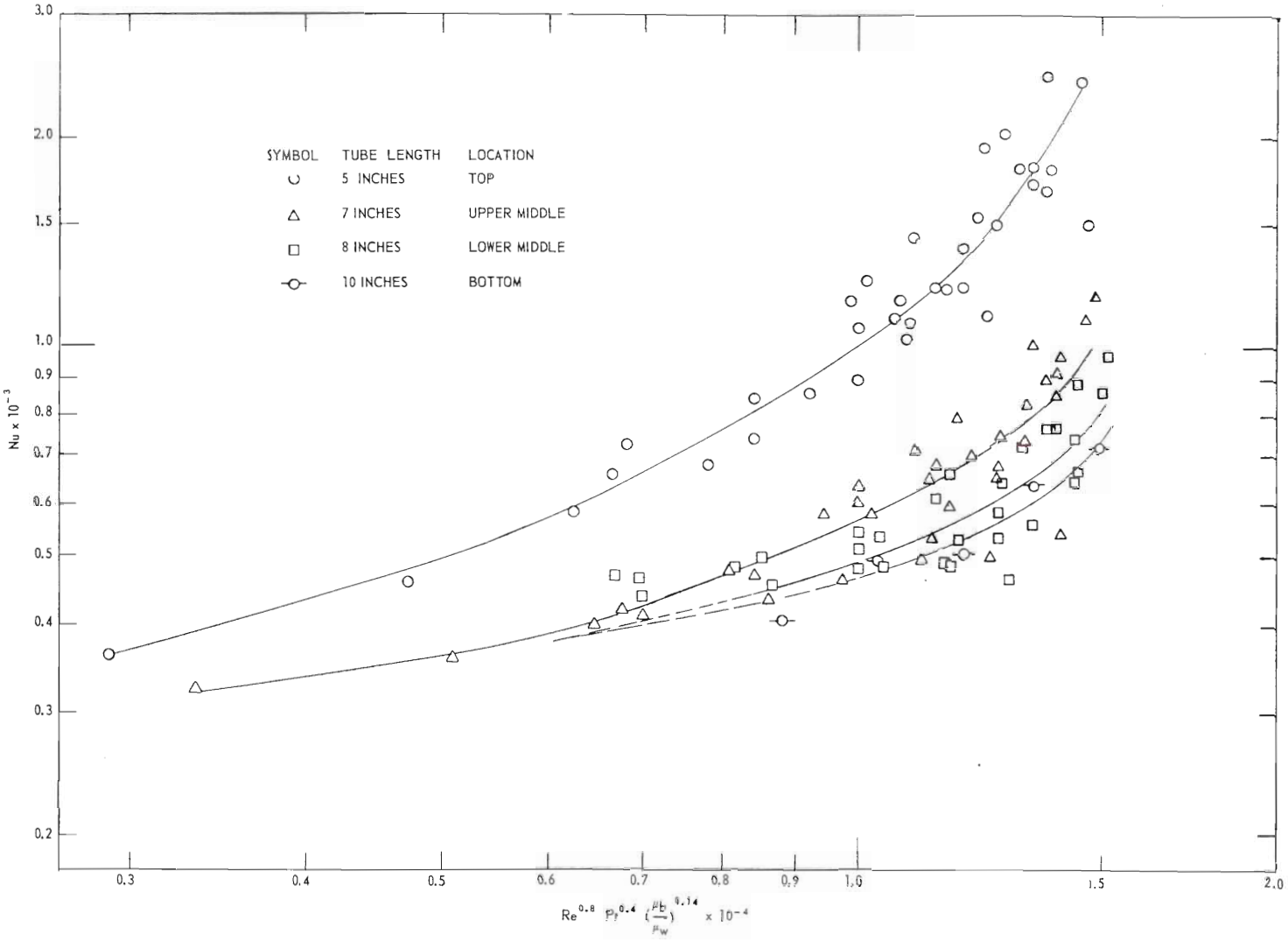

Figure 20. Correlation of Heat Transfer Data for Water.

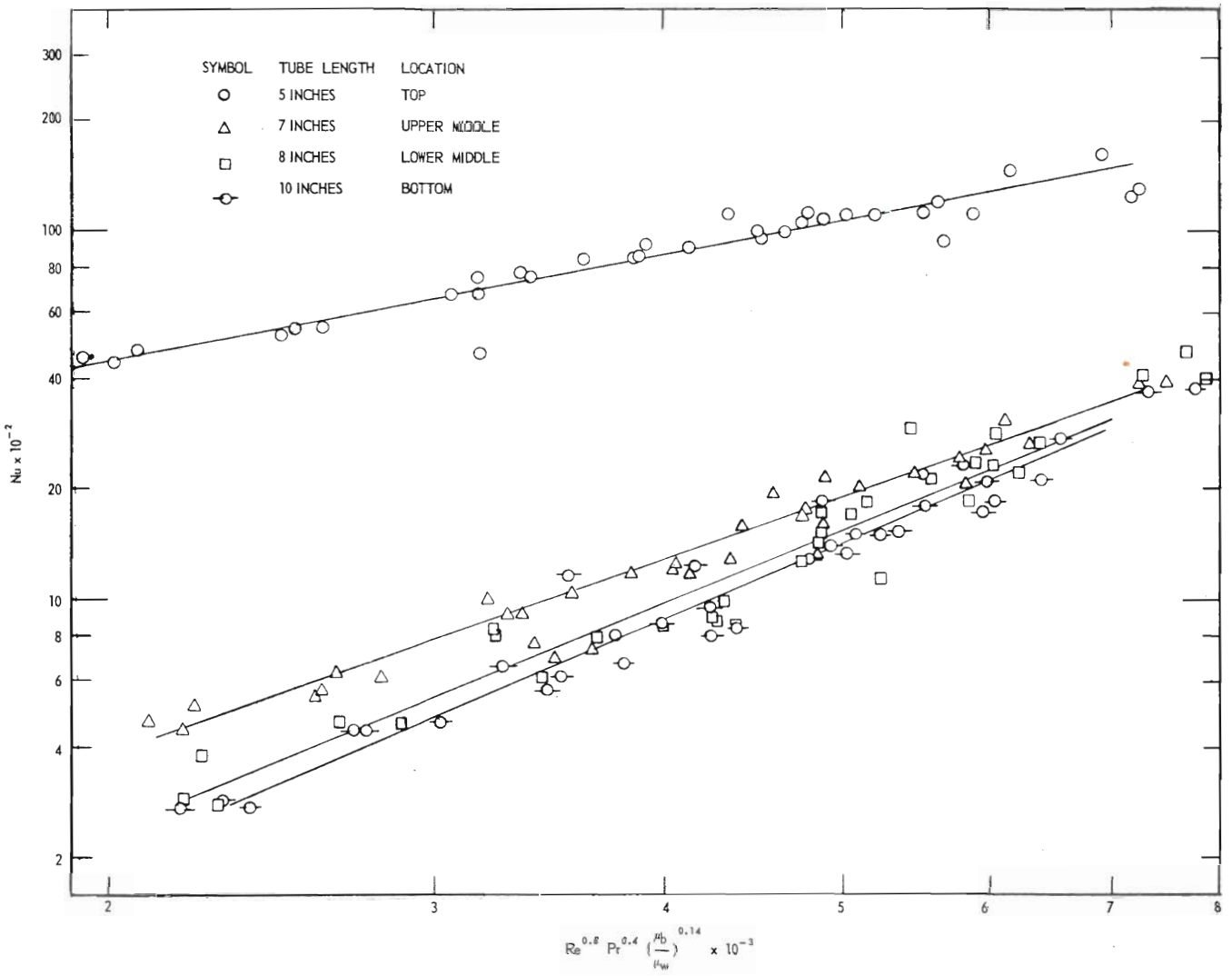

Figure 21. Correlation of Heat Transfer Data for Ethylene Glycol.

CHAPTER IV

DISCUSSION OF RESULTS

The results which were presented in Chapter II and which were analyzed in Chapter III generally involve two distinct types of experiment: flow characterization studies and heat transfer studies. These studies were presented separately for convenience; each topic is vital to an understanding of the performance of the system, and the results are necessarily related. A discussion of pertinent features of each of these topics is given in this Chapter, and a discussion of the overall performance of the complete system is presented.

Flow characterization studies.—The fixed impeller design used throughout this investigation was found to offer several advantages over other possible configurations. The device was simply fabricated from readily available materials. The basic design was quite versatile, since the flow characteristics of the assembly could be altered readily by changing the number of blades, the thread depth, the pitch or the major diameter. Operational difficulties and sealing problems to be expected with rotating propeller devices were completely avoided, and mechanical maintenance was unnecessary.

Undesirable characteristics of the fixed impeller include the difficulty of characterizing the flow pattern produced by the device and the static pressure required for its operation. Flow patterns from fixed-blade impeller devices of the type used in this investigation have at least

one characteristic in common: the flow leaving the channels between the blades is separated into distinct regions. The effect is produced by the fact that the blades occupy a finite cross-section in the outlet plane of the channel. The result is quite evident in Figs. 5 through 8, in which several distinct regions of flow may be noted, particularly near the impeller outlet. Additional non-uniformity within a given flow region at a point near the outlet of the impeller assembly can be detected also. This can be attributed to deformation of fluid streams leaving the impeller channels to the internal configuration of the tube. Fluid to occupy the space between the channels caused by the finite thickness of the blades is supplied from channel regions nearer the axis of the impeller assembly. Since this fluid did not have the same velocity distribution, the resulting flow pattern in the tube near the impeller was quite inhomogeneous and turbulent.

With increasing distance from the impeller, however, these inhomogenities were dissipated and the flow pattern became more uniform with angular position in the tube. This effect may be noted particularly in Table 3 in the Appendix and in Fig. 10. With increasing distance from the impeller the variation in tube wall static pressure with angular position became less pronounced. This resulted from increased turbulent mixing of the fluid, viscous dissipation of extremes in the turbulent field, and a change in the overall velocity distribution of the flow caused by gravitational acceleration. Indeed, these effects were so pronounced for distances from the impeller greater than fourteen inches that the tube wall static pressure was not measurable with the equipment used in the

flow characterization study.

The combination of effects noted above produced a flow pattern that was very difficult to characterize. Representative fluid velocities in the swirling film could not be obtained since these quantities were dependent on angular position, axial position, radial position and mass flow rate to the impeller assembly. For purposes of correlation of data from a particular study this fact does not present insurmountable difficulties, but the feasibility of theoretical treatment of the results is so reduced that extensions of the flow problem to a more general study cannot be made.

Of particular note in the flow characterization studies were the static pressure requirements of the impeller assembly. In general the static pressure in the fluid manifold was converted to kinetic energy of the fluid leaving the impeller and to friction losses in the system. These losses included several abrupt expansions and contractions of the fluid stream, friction losses in the tubing connecting the pressure manifold and the impeller assembly, and wall friction losses in the impeller channels.

The analysis which permitted the calculation of the apparent net friction loss of the system from measured values of manifold pressure, fluid flow rate and the dimensions of the system involved several approximations. First, the kinetic energy of the fluid entering the pressure manifold was calculated without regard to the distribution of velocity across the inlet plane of the system. The use of this assumption is generally reasonable for turbulent flow. In addition, if the

contribution of the kinetic energy of the fluid entering the system is only a small fraction of the total energy entering the system, as it was in this study, then the assumption of a negligible influence of the velocity distribution across the inlet plane of the system is quite appropriate.

The validity of the assumption regarding the kinetic energy of the fluid leaving the system was more difficult to evaluate. For the flow system used in this study it was considered necessary to include at least an estimate of the effects of variations of velocity across the outlet plane of the system. In the analysis velocity distributions measured and discussed by other investigators using similar systems were assumed to apply, since it was not considered feasible to experimentally determine velocity profiles in the impeller assembly devised for this study. Using three quite different velocity distributions in the outlet plane of the impeller channels three relations for the kinetic energy of the fluid leaving the system, Eqs. 37, 42 and 46, were developed. Since these expressions gave values of the fluid kinetic energy leaving the system which differed from each other by only approximately three per cent, it was decided that further investigation of the channel velocity distribution was unnecessary. Accordingly, the expression which was derived from the velocity distribution found most descriptive by other investigators, Eq. 46, was selected. It is considered that this relation gives a reasonable approximation to the kinetic energy of the fluid leaving the system.

A similar difficulty was encountered in the evaluation of an appropriate average static pressure over the outlet plane of the system. The tangential velocity distributions assumed in the development of the

kinetic energy relations were used to develop expressions for the average outlet pressure. The final expressions were Eqs. 53, 55, and 57. The maximum difference in the average pressure calculated from these relations for the experiments in this investigation was less than nine per cent. This value was obtained for the series of experiments using water as the working fluid at the maximum flow rate. For lower rates of flow and for the studies using ethylene glycol the difference was correspondingly smaller.

The final expression for the apparent friction loss was obtained by combining the mechanical energy equation and the derived expressions for the three assumed impeller channel velocity distributions. The resulting relations were Eqs. 58, 59, and 60. Apparent friction loss values predicted from these expressions differed by less than five per cent for the range of data from these experiments. Accordingly, the expression which embodied the velocity distribution found by other investigators to be most descriptive of this type of fluid motion, Eq. 60, was selected. It is considered that this equation gives a suitable means for characterizing the energy requirements for the impeller and for the data of this investigation.

For the correlation of the experimental data a Reynolds number based on the flow in the impeller channels was defined in the usual manner. Even though the calculated net friction loss for the system actually reflected the sum of individual contributions due to expansion, contraction and wall friction, each of which in general was a function of the appropriate local Reynolds number, it was considered that the

impeller Reynolds number would be the significant parameter. This choice was justified in part by the following considerations.

If it may be assumed that the total friction loss in any one test is composed of 1) a contraction loss as the fluid leaves the manifold and enters the connecting tubing, 2) a friction loss in the connecting tubing, 3) an expansion loss as the fluid enters the impeller jacket, 4) a contraction loss as the fluid enters an impeller channel, and 5) a friction loss as the fluid flows down the impeller channel, then the net apparent friction loss may be written

$$\Delta H_f = \sum_{j=1}^{5} (\Delta H_f)_j . \tag{74}$$

It has been empirically determined that, in general, the right member of Eq. 74 may be written

$$\Delta H_f = f_1(\mathrm{Re})_t \left[\frac{\overline{U}^2}{2g_c}\right]_t + f_2(\mathrm{Re})_t \left[\frac{\overline{U}^2}{2g_c}\right]_t \left[\frac{L}{D}\right]_t \tag{75}$$

$$f_3(\mathrm{Re})_t \left[\frac{\overline{U}^2}{2g_c}\right]_t + f_4(\mathrm{Re})_c \left[\frac{\overline{U}^2}{2g_c}\right]_c + f_5(\mathrm{Re})_c \left[\frac{\overline{U}^2}{2g_c}\right]_c \left[\frac{L}{D}\right]_c ,$$

where $f(\mathrm{Re})$ is a functional notation and subscripts t and c refer to tube and channel regions, respectively. Rearranging Eq. 75 gives

$$\frac{\Delta H_f}{\left(\frac{\overline{U}^2}{2g_c}\right)_c} = \left\{ f_1(\mathrm{Re})_t + f_2(\mathrm{Re})_t \left[\frac{L}{D}\right]_t + f_3(\mathrm{Re})_t \right\} \left[\frac{\overline{U}_t^2}{\overline{U}_c^2}\right] \tag{76}$$

$$+ f_4(\mathrm{Re})_c + f_5(\mathrm{Re})_c \left[\frac{L}{D}\right]_c .$$

Inspection of the right member of Eq. 76 leads to the observation that, for a given flow system, different fluids having identical channel Reynolds numbers should have identical friction loss ratios. In addition, for tube velocities which are small in comparison with the channel velocities, tests at different channel Reynolds numbers with the same fluid should give friction loss ratios primarily dependent on the channel Reynolds number, if the sum of the functions $f_1(\mathrm{Re})_t$, $f_2(\mathrm{Re})_t \left[\frac{L}{D}\right]_t$ and $f_3(\mathrm{Re})_t$ is less than or comparable in magnitude to the sum of functions $f_4(\mathrm{Re})_c$ and $f_5(\mathrm{Re})_c \left[\frac{L}{D}\right]_c$. For the system used in this study these restrictions are certainly fulfilled and a reasonable correlation of experimental data in the form proposed by Eq. 69 could be expected.

The resulting correlation of the experimental static pressure loss data was presented in Fig. 19. If the impeller efficiency is defined as the ratio of the fluid kinetic energy leaving the impeller to the total energy supplied to the impeller assembly, then this quantity can be estimated readily as a function of the channel Reynolds number from Fig. 19. The ordinate of this figure is the friction loss ratio, or the ratio of calculated friction loss to the kinetic energy of the fluid leaving the system. If the ratio of the average static pressure at the impeller outlet to the product of the fluid density and the fluid kinetic energy at the outlet plane is small in comparison to the fluid friction loss ratio, then the efficiency of the impeller assembly is approximately

$$\eta = \frac{1}{\dfrac{\Delta H_f}{\left(\dfrac{\overline{U}^2}{2g_c}\right)_c} + 1} \; .$$

Since the upper and lower bounds on the impeller friction loss ratio were approximately 7.0 and 0.4, the impeller efficiency ranged from 12.5 per cent to 71.5 per cent. It is readily apparent that the assembly was quite inefficient, and that the relative efficiency was quite sensitive to the Reynolds number of the fluid in the channel.

Improvements in the impeller design may be made which should markedly improve the efficiency of the assembly. The use of a pressure manifold and connecting tubing to supply fluid to the jacket of the impeller assembly is probably unnecessary for designs for relatively low mass flow rates, since in this case a uniform supply of fluid to the impeller channels is easily achieved. Application of this modification would permit a substantial reduction in abrupt expansion and contraction losses and in friction losses in the connecting tubing. An even greater improvement in performance could be achieved by shortening the impeller, since it is likely that this device provided the greatest resistance to flow in the system. If it is required that fluid in each channel make one complete revolution before leaving the impeller, then the overall length required for the present device would be somewhat less than an inch instead of the several inches used. One revolution of the fluid should certainly be sufficient to provide adequate swirling motion in the fluid leaving the device.

Heat transfer studies.—The results from the heat transfer studies included the experimental determination of the heat transferred in the exchange section, calculations of local average film heat transfer

coefficients from measured quantities, and correlation of the film coefficients with pertinent fluid parameters. The heat input to the heat exchange section was determined from the enthalpy of the steam entering the section, the enthalpy of the condensate leaving the exchange section, and the condensate flow rate. The determination of the steam enthalpy was performed using a calorimeter designed according to the Power Test Codes, ASME Series 1929, Instruments and Apparatus, Part 11. A thermometer certified by the National Bureau of Standards was used in conjunction with the calorimeter. In relating the measured temperature of the steam in the calorimeter at atmospheric pressure to the enthalpy of the steam in the high pressure main it was necessary to assume that the steam expanded isenthalpically. This restriction is generally acceptable for relatively low flow rates and for a well insulated system. These requirements were met with this device, and thus it is expected that a reasonable determination of the enthalpy of the steam entering the exchange section was effected. It should be noted that an isenthalpic expansion of the steam through the regulators into the heat exchange section was assumed also.

No attempt was made to determine experimentally the enthalpy of the condensate leaving the system. It was assumed that the condensate enthalpy was that of saturated water at the pressure prevailing in the heat exchange section; this assumption may be erroneous since there is a good possibility that the condensate was subcooled slightly. The error introduced by application of this assumption is considered to be small, however, and quite acceptable in view of the limitations on the accuracy

of the determination of the condensate flow rate.

The condensate flow rate was obtained by collecting and weighing the output from a conventional bucket-type steam trap which was connected to the inner region of the heat exchange section. The condensate from the inner region was separated from the condensate in the outer region by the adiabatic wall separator; thus, for steady-state operation, all of the condensate entering the steam trap from the inner region was produced by condensation on the copper heat exchange tube except for small quantities which could have been condensed on the upper and lower closure plates. Bucket-type steam traps are periodic in operation, which could introduce errors for collection in finite periods of time. Also, the condensate liberated from the trap was released at a pressure greater than atmospheric and was thus subject to flashing. Further, an additional error may be introduced by the fact that uncondensed steam was used to clear the trap of condensate. In all tests of this investigation approximately two liters of condensate were collected in an Erlenmeyer flask immersed in an ice bath. The collection of this quantity of condensate reduced the error involved in the periodic operation of the trap. The error introduced by losses of condensate from flashing was reduced and partially compensated by the condensation of a portion of the excess steam used to clear the trap. Thus it is considered that this measurement is the least accurate of those quantities required for the determination of the heat input to the system.

A second method for determining the heat input to the system was the measurement of the temperature increase of the heat transfer fluid

flowing through the heat exchange section. The flow rate of fluid to the system was obtained from rotameters which had been calibrated for both water and ethylene glycol. The rotameters were of the viscosity-compensating type; that is, the calibration of the rotameter for a particular fluid was essentially independent of changes in the viscosity of this fluid. The calibrations were sensitive to changes in the fluid density, however. For the range of inlet temperatures used in this study the density change was small, and the effect on the flow rate calibration was considered to be negligible.

The inlet temperature of the fluid was measured in the static pressure manifold. As shown in Fig. 14, the upper end of the manifold was surmounted by a tee. The branch of the tee was used for the determination of the static pressure in the manifold, and the run was used for the temperature sensing device. This consisted of a copper-constantan thermocouple mounted within a length of 1/4-inch O. D. copper tubing in such a way that the thermocouple head was imbedded in the end closed by soldering. The device was calibrated before installation at several temperatures using the oil bath described previously. The tubing containing the thermocouple was attached to the tee by means of a standard tubing fitting which had been drilled out to permit the installation of a polyethylene insulator.

In the installation of the sensing element, the tubing containing the thermocouple was inserted into the polyethylene insulator contained in the tubing fitting to a sufficient depth that the bead would be located at the plane of the fluid outlets in the manifold. The tubing fitting was

attached to the tee, and tightening the packing nut on the polyethylene insulator provided a tight seal. Thus the thermocouple was exposed to a well-mixed fluid entering the exchange section.

Possible errors inherent in the temperature sensing device include the effect of heat conduction away from the thermocouple junction down the thermocouple wire and the effect of heat conduction away from the thermocouple junction down the copper tubing. Heat conduction from the junction into the thermocouple wires would tend to reduce the temperature at the bead. This reduction in temperature would result in heat flow into the bead from the copper tube. Since the copper tube had a relatively large surface exposed to a well-stirred fluid, and since the cross-sectional area of the wire for heat conduction away from the bead was relatively small, it is expected that the error in the measurement temperature due to heat conduction in the thermocouple wires was negligible. Similarly, the surface of the copper tube exposed to the environment and subject to heat transfer by free convection was quite small compared to the surface exposed to the fluid, and thus the error in measured temperature caused by heat conduction in the tube wall is expected to be small.

The outlet temperature of the fluid was measured in the mixing device shown in Fig. 15. This device provided a well-mixed fluid for the temperature sensing element, since the fluid had to turn through a right angle before overflowing from the device. A temperature sensing element essentially identical to the one used in the pressure manifold was used to determine the outlet temperature. The element either was

mounted vertically in the bottom of the mixing device with the thermocouple junction approximately 1/2-inch beneath the surface of the fluid, or was inserted through the branch of the tee to a similar point, depending on whether the probe was being used to measure film temperatures. Errors in the temperature measurement from this device were similar to those for the element mounted in the pressure manifold, and thus are expected to be small as before.

A comparison of the heat into the exchange section as calculated from the steam condensation rate and the heat removed from the exchange section as calculated from the temperature increase of the fluid is given in Table 2. In general the comparison is quite good; the deviation between the two rates is on the order of a few per cent. The more accurate value is considered to be the value for the heat removed from the exchange section for the reasons given above.

Other temperatures which were measured in the heat transfer studies included the tube wall temperature and the fluid film temperature, both as a function of axial position. Tube wall temperatures were determined from thermocouples imbedded in a slot 0.100 inches deep and approximately one inch long. Errors involved in the measurement of the tube wall temperature included heat conducted from the junction down the thermocouple wires and the disturbance in the temperature field of the tube caused by the presence of the slot. Since several inches of thermocouple wire were exposed within the heat exchange section and since approximately one inch of wire was located in an essentially isothermal plane at the temperature of the thermocouple bead, the effect of heat

conduction down the wire on the measured temperature is expected to be small.

The disturbance of the temperature field caused by the removal of copper from the slot and subsequent replacement with an insulated thermocouple, tin solder and a new copper surface is difficult to evaluate. Considerable care was taken to minimize this effect by careful peening of the bead into the slot and by replacing as much of the copper in the slot as possible. The effect on the temperature field will be less for materials having high thermal conductivities than for those with low conductivities, however.

The errors involved in the measurement of the fluid film temperature with the probe assembly are difficult to evaluate. Possible sources of error other than probe location included the lack of a uniformly mixed fluid, variations of fluid temperature with both angular and radial position in the tube, heat conduction in the rubber thermocouple mounting device and heat conduction in the thermocouple wires. In an attempt to minimize the error in the film temperature, two thermocouples were used in diametrically opposed positions on the probe. In each test the temperature of each probe thermocouple was determined for two angular positions in the tube, and the film temperature at this location was obtained by calculating the arithmetic average of these values. At locations far removed from the impeller the deviation of any value from the average was small, but for locations near the impeller the deviation was significant. The maximum deviation was approximately 4°F. Heat conduction in the thermocouple wires away from the junction

was certainly possible. However, the wires were securely fastened to the thermocouple support and rubber mount, and were maintained at a temperature approaching the fluid temperature. Thus it is expected that this error is small. Since the rubber mount had a very low thermal conductivity and since an appreciable area of the mount was exposed to the fluid stream, it is expected the heat conduction from the thermocouple junction into the mount introduced only a very small error in the overall measurement. Accordingly, it is considered that the principal error in the film temperature determination was the lack of a well mixed fluid. This effect was, of course, most pronounced near the outlet of the impeller.

The location of the thermocouple probe within the heat exchange tube was important to the determination of local average film heat transfer coefficients. This was obtained by comparing reference points on the jointed segments of the thermocouple probe with a reference point on the mixing device. Thus it is expected that a reasonably accurate determination of this quantity was made for all tests.

The insertion of the probe into the heat exchange tube introduced a disturbance in the flow pattern which affected the amount of heat transferred to the fluid. This was particularly evidenced by the change in the amount of condensate collected during the four tests of a particular experiment. In general, the effect of the probe on the condensate flow rate was quite small for all but the last test with the probe quite close to the impeller outlet. The small effect was anticipated in part from the results from the flow visualization studies. Since the

disturbance in the flow pattern was small in the film upstream of the probe it is expected that the error introduced by this circumstance does not impair the validity of the film coefficients determined from these measurements.

The local average film heat transfer coefficients determined in this investigation, as shown in Table 2, were computed assuming a linear wall temperature variation and a linear fluid temperature variation in each test length. The assumption of linearity in the wall temperature variation was reasonable, as shown in Fig. 14, except near the upper end of the heated tube. The low temperature recorded at this point could be due to a number of effects: heat conduction out of the section, poor condensation rates in the zone of high steam velocity, or a poor thermocouple junction. In the treatment of the experimental data the effect of this point on the tube wall temperature was ignored; in general, this temperature would only affect the value of the first heat transfer coefficient, $\bar{h}_1$, and its effect in most cases would be small due to the high temperature differences between the wall and fluid.

The assumption of linearity in the fluid temperature over a particular length appeared to be reasonable for all but the section nearest the impeller. For that section the temperature increase of the fluid was often a large portion of the total temperature rise. Thus, the resulting curve giving the fluid temperature as a function of the distance from the impeller was non-linear; this curve in general indicated a rapid rise in temperature near the fluid inlet with a more linear relationship at distances further from the impeller. No consideration of this non-

linearity was attempted for the calculations of the film heat transfer coefficients. A graphical procedure to determine the average film heat transfer coefficient in the first section was considered, but it was felt that the temperature profile estimations that would be required would make this method of calculation less suitable than the one chosen. Thus, the procedure followed to determine the average local film heat transfer coefficients for the four regions of the heated tube selected involved only measured values.

The heat transfer coefficients obtained for water again illustrate the effect of the impeller on the fluid film. The region of high heat transfer and large heat transfer coefficients is that region near the impeller, where the tangential velocity and turbulence of the fluid is high. The next length of tube, in general, does not have the high turbulence and high tangential velocity and the heat transfer coefficient is somewhat reduced. The heat transfer coefficients in the third and fourth sections are even lower than those in the preceding sections and are of a similar magnitude; this illustrates the effect of viscosity in reducing the effect of swirling motion on the heat transfer coefficient in a manner similar to that noted for the fluid flow studies.

The heat transfer coefficients for the ethylene glycol studies were considerably lower than those obtained for water. In addition, it was found that the film heat transfer coefficient in the first length of the heated tube section was considerably greater than any of those in following sections. This result and the fact that the film coefficients in

the latter three sections were often quite similar in magnitude was principally due to the high viscosity of the glycol; this tended to reduce turbulence and the swirling motion much more rapidly.

The correlations of the heat transfer results shown in Figs. 20 and 21 indicate that the logarithm of the local Nusselt number is a function of the logarithm of the usual Reynolds-Prandtl-viscosity ratio product. A more general correlation of the local Nusselt numbers was not attempted. Difficulties involved in developing a more general correlation include the necessity of defining a local characteristic length and a local average velocity. Since values for these parameters were not obtained experimentally it was not considered feasible to attempt a general correlation of the experimental results.

CHAPTER V

CONCLUSIONS AND RECOMMENDATIONS

The conclusions which may be drawn from the reported investigations may be summarized as follows.

1. The postulate that superimposed swirling motion on linear flow of fluids can significantly improve the heat transfer characteristics of the flow has been demonstrated to be valid. Accordingly, the feasibility of applying this concept to the solution of novel heat transfer problems deserves further investigation.

2. Inducing swirling motion in a linearly flowing fluid provides a method for increasing the film heat transfer coefficients of that fluid.

3. Fixed impeller devices of the type used in this study are quite readily fabricated and are easily operated. The flow pattern produced by these devices is quite difficult to characterize, however.

4. Static pressure requirements for impellers of the type used in this investigation are quite high. Pumping requirements for inducing a high degree of swirling motion in the heat transfer fluid may be excessive.

5. In a system which utilizes a falling film having an initial swirling motion, the effect of the swirl is rapidly reduced with increasing distance from the impeller.

It is recommended that further study of the swirling flow concept be undertaken. Based on experience gained from this investigation it is suggested that the program be designed to permit theoretical studies of the fluid flow and heat transfer problem in conjunction with the experimental studies. Specifically, it is proposed that new studies include the following.

1. A fixed impeller device to induce the swirling motion is recommended. Varying degrees of swirl may be induced by changing the impeller dimensions. The use of machine-threaded stock for the impeller seems appropriate.

2. The impeller should produce a consistent influence on the heat transfer section. To achieve this objective it is suggested that the impeller extend at least through the entire length of the heated section. This feature will permit more accurate flow characterization and temperature measurement, thus permitting a more accurate evaluation of local average film heat transfer coefficients.

3. Consideration should be given to methods of producing a constant, uniform wall temperature. Attainment of this objective would simplify measurements, data reduction, and correlation of results, as well as simplifying the theoretical analysis.

APPENDIX

Table 3. Tube Wall Static Pressure Data.

Run Number*	Water Flow Rate (lbm/sec)	Impeller Pressure (psia)	Static Pressure at Stated Distance from Impeller									
			1.25 in. ($in. H_2O$)	2.05 in. ($in. H_2O$)	2.85 in. ($in. H_2O$)	4.05 in. ($in. H_2O$)	5.25 in. ($in. H_2O$)	6.85 in. ($in. H_2O$)	8.45 in. ($in. H_2O$)	10.85 in. ($in. H_2O$)	13.25 in. ($in. H_2O$)	15.65 in. ($in. H_2O$)
1	0.610	74.6	11.9	9.3	8.5	7.1	4.8	3.2	2.4	1.0	0.5	0.4
2	0.550	64.6	9.6	7.8	6.9	5.0	3.5	2.5	2.0	0.6	0.3	0.1
3	0.490	53.6	7.1	6.0	5.0	3.4	2.4	1.6	1.1	0.3	0.1	0.0
4	0.425	45.6	5.0	4.4	3.6	2.3	1.6	1.1	0.7	0.3	0.0	0.0
5	0.365	38.1	3.8	3.2	2.6	1.2	1.0	0.7	0.4	0.2	0.0	0.0
6	0.305	31.6	2.3	2.1	1.6	0.9	0.6	0.3	0.2	0.0	0.0	0.0
7	0.245	26.6	1.1	1.1	0.8	0.5	0.2	0.1	0.1	0.0	0.0	0.0
8	0.185	22.6	0.8	0.4	0.3	0.1	0.0	0.0	0.0	0.0	0.0	0.0
9	0.120	18.6	0.2	0.1	0.0	0.0	0.0	0.0	0.0	0.0	0.0	0.0
10	0.185	22.6	0.7	0.3	0.2	0.1	0.0	0.0	0.0	0.0	0.0	0.0
11	0.245	26.6	1.3	1.0	0.8	0.5	0.2	0.1	0.0	0.0	0.0	0.0
12	0.305	31.6	2.2	1.9	1.6	0.8	0.5	0.3	0.1	0.0	0.0	0.0
13	0.365	38.6	3.5	3.1	2.5	1.6	1.0	0.7	0.4	0.1	0.0	0.0
14	0.425	45.6	5.1	4.5	3.5	2.3	1.6	1.1	0.8	0.3	0.1	0.0
15	0.490	54.6	7.3	5.9	4.6	3.4	2.4	1.6	1.1	0.5	0.1	0.0
16	0.550	66.6	10.1	7.5	6.6	4.9	3.4	2.4	1.8	0.8	0.3	0.1
17	0.610	77.6	11.8	9.0	8.0	6.3	4.6	3.1	2.4	0.9	0.4	0.3
18	0.630	79.6	12.6	9.6	8.6	6.7	5.2	3.4	2.6	1.3	0.4	0.5
19	0.120	18.6	0.2	0.1	0.0	0.0	0.0	0.0	0.0	0.0	0.0	0.0
20	0.610	74.6	11.7	9.5	7.9	6.1	4.4	2.9	2.4	1.1	0.3	0.3
21	0.550	64.6	9.5	7.7	6.3	4.9	3.3	2.4	1.8	0.6	0.2	0.1
22	0.490	54.6	7.2	5.9	4.7	3.5	2.4	1.6	1.2	0.5	0.1	0.0
23	0.425	45.6	5.4	4.5	3.5	2.4	1.6	1.1	0.7	0.3	0.0	0.0
24	0.365	38.6	3.7	3.1	2.5	1.6	0.9	0.6	0.4	0.1	0.0	0.0
25	0.305	31.6	2.4	1.9	1.5	0.8	0.6	0.3	0.1	0.0	0.0	0.0
26	0.245	26.6	1.2	1.1	0.8	0.5	0.2	0.1	0.1	0.0	0.0	0.0
27	0.185	22.6	0.8	0.4	0.3	0.1	0.1	0.0	0.0	0.0	0.0	0.0
28	0.120	18.6	0.3	0.1	0.0	0.0	0.0	0.0	0.0	0.0	0.0	0.0

(Continued)

Table 3 (Continued). Tube Wall Static Pressure Data.

Run Number	Water Flow Rate (lbm/sec)	Impeller Pressure (psia)	Static Pressure at Stated Distance from Impeller									
			1.25 in. ($in. H_2O$)	2.05 in. ($in. H_2O$)	2.85 in. ($in. H_2O$)	4.05 in. ($in. H_2O$)	5.25 in. ($in. H_2O$)	6.85 in. ($in. H_2O$)	8.45 in. ($in. H_2O$)	10.85 in. ($in. H_2O$)	13.25 in. ($in. H_2O$)	15.65 in. ($in. H_2O$)
29	0.630	78.6	12.3	9.8	8.3	6.7	4.6	3.1	2.4	1.3	0.4	0.4
30	0.610	74.6	11.4	9.4	7.7	6.1	4.4	2.9	2.4	1.2	0.3	0.3
31	0.550	63.6	9.1	7.5	6.1	5.0	3.2	2.3	1.6	0.8	0.2	0.1
32	0.490	53.6	7.1	5.8	4.6	3.3	2.3	1.4	1.1	0.4	0.1	0.0
33	0.425	44.6	5.2	4.3	3.3	2.3	1.5	0.9	0.6	0.0	0.0	0.0
34	0.365	38.6	3.6	3.1	2.4	1.2	0.9	0.6	0.3	0.0	0.0	0.0
35	0.305	31.6	2.3	2.0	1.5	0.9	0.6	0.3	0.1	0.0	0.0	0.0
36	0.245	26.6	1.3	1.1	0.8	0.5	0.2	0.1	0.0	0.0	0.0	0.0
37	0.185	21.6	0.7	0.4	0.3	0.2	0.1	0.0	0.0	0.0	0.0	0.0
38	0.120	18.6	0.2	0.1	0.0	0.0	0.0	0.0	0.0	0.0	0.0	0.0
39	0.630	78.6	12.5	10.0	8.5	6.9	3.5	3.3	1.9	1.3	0.6	0.5
40	0.660	83.3	13.8	10.9	9.4	7.5	3.9	3.6	3.0	1.6	0.7	0.6
41	0.660	83.3	14.0	11.0	9.4	7.6	4.0	3.6	3.0	1.6	0.7	0.6
42	0.660	83.3	14.1	10.9	9.4	7.5	3.9	3.6	3.0	1.6	0.7	0.6
43	0.610	74.6	14.5	8.8	8.4	6.5	4.2	3.1	2.5	0.5	0.5	0.3
44	0.550	63.6	10.7	7.0	6.5	4.9	3.0	2.3	1.8	0.3	0.2	0.1
45	0.490	54.6	8.5	5.5	5.0	3.6	2.6	1.8	1.3	0.1	0.1	0.0
46	0.425	45.6	6.1	4.1	3.5	2.3	1.7	1.0	0.7	0.0	0.0	0.0
47	0.365	38.6	4.4	2.9	2.5	1.7	1.4	0.7	0.4	0.0	0.0	0.0
48	0.305	31.6	2.8	1.7	1.4	1.0	0.7	0.3	0.2	0.0	0.0	0.0
49	0.245	27.6	1.2	0.9	0.8	0.4	0.3	0.1	0.1	0.0	0.0	0.0
50	0.185	22.6	0.9	0.5	0.3	0.2	0.2	0.0	0.0	0.0	0.0	0.0
51	0.120	18.6	0.4	0.1	0.1	0.1	0.1	0.0	0.0	0.0	0.0	0.0
52	0.185	22.6	0.9	1.4	0.3	0.2	0.1	0.0	0.0	0.0	0.0	0.0
53	0.245	26.6	1.2	1.8	0.8	0.4	0.3	0.1	0.1	0.0	0.0	0.0
54	0.305	31.6	2.7	1.7	1.4	0.9	0.5	0.3	0.2	0.0	0.0	0.0
55	0.365	38.6	4.3	2.8	2.3	1.6	0.7	0.6	0.4	0.0	0.0	0.0
56	0.425	44.6	5.9	4.0	3.5	2.4	1.0	1.1	0.6	0.0	0.1	0.0

(Continued)

Table 3 (Continued). Tube Wall Static Pressure Data.

Run Number	Water Flow Rate (lbm/sec)	Impeller Pressure (psia)	Static Pressure at Stated Distance from Impeller									
			1.25 in. (in. H_2O)	2.05 in. (in. H_2O)	2.85 in. (in. H_2O)	4.05 in. (in. H_2O)	5.25 in. (in. H_2O)	6.85 in. (in. H_2O)	8.45 in. (in. H_2O)	10.85 in. (in. H_2O)	13.25 in. (in. H_2O)	15.65 in. (in. H_2O)
57	0.490	54.6	8.4	5.5	5.0	3.6	1.6	1.8	1.2	0.0	0.2	0.0
58	0.550	62.6	11.0	7.1	6.6	5.0	2.7	2.4	1.8	0.2	0.4	0.1
59	0.610	74.6	14.1	9.0	8.3	6.4	3.8	3.3	2.3	0.4	0.7	0.3
60	0.120	18.6	0.3	0.1	0.1	0.1	0.0	0.0	0.0	0.0	0.0	0.0
61	0.610	74.6	14.1	8.9	8.4	6.4	4.1	4.3	2.5	0.5	0.7	0.3
62	0.550	63.6	11.2	7.1	6.5	5.0	2.9	2.3	1.8	0.3	0.4	0.1
63	0.490	54.6	8.6	5.5	6.0	3.6	2.1	1.8	1.3	0.1	0.2	0.0
64	0.425	44.6	6.1	4.1	3.6	2.4	1.3	1.1	0.7	0.0	0.1	0.0
65	0.365	38.6	4.4	2.9	2.5	1.8	0.9	0.7	0.4	0.0	0.0	0.0
66	0.305	31.6	2.7	1.7	1.4	1.0	0.5	0.3	0.2	0.0	0.0	0.0
67	0.245	26.6	1.6	0.9	0.9	0.4	0.3	0.1	0.1	0.0	0.0	0.0
68	0.185	22.6	0.9	0.5	0.3	0.2	0.1	0.1	0.0	0.0	0.0	0.0
69	0.120	18.6	0.3	0.1	0.1	0.1	0.0	0.0	0.0	0.0	0.0	0.0
70	0.630	78.6	15.2	9.4	8.8	6.8	4.5	3.4	2.5	0.7	0.7	0.3
71	0.660	83.6	16.9	10.4	9.6	7.3	5.1	3.7	2.7	0.8	0.8	0.5
72	0.630	78.6	15.9	9.7	9.0	6.9	4.9	3.6	2.6	0.7	0.7	0.4
73	0.660	82.6	16.4	10.2	9.4	8.3	5.2	3.8	2.7	0.8	0.7	0.5
74	0.630	79.6	17.9	9.8	9.1	7.1	5.0	3.6	2.6	0.7	0.7	0.4
75	0.660	82.6	16.5	10.1	9.4	7.3	5.2	3.7	2.7	0.7	0.7	0.5
76	0.610	74.6	14.3	9.0	8.3	6.4	4.3	3.3	2.4	0.4	0.7	0.3
77	0.550	62.6	11.1	7.1	6.6	5.0	3.0	2.4	1.9	0.3	0.5	0.1
78	0.490	53.6	8.4	5.5	5.0	3.6	2.3	1.8	1.3	0.0	0.2	0.0
79	0.610	78.6	13.6	10.6	9.7	6.0	5.6	3.5	2.7	1.3	0.8	0.5
80	0.550	67.6	11.6	8.8	8.0	4.9	4.8	2.9	2.2	1.1	0.6	0.4
81	0.490	54.6	7.5	6.3	5.0	3.3	3.0	1.8	1.3	0.6	0.4	0.1
82	0.425	44.6	5.8	4.7	3.5	2.4	1.9	1.2	0.9	0.4	0.2	0.0
83	0.365	38.6	4.1	3.2	2.2	1.6	1.1	0.7	0.5	0.2	0.1	0.0
84	0.305	31.6	3.0	2.3	1.5	1.1	0.9	0.4	0.3	0.1	0.0	0.0

(Continued)

Table 3 (Continued). Tube Wall Static Pressure Data.

Run Number	Water Flow Rate (lbm/sec)	Impeller Pressure (psia)	Static Pressure at Stated Distance from Impeller									
			1.25 in. ($in. H_2O$)	2.05 in. ($in. H_2O$)	2.85 in. ($in. H_2O$)	4.05 in. ($in. H_2O$)	5.25 in. ($in. H_2O$)	6.85 in. ($in. H_2O$)	8.45 in. ($in. H_2O$)	10.85 in. ($in. H_2O$)	13.25 in. ($in. H_2O$)	15.65 in. ($in. H_2O$)
85	0.245	26.6	1.7	1.2	0.8	0.5	0.3	0.1	0.2	0.1	0.0	0.0
86	0.185	22.6	0.8	0.5	0.2	0.2	0.1	0.1	0.1	0.0	0.0	0.0
87	0.120	18.6	0.4	0.2	0.1	0.1	0.1	0.1	0.1	0.0	0.0	0.0
88	0.185	21.6	0.8	0.4	0.2	0.1	0.1	0.1	0.1	0.0	0.0	0.0
89	0.245	26.6	1.8	1.3	0.8	0.5	0.3	0.2	0.1	0.0	0.0	0.0
90	0.305	31.6	2.9	2.2	1.3	1.1	0.5	0.3	0.2	0.1	0.0	0.0
91	0.365	37.6	4.2	3.4	2.2	1.5	0.8	0.6	0.4	0.2	0.1	0.0
92	0.425	44.6	5.6	4.7	3.5	2.4	1.4	1.3	0.9	0.4	0.2	0.0
93	0.490	54.6	8.1	6.6	5.1	3.5	2.5	1.9	1.2	0.6	0.4	0.0
94	0.550	63.6	9.7	8.3	6.6	4.3	3.3	2.4	1.7	0.9	0.6	0.2
95	0.610	74.6	12.1	10.3	8.6	5.6	5.0	3.4	2.5	1.2	0.7	0.5
96	0.120	18.6	0.4	0.2	0.1	0.1	0.1	0.1	0.1	0.1	0.1	0.0
97	0.610	74.6	12.0	10.3	8.7	5.6	4.7	3.3	2.5	1.2	0.7	0.5
98	0.550	62.6	9.5	8.1	6.6	4.4	3.2	2.4	1.7	0.9	0.6	0.3
99	0.490	54.6	7.7	6.6	5.2	3.5	2.6	1.9	1.4	0.7	0.4	0.1
100	0.425	44.6	5.6	4.8	3.6	2.4	1.6	1.2	0.9	0.4	0.2	0.0
101	0.365	38.6	4.2	3.5	2.5	1.7	1.0	0.7	0.5	0.2	0.1	0.0
102	0.305	31.6	2.8	2.2	1.4	1.1	0.7	0.3	0.2	0.1	0.0	0.0
103	0.245	26.6	1.7	1.3	0.8	0.5	0.3	0.2	0.2	0.0	0.0	0.0
104	0.185	22.6	0.9	0.5	0.3	0.2	0.1	0.1	0.2	0.0	0.0	0.0
105	0.120	18.6	0.4	0.2	0.1	0.1	0.1	0.1	0.2	0.0	0.0	0.0
106	0.630	78.6	13.6	12.2	10.6	6.4	5.2	3.7	3.0	1.5	0.8	0.6
107	0.660	83.6	14.7	12.4	11.5	7.1	6.0	4.2	3.3	1.7	0.9	0.7
108	0.630	78.6	13.6	11.2	10.4	6.4	5.2	3.7	3.0	1.5	0.8	0.6
109	0.660	83.6	14.6	12.3	11.5	7.2	6.1	4.3	3.3	1.7	1.0	0.8
110	0.630	78.6	13.8	11.2	10.5	6.4	5.2	3.7	3.0	1.6	0.7	0.6
111	0.660	83.6	14.7	12.2	11.5	7.1	6.0	4.2	3.3	1.7	0.9	0.8

*Runs 43 through 78 were made with the tube rotated 150° with respect to the original position; runs 79 through 111 were made with the tube rotated 75° with respect to the original position

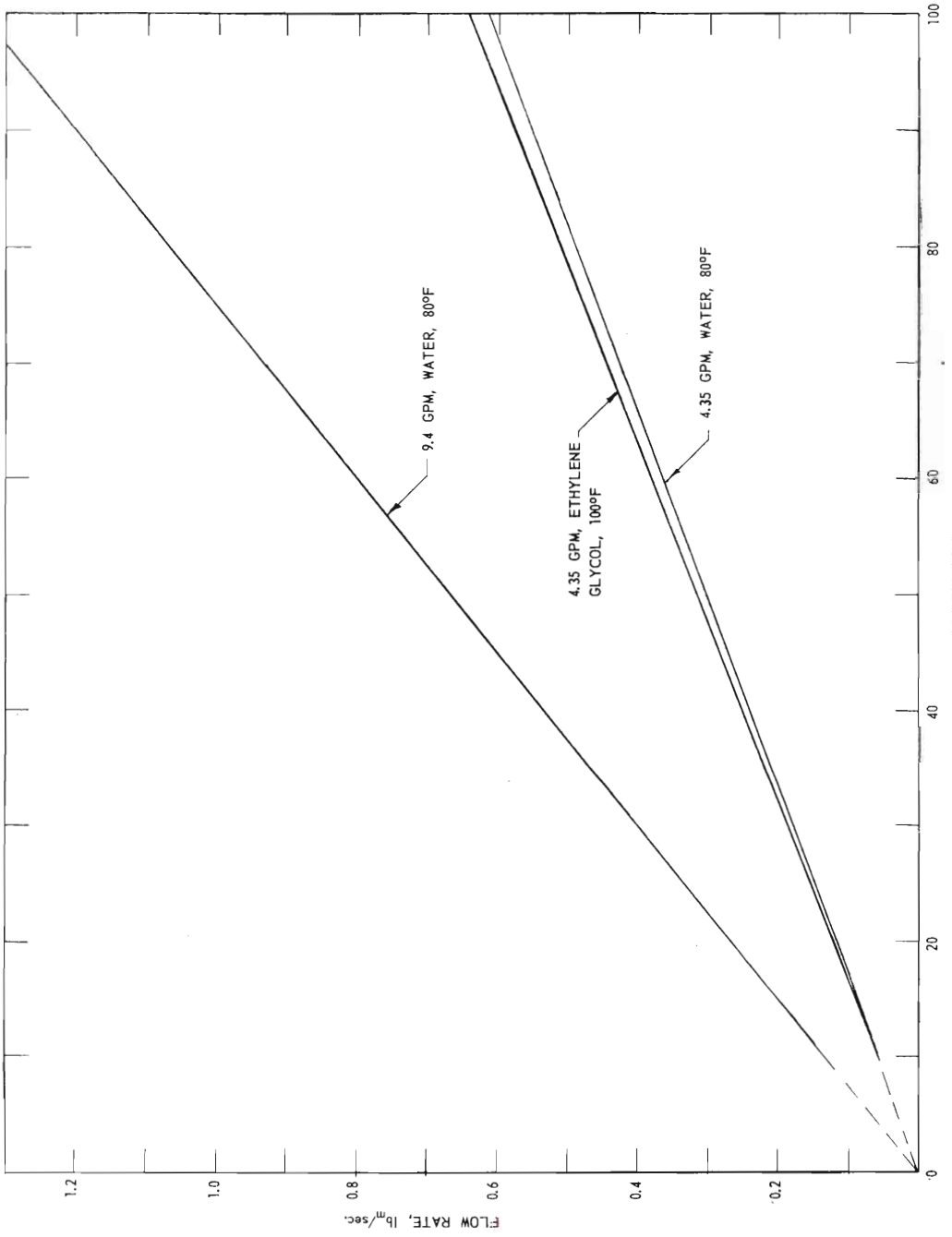

Figure 22. Rotameter Calibration.

BIBLIOGRAPHY

BIBLIOGRAPHY

1. Wattendorf, F. L., "A Study of the Effect of Curvature on Fully Developed Turbulent Flow", Proceedings of the Royal Society of London, Series A, 148, (1935), pp. 565-598.

2. Rayleigh, J. W. S., "On the Dynamics of Revolving Fluids", Proceedings of the Royal Society of London, Series A, 6, (1916), pp. 148-154.

3. Eskinazi, S., and Yeh, H., "An Investigation on Fully Developed Turbulent Flows in a Curved Channel", Journal of the Aeronautical Sciences, 23, (1956), pp. 23-42.

4. Yeh, H., "Boundary Layer Along Annular Walls in a Swirling Flow", Transactions of the American Society of Mechanical Engineers, 80, (1958), pp. 767-776.

5. Lay, J. E., "An Experimental and Analytical Study of Vortex Flow Temperature Separation by Superposition of Spiral and Axial Flows", Transactions of the American Society of Mechanical Engineers, Series C, Journal of Heat Transfer, 81, (1959), pp. 202-222.

6. Hartnett, J. P., and Eckert, E. R. G., "Experimental Study of the Velocity and Temperature Distribution in a High-Velocity Vortex-Type Flow", Transactions of the American Society of Mechanical Engineers, 79, (1957), pp. 751-758.

7. Talbot, L., "Laminar Swirling Pipe Flow", Journal of Applied Mechanics, 21, (1954), pp. 1-7.

8. Kreith, F., "The Influence of Curvature on Heat Transfer to Incompressible Fluids", Transactions of the American Society of Mechanical Engineers, 77, (1955), pp. 1247-1256.

9. Kreith, F., and Margolis, D., "Heat Transfer and Friction in Swirling Turbulent Flow", Institute of Heat Transfer and Fluid Mechanics Preprints, (1958), pp. 126-142.

10. Seigel, R., and Perlmutter, M., "Heat Transfer in Swirling Laminar Pipe Flow", Journal of Applied Mechanics, 25, (1958), pp. 295-297.

11. Fleming, J. D., Jr., Heat Transfer from Thin Gold Films to Water in Swirling Flow, Ph.D. Thesis, Georgia Institute of Technology, (1959).

12. Gambill, W. R., and Greene, N. D., "A Preliminary Study of Boiling Burnout Heat Fluxes for Water in Vortex Flow", Second National Heat Transfer Conference, AIChE-ASME, Preprint 29, (1958).

13. Sineath, H. H., Operation Characteristics of Fixed Impeller Hydroclones, Ph.D. Thesis, Georgia Institute of Technology, (1955).

14. Orr, C., Jr., The Transference of Heat Between a Pipe Wall and a Liquid-Solid Suspension Flowing Turbulently Inside the Pipe. The Thermal Conductivity and Viscosity of a Liquid-Solid Suspension, Ph.D. Thesis, Georgia Institute of Technology, (1952).

15. Keenan, J. H., and Keyes, F. G., The Thermodynamic Properties of Steam, New York: John Wiley and Sons, Inc., (1936).

16. Perry, J. H., ed., Chemical Engineers' Handbook, 3rd ed., New York: McGraw-Hill Book Company, Inc., 1950, p. 225.

17. Carbide and Carbon Chemicals Company, Glycols, New York, (1957).

18. Carbide and Carbon Chemicals Company, Physical Properties of Synthetic Organic Chemicals, New York, (1958).

VITA

Thomas Edward Stonecypher was born in Savannah, Georgia, on June 20, 1934. He attended elementary schools in Savannah and was graduated from high school in Albany, Georgia. In 1951 he entered the Georgia Institute of Technology in the School of Chemical Engineering. In 1955 he was awarded the degree of Bachelor of Chemical Engineering with Honor. In June 1955 he enrolled in the Graduate Division of the Georgia Institute of Technology and was employed as a research assistant in the Engineering Experiment Station until September 1957. He was awarded the Dow Chemical Company fellowship in the School of Chemical Engineering for the 1957-1958 academic year. Since November 1958 he has been employed as a Research Engineer by the Redstone Arsenal Research Division of Rohm & Haas Company

In 1956 he was married to the former May Davis Muse of Albany, Georgia. They have one daughter, Lynn.